

# Department of Electrical and Computer Systems Engineering

## Technical Report MECSE-13-2003

Modelling of Dispersion managed optical fibre  
communications systems

Le Nguyen Binh

**MONASH**  
**UNIVERSITY**

**MODELLING PLATFORM  
FOR  
ULTRA-LONG ULTRA-HIGH-SPEED DISPERSION-  
MANAGED DWDM OPTICAL FIBRE COMMUNICATION  
SYSTEMS**

*Le Nguyen Binh*

*Laboratory for Optical Communications and Applied Photonics*

*Department of Electrical and Computer Systems Engineering*

*Monash University, Clayton Campus, Clayton, Victoria 3168 Australia*

*Internet: [le.binh@eng.monash.edu.au](mailto:le.binh@eng.monash.edu.au)*

## Summary

*Optical fibre communications beyond the dispersion limit and multiplexing of several optical carriers are currently the most intense research and fastest growing areas of communications community worldwide. It is expected that the wavelength division multiplexed optical fibre communication networks will be deployed extensively throughout the world. As the complexity of these optical communications systems increases, the demand for a computer aided design facility is very necessary. The design, testing and optimisation of the performance of a communication system and its components can be difficult, time-consuming and expensive unless they are properly planned and estimated.*

*This monograph presents a computer simulation for wavelength division multiplexed (WDM) optical communication with special emphasis on the dispersion compensation for ultra-long and ultra-high speed transmission in the Gb/s and thousand of kilometres line. This simulation has been designed in modular structures so that it can be a universal modelling platform for long-haul high speed WDM optical communication system.*

*In compensating the dispersion effects impinged on the optical pulses during its transmission over a long haul length of optical fibres there are a number of compensation techniques such as pre-distortion dispersion using fibre gratings, mid-way dispersion compensation using optical phase conjugator or dispersion compensation fibres. In this monograph the dispersion compensated fibres are chosen due to its wide band, of more than few decades of nanometres of wavelength range, properties in generating large negative dispersion factor.*

*Therefore optical fibres can be designed on window platform so that users can design or select appropriate fibre types which are standard single mode optical fibres, dispersion shifted fibres, dispersion flatten fibres and multi-layer refractive index-profile fibres.. Further facilities for design of dispersion shifted and compensated optical fibres are also included using multiple clad refractive index profiles to suppress the waveguide dispersion factor to a desirable level to compensate to that of the material dispersion factor.*

*The modelling module for semiconductor lasers is described. Laser operations can be under continuous waves region or in the direct modulation case. The laser rate equations are solved numerically for practical laser implementation under direct current modulation or operating in a continuous mode. Sources of different wavelength and variable spectrum can be designed. External modulators are also included for high speed operating bit rates up to 60 Gbit/sec. Multiple laser sources are also included for WDM modelling.*

*Multiplexers and demultiplexers are also essential modelled for WDM operations and are integrated as a module of the design package. The propagation of the optical electric field components is performed in a split step method of the nonlinear Schrodinger equation representing the linear and nonlinear effects including the self-phase modulation, cross phase modulation and four-wave mixing.*

*Systems modelling is possible with multiple inclusion of optical amplifiers and their associated noises effects. The laser spatial rates equations are also used to model accurately the performance of optical amplifiers in particular its optical gain can be adjusted with the optical pump power and its Er doped fibre length to optimise the performance of the systems depending on the location of the optical signals along the transmission link.*

*Case studies are investigated to prove the accuracy and effectiveness of our modelling platform. Single channel operating at 2.5 Gb/s. and 20 Gb/s. and for four wavelength channels or higher number of channels are investigated with transmission distance over thousands of kms of dispersion shifted and compensated fibres.*

## **1 Introduction**

Optical fibre communications technology has been extensively employed and deployed in global communications networks and throughout terrestrial systems; from fibre-to-the-home schemes in several countries to internetworking between countries and major cities. During this last decade of the 20<sup>th</sup> century and the coming 21st century we have witnessed and will be certain that an increasing deployment of communication capacity will be demanded by information-hungry societies..

The enormous bandwidth of optical fibres and advancement of Optical communications technology together with the direct photon-photon amplification make possible several innovative configurations of optical transmission systems and distribution networks. Current deployment of optical signals over single mode optical fibres in the field are only based on single channels either at 1310 nm or 1550 nm windows, except in some field trail systems and networks. It is essential that the these enormous bandwidth regions should be used extensively. Intense investigation and experiments of ultra-long and ultra-high speed optical communication systems have been carried out together with interests in the multiplexing of optical carriers in the same fibre channel, the wavelength division multiplexing techniques have been used as the unique technology. These systems benefit from the availability of erbium-doped optical amplifiers (EDFA) which can amplify

multiple optical carriers with its certain flat optical gain spectrum without significant channel cross talk.

The complexity of optical communication systems employing WDM requires a comprehensive computer aided modelling platform in order to optimise design and experimental costs and evaluate the performance of the implemented networks. This monograph focuses on the development of a computer simulation package for optical communication systems, in particular the emerging technique WDM or multichannel optical systems would be closely investigated. The Monash Optical Communication Systems Simulator MOCSS<sup>©</sup> for optical communication systems in which three main modules, namely the transmitter module, the fibre module and the receiver module. These modules consist of sub-modules which represent all possible associated optical components for an ultra-high speed ultra-long optical communications systems. Thus our simulator would model optical communication systems for WDM high speed up to bit rate in order of 40-50 Gbits/sec. using external modulators and optical solitons as well as direct modulation of the semiconductor lasers for moderate high speed at around 2.5 to 5 Gbits/sec.

Our MOCSS<sup>©</sup> modelling facility consists of both a linear model processing the signal transmission in the frequency domain for moderate high speed optical communication systems and a nonlinear modelling employing temporal and spatial propagation technique, the nonlinear Schrodinger equation (NSE) for signal processing along long distance multi-channel optical transmission.

Detailed syntheses of all essential optical components including optical amplifiers for loss compensation, dispersion compensating fibres for dispersion compensation, tunable transmitters for multi-wavelength carrier generation, an external modulator for high bit rate signal generation, and a multiplexer/demultiplexer for channels combination and separation. The MOCSS<sup>©</sup> simulators are developed on MATLAB<sup>©</sup> for Windows platform, and are available to run on a personal computer environment or Unix workstation and supercomputing systems.

The monograph is organised as follows. In Section 2 modelling of optical modules of the simulator are presented in details from analytical formulation to computer modelling. They form the modular structures for integration into a composite system for modelling of comprehensive optical communications. The laser rate equations are given and used to generate lightwaves in CW or pulse modes, that means lightwaves pulses can be generated by direct modulation of the laser current or by an external modulator. Both of these modulators are given in details.

The optical single mode fibres can be designed using the fibre design module. Several types of optical fibres can be designed using this module from standard single core single cladding layer to dispersion shifted and compensated fibres with multiple core and cladding layers can be accurately modelled.

Optical pulses are propagated through the optical fibres influenced by linear and nonlinear effects such as linear dispersion factor, self-phase-modulation, cross-phase-modulation etc. are included. The nonlinear Schrodinger equation is used extensively for propagation of lightwaves beams through the transmission medium.

Further the important optical amplifiers are also accurately modelled by a spatial propagation technique and integrated or inserted into to the fibre propagation module. The optical signals sequences can be detected through a detection and receiving module with electrical equalisers and optical detectors. Electrical and quantum noises are included extensively in these modules giving an accurate model closely confirmed with practical system implementation. This is presented in Section 3. In Section 4 case studies of a number of WDM optical fibre communications systems are described to demonstrate the modelling facility and its accuracy. In Section 5 gives a number of important issues as conclusion to the monograph.

## 2 Modelling of Optical Modules

In the following sub-sections we describe the design and implementation of optical transmission channels. These include single mode standard (NDSF) or dispersion shifted fibres and dispersion compensated fibres, optical transmitters consisting of optical carriers generators and modulators; optical amplification devices mainly the Er doped fibre amplifiers and the multiplexing and demultiplexing optical devices for WDM and the optical receivers and demodulators. The modules are designed in modular form so that they can be interconnected as required by the system modellers.

### 2.1 Optical Fibre Channels and Dispersion Compensating Fibres

Single mode fibres is modelled with dominant linear dispersion factor being chromatic or group velocity dispersion (GVD), due to fibre index variation with the optical spectrum. Different lightwaves of the spectra propagate at different phase velocities and thus generate pulse broadening. In another word different spectral components are modulated by the pulse envelope travel at slightly different group velocities and arrive at slightly different times. Chromatic dispersion

includes effects due to fibre materials and waveguide propagation phasors as function of optical wavelength . Polarisation mode dispersion (PMD), due to differential group delay between the two orthogonal linearly polarised modes of a pulse and the random birefringence of the fibre caused by microbending, is not included in this modelling version. Although the PMD is very small (below 0.1 ps/nm/km) as compared with that of the standard single mode optical fibre it is significant compared with that of the dispersion shifted fibre. The PMD can be included at ease in our model. These PMD effects would also reduce the nonlinear effects in WDM systems. Nonlinear self-phase-modulation (SPM) and cross phase modulation due mixing of optical waves of different wavelengths are also included.

To ensure that the pulse shape remains unchanged due to dispersion effects over the long distance transmission, it is necessary to tailor the dispersion of optical fibres with a desire dispersion factor that would balance almost the dispersion effects generated during the propagation of optical pulses in a standard fibre at a certain length. The fibre module in MOCSS<sup>®</sup> is extended to include fibre design for dispersion compensating fibres. For multi-wavelength systems, it is desirable to compensate for all channels over an entire wavelength window. This was found to be achievable with multi-clad fibres. To this end, two-clad and three-clad fibres are developed.

## 2.2 Design of Dispersion-Modified Fibre

There are several main parameters in the design of a dispersion-modified fibre. With a single mode fibre, the dispersion factor in a fibre is contributed mainly material dispersion and waveguide dispersion [2]. The total dispersion factor  $D$  is thus simply the sum of two terms: the material dependent term and waveguide dependent factor as

$$D = D_M + D_W \tag{1.1}$$

where the material dispersion factor defined as

$$D_M = -\frac{\lambda}{c} \frac{d^2 n_1}{d\lambda^2} \tag{1.2}$$

and the waveguide dispersion factor by

$$D_W = -\left(\frac{n_1 - n_2}{\lambda c}\right) V \frac{d^2(Vb)}{dV^2} \tag{1.3}$$

where  $\lambda$  is the operating optical wavelength,  $n_1$  and  $n_2$  the respective refractive index of the core and cladding,  $V$  the normalised frequency,  $b$  the normalised propagation constant, and  $V(d^2(Vb)/dV^2)$  is a universal parameter which describes the waveguide-dependent dispersion characteristics of an optical fibre.

The material dependent dispersion factor of a silica-based optical fibre is due to variation of the refractive index  $n_1$  of silica with the optical carrier frequency, can be approximated by the Sellmeier equation as

$$n_1^2(\lambda) = 1 + \sum_{j=1}^N \frac{B_j \lambda^2}{\lambda^2 - \lambda_j^2} \tag{1.4}$$

where  $\lambda_j = 2\pi c/\omega_j$  is the resonance wavelength at which electrons oscillate and  $B_j$  is the oscillator strength. These two parameters are calculated from an empirical fit of (1.4) to the measured dispersion curves and are tabulated up to  $N=3$  for a number of fibres with different dopant concentrations in the core. The material dispersion factor generally does not alter when the resonance frequencies in the core region are stable at the operating frequency. Thus in order to synthesize the dispersion of an optical fibre it is required to select certain fibre material and the specifying its waveguide dispersion characteristics. From (1.3),  $D_W$  allows for two degrees of freedom in modifying its value. The relative index difference  $\Delta=(n_1-n_2)/n_1$  and the waveguide parameter  $V(d^2(Vb)/dV^2)$  can be altered to achieve a dispersion value, but the two parameters often conflict in regard to fibre performance and may require compromises with one another. For single mode fibre, current development keeps the refractive index difference at about 1% or less. However, for adequate power confinement within the core, it is desired to start the design with a high normalised frequency  $V$ , an important parameter that combines in an useful way the index difference  $\Delta$ , the core radius  $a$  and the operating wavelength  $\lambda$  as defined by:

$$V = \frac{2\pi}{\lambda} a n_1 (2\Delta)^{\frac{1}{2}} \tag{1.5}$$

Large  $V$  is required to reduce power leakage into the cladding, due to the variation of the spot size  $r_0$  with  $V$ , which is approximated to within 1% accuracy by fitting the exact field distribution of the fundamental mode to a Gaussian distribution to give [2][3]

$$\frac{r_0}{a}(V) = 0.65 + 1.619V^{-\frac{3}{2}} + 2.879V^{-6}, \quad 1.2 \leq V \leq 3$$

$$\text{or} \quad \frac{r_0}{a}(\lambda) = 0.65 + 0.434 \left(\frac{\lambda}{\lambda_c}\right)^{\frac{3}{2}} + 0.0149 \left(\frac{\lambda}{\lambda_c}\right)^6, \quad 0.8 \leq \frac{\lambda}{\lambda_c} \leq 2.0 \tag{1.6}$$

where  $r_0$  is the wavelength dependent field radius or spot size, and  $a$  is the core radius.

$\lambda_c$  is the cut-off wavelength **above** which a fibre supports only one mode, and it is related to  $V$  as

$$\frac{\lambda_c}{\lambda} = \frac{V}{V_c} \tag{1.7}$$

where  $V_c$  is the cut-off value **below** which only the fundamental mode is supported.  $V_c$  is theoretically 2.405 but can practically be 3.0. The upper limit on  $V$  in (1.6) is therefore to constrict the fibre to guide only the fundamental mode and reject all higher order modes, and the lower limit defines the range of curve fitting. From (1.5) large  $V$  requires large  $\Delta$ , therefore the design while catering for the power will pay for a higher index difference.

An approximation of the waveguide parameter  $V(d^2(Vb)/dV^2)$  as a function of  $V$  is given by the following empirical formula to less than 5% error [4]

$$V \frac{d^2(Vb)}{dV^2} \cong 0.080 + 0.549(2.834 - V)^2, \quad 1.2 \leq V \leq 2.6 \quad (1.8)$$

Eq. (1.8) is plotted in Figure 1.1, together with the normalised propagation constant  $b(V)$  which is approximated using the eigen-value of the fibre cladding with less than 2% error over the similar range of  $V$  as

$$b(V) = \left(1.1428 - \frac{0.996}{V}\right)^2, \quad 1 \leq V \leq 3 \quad (1.9)$$

and the spot size variation with wavelength in (.6) is also plotted.

A dispersion compensating fibre is usually required to be short to minimise loss and thus required a high dispersion level in the anomalous region to cancel the normal dispersion in existing standard fibre. With eq.(1.3), a high dispersion requires a large waveguide parameter and it is obvious from Figure (1.1) that the waveguide parameter and the normalised spot size are conflicting. As the waveguide parameter gets larger, the normalised spot size  $r_0/a$  also grows, which implies some fraction of mode field penetrates into the fibre cladding. The fraction of mode power confined in the core can be determined by [2]

$$\frac{P_{core}}{P_{Total}} = 1 - \exp\left(-\frac{2a^2}{w^2}\right) \quad (1.10)$$

where for  $V=2.4$ , 75% of mode power is contained in the core. This reduces to 22% when  $V=1.2$ . As the approximation for the waveguide parameter given in (1.8) is valid only in the range  $1.2 \leq V \leq 2.6$ , it can not be made any larger for a large dispersion. Instead the index difference  $\Delta$  has to be altered to achieve the required waveguide dispersion according to (1.3). When  $\Delta$  gets larger, the core diameter by (1.5) will get smaller. This will cause more loss of mode power in the cladding, and eventually an upper limit of dispersion value realisable will be reached beyond which the core diameter will be too small for light guiding or  $\Delta$  will be too large to realise. Therefore we concern

with two main parameters in the design of an optical fibre: the *core radius*  $a$  and the *index difference*  $\Delta$  at an operating wavelength  $\lambda$  or within a window of a wavelength range.

### 2.3 Dispersion Modified Fibre Design Algorithm

A study of the variation of the radius and index difference with a set of negative dispersion curves found that minimum  $\Delta$  could be obtained with the minimum  $V$  at 1.2, and maximum radius could be obtained at a common  $V$  close to 1.48. A design algorithm for a dispersion compensating fibre is derived as follows

Given operating wavelength  $\lambda_o$ , core index  $n_1$ , dispersion  $D$

Compute  $D_M = -\lambda_o / c(d^2 n / d\lambda^2)$

Compute  $D_W = D - D_M$

Either

**Design for  $V = 1.2$  to minimise index difference**

Or

**Design for  $V = 1.48$  to maximise radius**

Compute  $(Vd^2(Vb)/dV^2) = 0.08 + 0.549(2.834 - V)^2$

Compute  $\Delta$  from  $D_W = -(n_1 - n_2) / (\lambda_o c)(Vd^2(Vb)/dV^2)$

Compute **radius** from  $V = 2\pi a n_1 (2\Delta)^{1/2} / \lambda_o$

while **radius** > 4.5um and  $V > 1.2$

Reduce  $V$  by 0.002

Compute  $(Vd^2(Vb)/dV^2) = 0.08 + 0.549(2.834 - V)^2$

Compute  $\Delta$  from  $D_W = -(n_1 - n_2) / (\lambda_o c)(Vd^2(Vb)/dV^2)$

Compute **radius** from  $V = 2\pi a n_1 (2\Delta)^{1/2} / \lambda_o$

end

For any specified value of dispersion, the design starts with either  $V=1.2$  or  $V=1.48$ . When the radius is too large,  $V$  is reduced slowly and the waveguide dispersion value is achieved from (1.3) by moving along the waveguide parameter curve given by (1.8) within the limit of  $1.2 \leq V \leq 2.6$ , until the radius gets below the practical value of 4.5um.  $V$  theoretically can not take any value lower than 1.2.

## 2.4 Attenuation Associated With Compensating Fibres

A number of important fibre parameters, such as the core radius, the index difference, the mode field diameter and the cut-off wavelength, need to be considered in the course of designing a fibre, as they generate serious effects on the system performance. A compensating fibre however has relatively high intrinsic loss due to the high index difference. In addition to insertion loss, additional losses incurred by radii and index mismatch at the fibre-fibre junction are

$$Loss_{\text{int}} = -10 \log \left( \frac{a_2 NA_2}{a_1 NA_1} \right)^2 \quad (1.11)$$

where  $a_1$  and  $a_2$  are the conventional and compensating fibre core radii, and  $NA_1$  and  $NA_2$  are the numerical aperture of the two fibres respectively.

## 3 Optical Transmitter Modelling

In WDM optical communications systems the bit rate can vary from a minimum moderate bit rate of 2.48 Gbits/sec (STM-16) to 20 Gbits/sec for ultra-high speed operation. Under these operating condition the optical transmitter can be a direct modulated semiconductor laser source connected to a single mode optical fibre or it can be a semiconductor laser diode operating in the continuous waves mode coupled to an external modulator of  $\text{LiNbO}_3$  or electro-optic absorption modulator that would modulate the lightwaves at very high speed. The direct modulation optical transmitter is normally operating at moderate bit rate and the externally modulated optical transmitter are usually employed at very high bit rate of multi-gigabits per second.

In this section we present the modelling of the semiconductor laser diodes which can operate under direct current modulation or in the continuous wave mode for external modulation.

### 3.1.1 Semiconductor lasers under CW and modulated conditions

#### 3.1.1.1 Single Mode Optical Laser Rate Equations

The operating characteristic of semiconductor lasers are well described by a set of rate equations which govern the interaction of photons and electrons inside the active region. A rigorous derivation of these rate equations generally starts from Maxwell's equations together with a quantum-mechanical approach for the induced polarisation[1]. However, the rate equations can also be obtained heuristically by considering the physical phenomena through which the number of

photons  $S$  and the number of electrons  $N$  change with time inside the active region as illustrated in Figure 2.1.

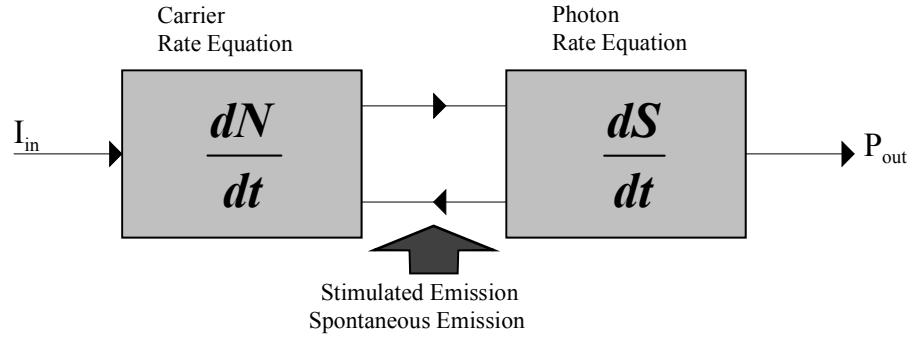


**Figure 2.1** Single mode rate equation for modelling laser.

For a single-mode laser, three rate equations are given in eqs (2.1), (2.2) and (2.3) which can be used for simulation of the frequency chirp and the output power modulated waveform corresponding to a sequence of input signals

$$\frac{dS(t)}{dt} = \left( \Gamma a_0 v_g \frac{N(t) - N_0}{1 + \epsilon S(t)} - \frac{1}{\tau_p} \right) S(t) + \frac{\beta N(t)}{\tau_n} \quad (2.1)$$

$$\frac{dN(t)}{dt} = \frac{I(t)}{qV_a} - \frac{N(t)}{\tau_n} - v_g a_0 \frac{N(t) - N_0}{1 + \epsilon S(t)} S(t) \quad (2.2)$$

$$\frac{d\phi_m(t)}{dt} = \frac{\alpha}{2} \left( \Gamma v_g a_0 (N(t) - N_0) - \frac{1}{\tau_p} \right) \quad (2.3)$$

where the parameters of the above rate equations are:  $\Gamma$  - optical waveguide confinement factor,  $v_g$  - guided lightwaves group velocity,  $a_0$  - gain coefficient,  $N_0$  - carrier density at transparency,  $\epsilon$  - gain compression factor,  $\tau_p$  - photon lifetime,  $\beta$  - fraction of spontaneous emission coupled into the lasing mode,  $\tau_n$  - electronic carrier lifetime,  $q$  - electronic charge,  $V_a$  - active layer volume,  $\alpha$  - optical linewidth enhancement factor,  $\phi_m$  - optical phase.

In (2.2) the electron density  $N(t)$ , increases due to the injection of a current  $I(t)$  into the active layer volume  $V_a$ , and decreases due to stimulated and spontaneous emission of photon density  $S(t)$ . Similarly in (2.1) the photon density  $S(t)$ , is increased by stimulated and spontaneous emission  $S(t)$  and decreased by internal and mirror losses with a photon lifetime  $\tau_p$  given by

$$\tau_p = \frac{1}{v_g(\alpha_i + \alpha_m)} \quad (2.4)$$

where  $\alpha_i$  and  $\alpha_m$  denotes waveguide loss and  $\alpha_m$  the mirror loss respectively. The carrier lifetime,  $\tau_n$  is related to the loss of electrons due to both spontaneous emission and non-radiative recombination [1] given by

$$\tau_n = \frac{N(t)}{R_{sp} + R_{nr}} \tag{2.5}$$

where  $R_{sp}$  denotes rate of spontaneous emission and  $R_{nr}$  denotes non-radiative recombination. The time variations of the optical power output is thus given by

$$m(t) = \frac{S(t)V_a\eta_0 h\nu}{2\Gamma\tau_p} \tag{2.6}$$

where  $h\nu$  denotes the photon energy and  $\eta_0$  denotes the total differential quantum efficiency.

### 3.1.1.2 Dynamic Response of Laser Source

The dynamic behaviour of the injection laser is critical, especially when it is used in ultra-long high-speed optical fibre communication systems. The application of a step current to the device results in a switch-on delay, often followed by high frequency damped oscillations ( $\approx 10$  GHz) known as relaxation oscillations (RO). RO occurs when the electron ( as the carrier ) and photon populations within the structure come into equilibrium and are illustrated in Figure 2.2. The input electrical pulse causes the electron density to rise to a maximum, which is maintained during a turn-on delay until a large photon density builds up and depletes the carriers. This behaviour is easily seen from the carrier rate eqn. (2.2).

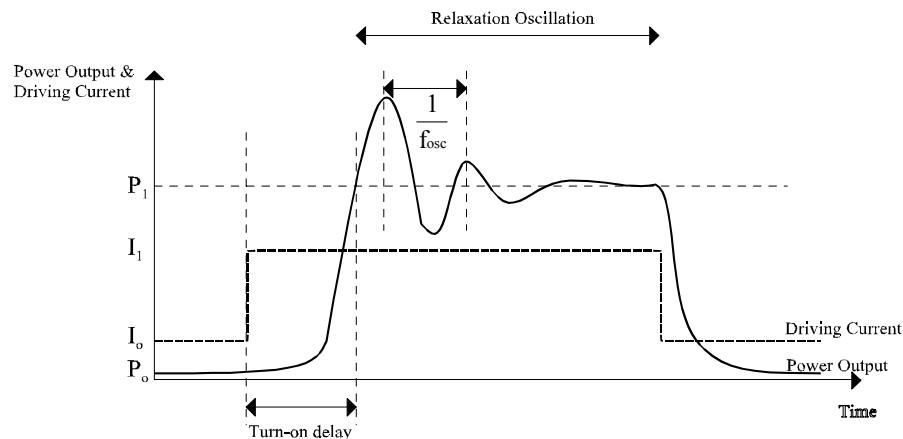


**Figure 2.2:** Typical response to a drive rectangular pulse

In addition, when a current pulse reaches a laser which has significant parasitic capacitance after the initial delay time, the pulse will be broadened because the capacitance provides a source of current

over the period that the photon density is high. The turn-on delay is caused by the initial build-up of photon density resulting from stimulated emission. It is related to the minority carrier lifetime and the current through the device. It can be reduced by biasing the laser current near threshold current level (pre-biasing). However, further increase in laser current will decrease the extinction ratio ( $P_1/P_0$ ). Resonance or oscillation frequency  $f_{OSC}$  can be increased by increasing  $I_1$ . Overshoot can be reduced by shaping electrical input pulse [5-8].

### 3.1.1.3 Frequency Chirp

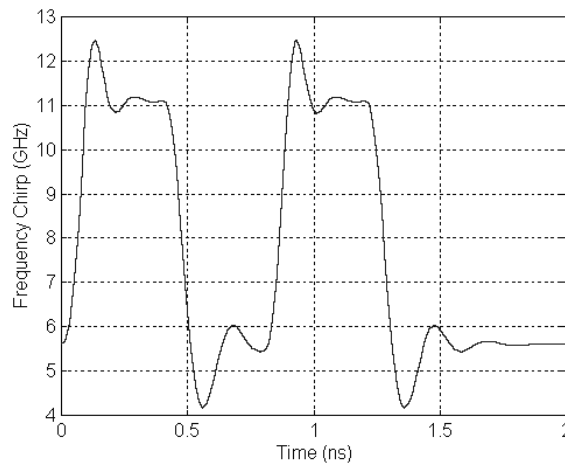


**Figure 2.3** Frequency Chirp

The direct current modulation of a single longitudinal mode semiconductor laser can cause a dynamic shift of the peak wavelength emitted from the device [7]. This phenomenon, which results in dynamic line-width broadening under direct modulation of injection current, is refer to as frequency chirping. It arises from gain-induced variations in the laser refractive index due to the strong coupling between the free carrier density and the index of refraction which is present in any semiconductor structure [11]. Hence, even small changes in carrier density will result in a phase shift of the optical field, giving an associated change in the resonance frequency within both *FP* and *DFB* laser structures.

$$\Delta \nu(t) = \frac{1}{2\pi} \left( \frac{d\phi_m(t)}{dt} \right) = \frac{1}{2\pi} \left[ \frac{\alpha}{2} \left( \Gamma v_g a_o (N(t) - N_o) - \frac{1}{\tau_p} \right) \right] \quad (2.7)$$

where  $\Delta \nu$  denotes frequency chirp,  $N(t)$  denotes the carrier density and  $d\phi_m/dt$  denotes optical phase rate eqn. (2.3).

A number of techniques can be employed to reduce the frequency chirp effects by:

- (i) Biasing the laser sufficiently above threshold so that the modulation current does not drive the device below the threshold where the rate of change of optical output power varies rapidly with time. However, this method gives an extinction ratio penalty of the order of several decibels at the receiver.
- (ii) Damping the relaxation oscillations by shaping the electrical drive pulses which will result in small power fluctuations [8].
- (iii) Using quantum well lasers, Bragg wavelength detuned *DFB* lasers and multi-electrode *DFB* lasers which provides an improvement in frequency chirp. However, it requires complex fabrication process.
- (iv) Using external modulator such as LiNbO3 Mach-Zehnder interferometric amplitude type with the laser source emits continuously lightwaves with appropriate wavelength[9].

#### 3.1.1.4 Laser Noises

The output of a semiconductor laser exhibits fluctuations in its intensity, phase, and frequency chirp even when the laser is biased at a constant current with negligible current fluctuations. This is due to two fundamental noise mechanism, the spontaneous emission and the electron-hole recombination ( shot noise ). Usually the noises in semiconductor lasers is dominated by photons randomly generated by spontaneous emission. The intrinsic intensity fluctuation in a semiconductor laser is a noise source in direct modulated optical communication systems and in some specific applications may significantly reduce the signal-to-noise ratio (*SNR*), whereas phase fluctuation leads to a limited spectral line-width when semiconductor lasers are operated continuously at a constant current. The rate equations can be used to study laser noises by adding an extra noise term, known as the Langevin force, to each of them. The rate equations thus become

$$\frac{dS(t)}{dt} = \left( \Gamma a_o v_g \frac{N(t) - N_o}{1 + \epsilon S(t)} - \frac{1}{\tau_p} \right) S(t) + \frac{\beta \Gamma N(t)}{\tau_n} + F_S(t) \quad (2.8)$$

$$\frac{dN(t)}{dt} = \frac{I(t)}{qV_a} - \frac{N(t)}{\tau_n} - v_g a_o \frac{N(t) - N_o}{1 + \epsilon S(t)} S(t) + F_N(t) \quad (2.9)$$

$$\frac{d\phi_m(t)}{dt} = \frac{\alpha}{2} \left( \Gamma v_g a_o (N(t) - N_o) - \frac{1}{\tau_p} \right) + F_\phi(t) \quad (2.10)$$

where  $F_S(t)$ ,  $F_N(t)$  and  $F_\phi(t)$  denote Langevin noise sources due to the spontaneous emission, the carrier generation recombination process in photon number and generated phase respectively[12].

They are assumed to be Gaussian random process with zero mean. Under the Markovian assumption (system has no memory ) and the correlation function of the form by Markovian approximation is

$$\langle F_i(t)F_j(t') \rangle = 2D_{ij}\delta(t-t') \quad (2.11)$$

where  $i, j = S, N, \text{ or } \phi$ , angle brackets denote the ensemble average, and  $D_{ij}$  is called the diffusion coefficient [18] and are listed in eqns. (2.12), (2.13) and (2.14).

$$D_{SS} = \frac{\beta V_a N_{sd} (V_a S_{sd} + 1)^3}{\tau_n} \quad (2.12)$$

$$D_{NN} = \frac{V_a N_{sd}}{\tau_n} [\beta V_a S_{sd} + 1] \quad (2.13)$$

$$D_{\phi\phi} = \frac{R_{sp}}{4S} \quad (2.14)$$

where  $N_{sd}$  and  $S_{sd}$  represent the steady-state average values of the carrier and photon populations respectively ( eqns. (2.15) and (2.16) ), and  $R_{sp}$  denotes rate of spontaneous emission ( eqn. 2.17 ).

$$N_{sd} = \frac{1}{\Gamma a_o v_g \tau_p} + N_o \quad (2.15)$$

$$S_{sd} = \frac{\tau_p}{\tau_n} N_{sd} \left( \frac{I}{I_b} - 1 \right) \quad (2.16)$$

$$R_{sp} = 2\Gamma v_g \sigma_g (N(t) - N_o) \quad (2.17)$$

where  $I_b$  denotes bias current and  $\sigma_g$ , the gain cross section normally is  $2 \times 10^{-20} \text{ m}^2$  By making use of the Wiener-Kinchen theorem, which states that the Fourier transform of the auto-correlation function of a process is equal to the power spectral density of that process, we take the Fourier transform of a delta function is simply white Gaussian noise. For ergodic random process,  $\langle F_i^2 \rangle = \overline{F_i^2}$  and since  $\overline{F_i} = 0$ , variance of  $F_i$  or  $\text{VAR}(F_i) = 2D_{ij}$ , ( refer to Eqn. 2.11 ). Thus, the

Langevin force is white Gaussian with a mean of zero and standard deviation of  $\sqrt{2D_{ij}}$  given as

$$F_S(t) = N(0,1)\sqrt{2D_{SS}} \quad (2.18)$$

$$F_N(t) = N(0,1)\sqrt{2D_{NN}} \quad (2.19)$$

$$F_{\phi}(t) = N(0,1)\sqrt{2D_{\phi\phi}} \quad (2.20)$$

where  $N(0,1)$  denotes Gaussian distributed random process with mean 0 and standard deviation of 1 and these three Langevin forces are to be fitted in Eqn. 2.8, 2.9 & 2.10. The noise power spectrum

$s(f)$  of the photon density as a function of the Fourier frequency,  $f$  is written using the rate equation. as

$$s(f) = \frac{\tau_p f_r^4 \langle F_N^2 \rangle + \Psi^2 \frac{\langle F_s^2 \rangle}{4\pi^2} + \tau_p f_r^4 \Psi \frac{\langle F_s F_N \rangle}{\pi} + \frac{\langle F_s^2 \rangle}{4\pi^2} f^2}{(f^2 - f_r^2) + \Psi^2 f^2} \quad (2.21)$$

and Relative Intensity Noise (  $RIN$  ) of laser source is given by

$$RIN = 10 \text{Log}_{10} \frac{s(f)^2}{S_{sd}^2} \quad (2.22)$$

where  $f_r$  denotes the resonant frequency given by

$$f_r = \frac{1}{2\pi} \sqrt{\frac{1}{\tau_p \tau_n} (1 + \Gamma a_o v_g N_o \tau_p) \left( \frac{I}{I_b} - 1 \right)} \quad (2.23)$$

and  $\langle F_s F_N \rangle$  denotes cross-correlation given by

$$\langle F_s F_N \rangle = -\frac{\beta V_a N_{sd} (V_a S_{sd} + 1)}{\tau_N} + \frac{V_a S_{sd}}{\tau_p} \quad (2.24)$$

and constant  $\Psi$  denotes

$$\Psi = \frac{1}{2\pi} \left( \Gamma a_o v_g S_{sd} + \frac{1}{\tau_n} \right) \quad (2.25)$$

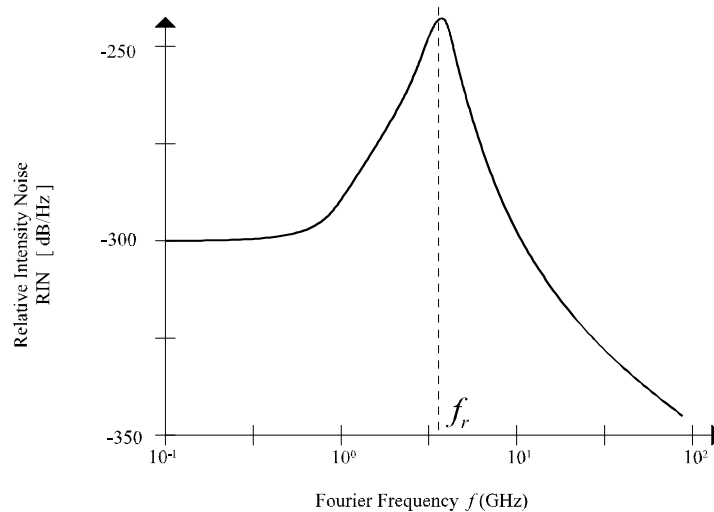
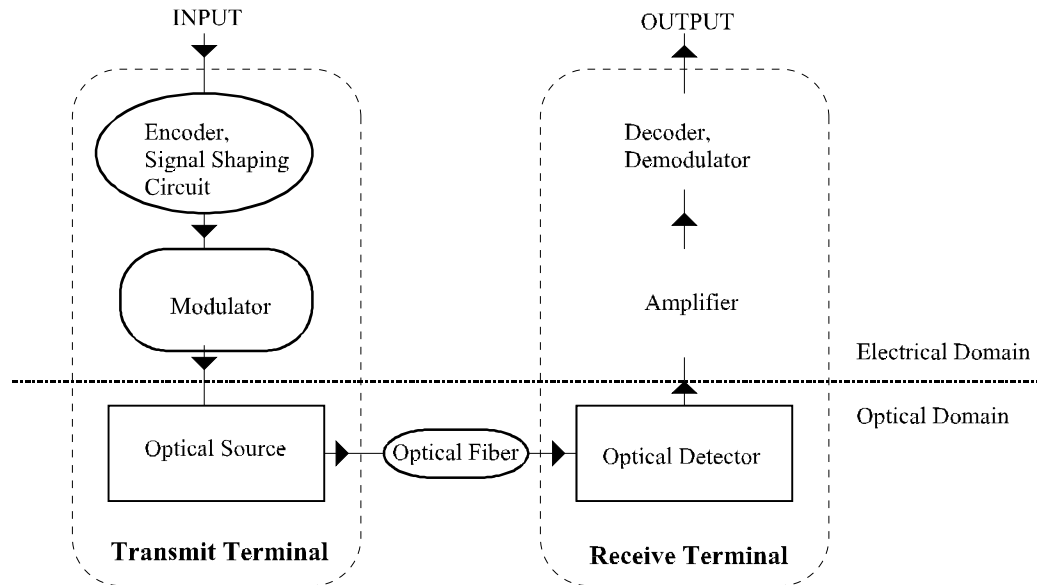


**Figure 2.3** Relative Intensity Noise for Intensity Modulation

### 3.1.2 Modelling and Development of Optical Transmitters

A typical block diagram of an optical transmitter is shown in Figure 2.4. The input to the optical source is represented by coded output of a data signal generator. Users are required to specify the

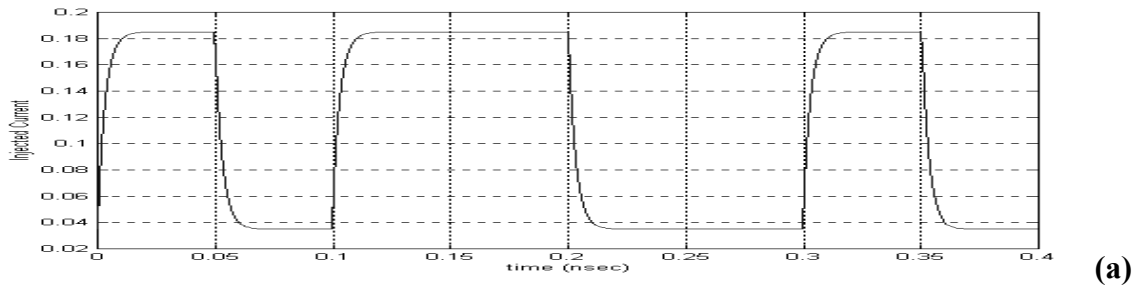
binary number input sequence in the 'Transmitter Main Menu' . The source output is coupled to a transmitting optical components block. These components may be connectors, couplers, or filters. The optical output power is usually directly modulated by varying the drive current, but external optical modulation is also possible [21].

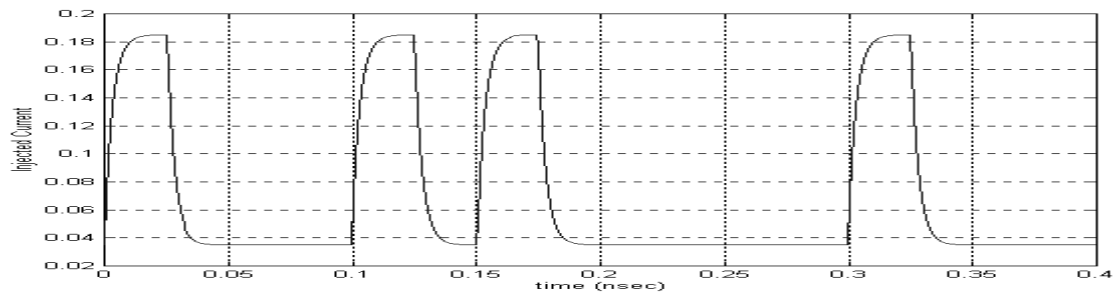


**Figure 2.4** Transmitter block diagram

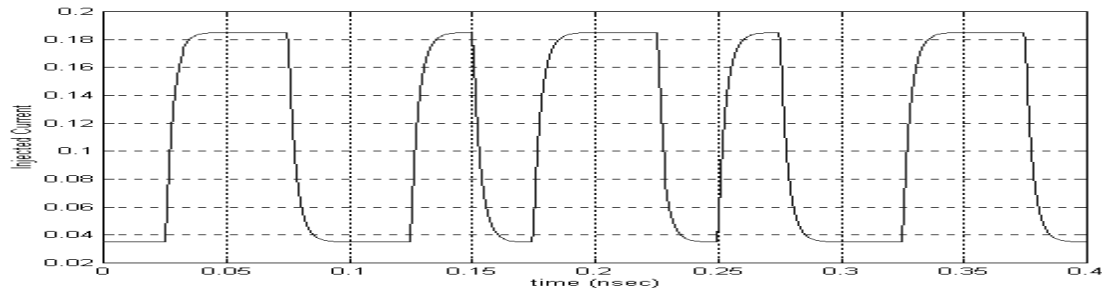
### 3.1.2.1 Line Coding

Currently, non-return zero (*NRZ*), return zero (*RZ*), and Manchester (*MAN*) are the most common coding schemes used in optical communications [22]. *NRZ* codes are simple and easy to implement. The *RZ* and *MAN* codes increase the bandwidth requirements, but this is not a serious concern at present with single-mode optical fibre transmission. The resulting waveforms of these coding schemes, generated using **MOCSS**<sup>®</sup>, are shown in Figure 2.5.





(b)



(c)

**Figure 2.5** Output waveform of (a) NRZ, (b) RZ and (c) MAN line coding

When a *NRZ* code is employed, the binary one level is held for the whole bit period. In this case there are two bit periods in one wavelength. Hence the maximum bandwidth  $B_{\max}$  is one half of the maximum data rate, eg 10 GHz data rate produces  $B_{\max}$  of 5 GHz (Figure 2.6). However, when *RZ* or *MAN* is considered, the binary one level is held for only half of the bit period. For this signalling scheme the data rate is equal to the bandwidth, eg. 10 GHz data rate produces  $B_{\max}$  of 10 GHz (Figure 2.7). The advantage of *MAN* over *RZ* or *NRZ* is to overcome 'DC built-up' by having long consecutive input bits stream of all 'ones' which could overheat the driving circuitry of the laser source [ 1 ].

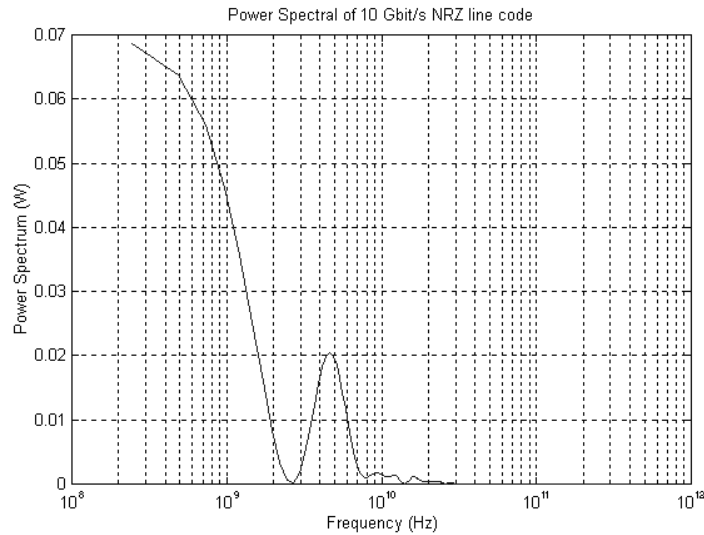


**Figure 2.6** Bandwidth display of NRZ line code at 10 Gbit/s



**Figure 2.7** Bandwidth display of RZ line code at 10 Gbit/s

### 3.1.2.2 The Runge Kutta Algorithm for Laser Rate Equations

Laser rate equations given in (2.1), (2.2) and (2.3) are in the ordinary differential equations. A few differential equations can be integrated exactly to give a solution which can be written in terms of elementary functions. In general, a numerical method must be used to find an approximate solution to the first order differential equation, which follows the general form

$$\frac{dy}{dt} = f(t, y) \tag{2.26}$$

where  $f$  is a given function of both  $t$  and  $y$ . In these equations we are seeking an unknown function  $y(t)$  which satisfies this eqn. for all values of  $t$  larger than some given initial value  $t_0$ , at which the initial value of  $y$  is also specified. Available methods to solve these differential equations are Euler's Method or the Improved Euler Method and Runge-Kutta Method. To solve the rate equations in this simulation, Runge-Kutta Method is used as in most application, it gives a very accurate results provided very small step size is used for iteration.

There are two library files available in *MATLAB* to solve ordinary differential equations using Runge-Kutta method, *ODE23* and *ODE45*, *ODE23*(FunFcn,  $t_0$ ,  $t_{final}$ ,  $y_0$ ,  $tol$ ,  $trace$ ) and *ODE45*(FunFcn,  $t_0$ ,  $t_{final}$ ,  $y_0$ ,  $tol$ ,  $trace$ ). The *ODE23* integrates a system of ordinary differential equations using 2nd and 3rd order Runge-Kutta formulas whereas *ODE45* integrates a system of ordinary differential equations using 4th and 5th order which appears to provide more accurate numerical solution but it takes larger computation time. ***tol*** is the desired accuracy for Runge-Kutta computation and it has value 0.0000001 by default. In **MOCSS**<sup>®</sup> *ODE45* with 0.0000001 accuracy is adopted for simulation analysis.

### 3.2 Optical Source Modelling

A block diagram of optical transmitter system to be considered is illustrated in Figure 2.5. Input signal will be electrically encoded by using laser drive circuit. The optical source is assumed to be single-longitudinal mode semiconductor laser which the injected laser current  $I(t)$  is a digital pulse waveform

$$I(t) = I_{bias} + \sum_{k=-\infty}^{\infty} A_k I_p(t - kT) \tag{2.27}$$

where  $A_k$  is the input data sequence (  $A_k = 0$  or  $1$  for each  $k$  ),  $I_p(t)$  is the transmitted current pulse shape ( *RZ*, *NRZ* and *MAN* signalling formats are considered ),  $T$  is the bit period,  $I_{bias}$  is the bias current. Current pulse shape is assumed to be of the form [22]

$$I_p(t) = \begin{cases} 0 & t < 0 \\ I_m \left[ 1 - \exp(-t^2 / \tau_r^2) \right] & 0 \leq t \leq T \\ I_m \left[ 1 - \exp(-T^2 / \tau_r^2) \right] \cdot \exp(-t^2 / \tau_r^2) & t > T \end{cases} \tag{2.28}$$

where  $I_m$  is the peak modulation current and  $\tau_r$  determines the pulse rise time and fall time. The photon density, carrier density and optical phase of the semiconductor laser, in response to the injected current  $I(t)$ , are determined by numerically solving rate eqn.s which describe the non-linear

modulation dynamics of the device. A *fourth-fifth order Runge-Kutta algorithm* is used to integrate the coupled set of first-order differential equations for the photon density  $S(t)$ , carrier density  $N(t)$ , and optical phase  $\phi_m(t)$ . Laser noise due to spontaneous emission and electron-hole recombination (shot noise) can be represented by Langevin noise. **MOCSS**<sup>©</sup> uses *MATLAB's* built in Runge-Kutta algorithm to solve these complex rate equations

$$\frac{dS(t)}{dt} = \left( \Gamma a_o v_g \frac{N(t) - N_o}{1 + \epsilon S(t)} - \frac{1}{\tau_p} \right) S(t) + \frac{\beta \Gamma N(t)}{\tau_n} + N(0,1) \sqrt{2 \left( \frac{\beta V_a N_{sd} (V_a S_{sd} + 1)^3}{\tau_n} \right)} \quad (2.29)$$

$$\frac{dN(t)}{dt} = \frac{I(t)}{q V_a} - \frac{N(t)}{\tau_n} - v_g a_o \frac{N(t) - N_o}{1 + \epsilon S(t)} S(t) + N(0,1) \sqrt{2 \left( \frac{V_a N_{sd}}{\tau_n} (\beta V_a S_{sd} + 1) \right)} \quad (2.30)$$

$$\frac{d\phi_m(t)}{dt} = \frac{\alpha}{2} \left( \Gamma v_g a_o (N(t) - N_o) - \frac{1}{\tau_p} \right) + N(0,1) \sqrt{\frac{\Gamma v_g \alpha (N(t) - N_o)}{S(t)}} \quad (2.31)$$

where  $N(0,1)$  denotes Gaussian distributed random process with mean 0 and standard deviation of 1. Photon density  $S(t)$ , carrier density  $N(t)$  and optical phase  $\phi_m(t)$ , simulated by **MOCSS**<sup>©</sup> are shown in Figure 2.8.

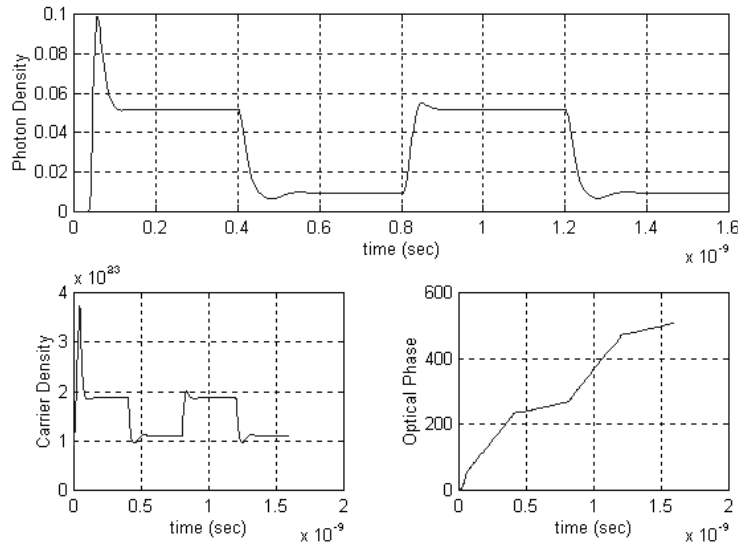
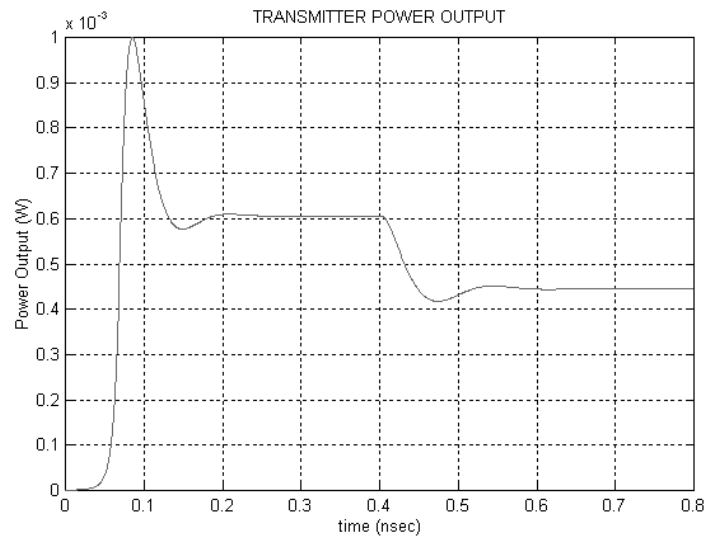


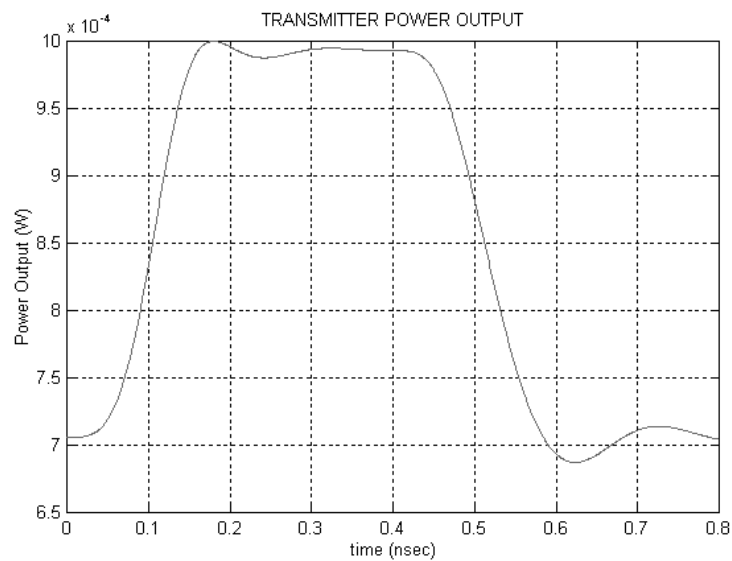
**Figure 2.8** Photon density, carrier density and optical phase

In modelling an optical transmitter, the important characteristics are the optical spectrum and the optical power output waveform. The source optical spectrum is one of the inputs needed to calculate the single-mode fibre transfer function. The time variations of the optical power and the laser chirp are given by eqs. (2.6) and (2.7) respectively.

### 3.2.1 Initial Conditions for the Laser Rate Equations - Direct Modulation



(a)



(b)

**Figure 2.9** : Direct modulation of a semiconductor laser (a) Switch On State (b) Continuous State  
 In modelling the initial response of the laser source there are two possible initial states as shown in Figure 2.18, the switch-on and continuous states. In the switch-on state, we assume a step current is introduced to the laser driving circuitry and this causes a switch-on delay. A sharp overshoot may occur before the photons and electrons have reached an equilibrium state. Therefore, this phenomena is called the '*Switch-On*' state of the laser.

In the second case, we assume the laser source has been turned on for a period of time whereby the equilibrium state of the photons and electrons have been reached. Thus, there is no sharp overshoot

but switch-on delay is still in effect due to the turn on period in the earlier point of time. Hence, this phenomena is called the 'Continuous' state of the laser. Both states can be modelled by using the basic laser rate equations and with a few boundary conditions.

At  $t=0$ , fraction of the photons produced by spontaneous emission can be ignored, i.e. the second term of (2.1) :

$$\frac{\beta \Gamma N(t)}{\tau_n} = 0 \tag{2.32}$$

Since  $dS(t)/dt$  at  $t=0$  must be a positive number :

$$\left. \frac{dS(t)}{dt} \right|_{t=0} > 0 \tag{2.33}$$

Hence

$$\Gamma a_o v_g \frac{N(t) - N_o}{1 + \varepsilon S(t)} > \frac{1}{\tau_p} \tag{2.34}$$

$$N(0) = N_o + \frac{1 + \varepsilon S(0)}{\Gamma a_o v_g \tau_p} \tag{2.35}$$

Thus, initial state of the carrier density is given by Eqn. (2.35) which is valid for the following two cases.

### 3.2.1.1 Switch On State

We now define a threshold current as the  $I(t)$  required to sustain  $N(t) = N_{th}$  when  $S(t) = 0$ . From Eqn. (2.1), this is

$$\frac{I_{th}}{qV_a} = \frac{N_{th}}{\tau_n} \tag{2.36}$$

This gives the current required to sustain an excess electron concentration,  $N(t)$ , when spontaneous emission is the only decay mechanism. We can use Eqn. (2.2) to find  $S(t)$  for the 'switch-on' state. By substituting Eqn. (2.36) into (2.1) and considering (2.34), we obtain

$$S(t) = \frac{\tau_p}{qV_a} (I(t) - I_{th}) \tag{2.37}$$

since,  $I_m = I_{th}$ ,  $I_{bias} = 1.1I_m$ ,  $I(0) = 1.1I_m$  ;

$$S(0) = \frac{\tau_p}{qV_a} (0.1 \times I_m) \tag{2.38}$$

Thus, the initial state,  $S(0)$  for 'switch-on' state is given by (2.38).

### 3.2.1.2 Continuous State

The initial conditions for photon density,  $S(0)$  and Carrier Density,  $N(0)$  can be obtained by considering the steady-state solutions to the rate equations. These solutions can be found by setting

$$\frac{dS(t)}{dt} = 0 \tag{2.39}$$

$$\frac{dN(t)}{dt} = 0 \tag{2.40}$$

Laser source rate equations are given by (2.1) and (2.2). By applying the steady-state conditions at  $t = 0$  in (2.39) and (2.40) :

$$\Gamma \left( \frac{a_0 v_g N(0) S(0)}{1 + \varepsilon S(0)} - \frac{N_0 a_0 v_g S(0)}{1 + \varepsilon S(0)} \right) - \frac{S(0)}{\tau_p} + \frac{\beta \Gamma N(0)}{\tau_n} = 0 \tag{2.41}$$

for  $I(0) = I_{bias}$ ,

$$\frac{I_{bias}}{q V_a} - \frac{N(0)}{\tau_n} - \left( \frac{a_0 v_g N(0) S(0)}{1 + \varepsilon S(0)} - \frac{N_0 a_0 v_g S(0)}{1 + \varepsilon S(0)} \right) = 0 \tag{2.42}$$

Equating (2.41) and (2.42) we obtain

$$\frac{I_{bias} \Gamma}{q V_a} - \frac{N(0) \Gamma}{\tau_n} - \frac{S(0)}{\tau_p} + \frac{\beta \Gamma N(0)}{\tau_n} = 0 \tag{2.43}$$

finally, we have

$$N(0) = \frac{\tau_n}{(\beta - 1)} \left( \frac{S(0)}{\Gamma \tau_p} - \frac{I_{bias}}{q V_a} \right) \tag{2.44}$$

Equating (2.45) and (2.36) :

$$N_0 + \frac{1}{\Gamma a_0 v_g \tau_p} + \frac{\varepsilon S(0)}{\Gamma a_0 v_g \tau_p} = \frac{\tau_n S(0)}{(\beta - 1) \Gamma \tau_p} - \frac{\tau_n I_{bias}}{(\beta - 1) q V_a} \tag{2.45}$$

$$S(0) = \frac{q V_a (\beta - 1) [1 + N_0 \Gamma a_0 v_g \tau_p] + \tau_n I_{bias} \Gamma a_0 v_g \tau_p}{q V_a [\tau_n a_0 v_g - \varepsilon (\beta - 1)]} \tag{2.46}$$

Thus, the initial state,  $S(0)$  for 'continuous' state is given by (2.46).

### 3.2.2 Effects of the Parameters of the Rate Equations on the Laser Response

The response of the laser power output is governed by the parameters in the photon rate equations given in (2.1) and the modulation current stated in (2.27) and (2.28). Each parameter has significant effects on the physical structure of a semiconductor laser on its behaviour and consequently its optical responses. Thus in order to design a laser source, it is essential that the effects of each

individual factor or a combination of these parameters to the laser optical response. We can then model the semiconductor laser source without resorting to any tedious or time consuming experiment.

Therefore the effects of each parameter are considered in this section. The following important parameters are examined :  $T_{\text{rise}}$  - rise ( or fall ) time constant,  $\Gamma$  - optical confinement factor,  $\alpha$  - linewidth enhancement factor,  $\eta$  - differential quantum efficiency,  $\tau_p$  - photon lifetime,  $\tau_n$  - carrier lifetimes and  $\varepsilon$  - gain compression factor.

### 3.2.2.1 Effects of the Laser Source Rise Time Constant

Ultra-long high-speed optical communication systems are very much limited by the laser source rise time constant. For high-speed modulated laser, a short laser rise time constant is essential. However, a short laser rise time constant would cause higher initial overshoot in its time response. In the case where the rise time constant is about 5ps, the overshoot is observed about 75%. No overshoot effect is observed for rise time constant of 50ps, 80ps and 120ps, but these lasers render low-speed modulation capability.

The second observable effect is the turn-on delay which has been illustrated in Figure 2.10. As expected, larger laser rise time constant would give rise to longer turn-on delay and hence, slower laser output response. Referring to Figure 2.10, the average turn-on delay is about 20% of the bit period (5ns).

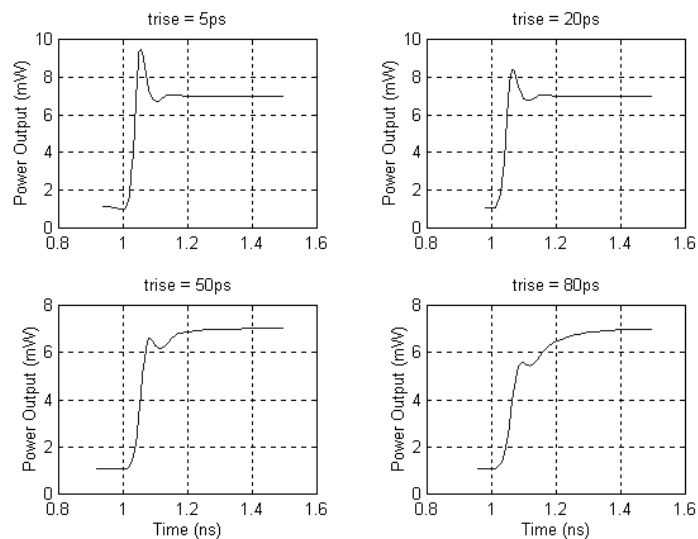


**Figure 2.10 :** Power output lightwaves of various rise time constants at 2 Gbit/s bit rate.

Therefore in order to design a good, reliable, stable and high-speed modulation laser source, optimum results should be drawn from the balance effect of overshoot and the rise time.

### 3.2.2.2 Effects of the optical confinement factor - $\Gamma$

The optical confinement factor,  $\Gamma$  is defined as the ratio of the fractional optical power confined in the core region to the total power. This factor is important for a semiconductor laser having optical gain in the core region, because it is related to the mode gain. In Figure 2.11, it is clearly seen that optical confinement factor has great effect on the turn-on delay time. When a laser medium is excited suddenly by a pulsed excitation source, the laser cannot start to oscillate immediately. The laser begins to oscillate after delay time  $t_d$ , the characteristic time it takes for the population to build up to a level corresponding to threshold.

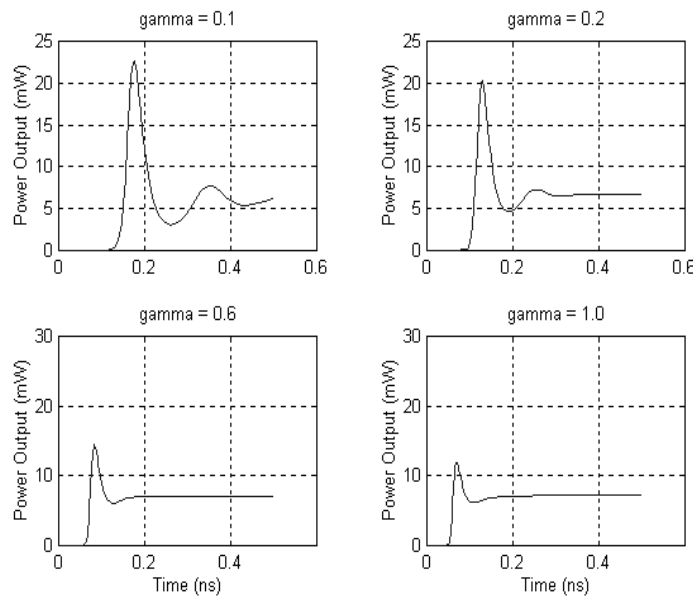


**Figure 2.11 :** Power output of various optical confinement factor at 2 Gbit/s

It is also observed that a smaller optical confinement factor contributes considerably to longer delay time of the output pulse. In the case of  $\Gamma = 0.1$ , the delay time is about 30% of the bit period ( 5ns ) whereas compare to  $\Gamma = 1.0$ , the delay time is greatly reduced to only 1% of the bit period. Thus, by increasing the optical confinement factor in the active layer of the semiconductor, we can reduce the delay time considerably. Further more, for higher value of optical confinement factor, the overshoot effect has been reduced too. Take for example  $\Gamma = 0.1$ , the overshoot is about 400% whereas  $\Gamma = 1.0$  only give rise to about 100% overshoot. The final advantage of having large optical confinement factor is the good damping effect. For  $\Gamma = 0.1$ , the pulse is oscillating over the whole bit period which would create an additional unnecessary bandwidth in the communication channel. In conclusion, a high performance laser source design should maximise the optical confinement factor in the active layer. With a reasonable value, we can reduce the pulse distortion due to the

delay time, overshoot and relaxation oscillation effect of the response. This maximisation can be pursued during the design and fabrication of the laser structure so that the optical guided waves in the channel structure if the active region is optimised such that its energy is concentrated. This however restricts the propagation of the guided waves and can generate further propagation of the guided waves.

### 3.2.2.3 Effects of the line-width enhancement factor - $\alpha$

Low frequency chirp single frequency laser diodes are extremely important for coherent optical communication systems. The principles of laser chirp has been discussed in previous sections and various methods of reducing this effect have been recommended. In this section, we analyse the effect of line-width enhancement factor,  $\alpha$  to the frequency chirp. As we can see from (2.1), the magnitude of frequency chirp ( measured in Hz ) is proportional to  $\alpha$ . In this experiment, we assume direct intensity optical modulation scheme. No external modulator is used or otherwise the chirping effect is virtually non-existing.

From Figure 2.12, we expect to see the linear relationship between frequency chirp and the line-width enhancement factor,  $\alpha$ . There is about an increase of 5.5 GHz for each unit increment of alpha. Thus, frequency chirp ( undesirable effect ) can be reduced by minimising the factor  $\alpha$ . Also, we can deduce from (2.8) that frequency chirp is proportional to carrier density,  $N(t)$  and hence the input pulse. Therefore, in Figure 2.12, the magnitude of frequency chirp follows the sequence of the input pulse.

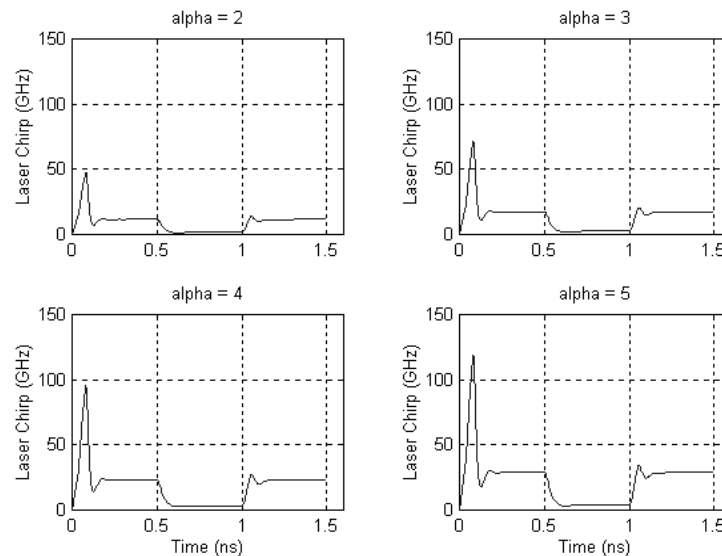


**Figure 2.12** Power output of various line-width enhancement factor at 2 Gbit/s

In conclusion, design implementation of laser source should remove the chirping effect as much as possible if not all, by minimising the value of  $\alpha$ . For example, high performance tuneable 1.5  $\mu\text{m}$  InGaAs/InGaAsP multiple-quantum well *DFB* lasers are designed by AT&T Bell Laboratories in 1988 [31] with the value  $\alpha = -3.5$ .

### 3.2.2.4 Effects of differential quantum efficiency - $\eta$

Differential quantum efficiency,  $\eta$  can be best understood by quantifying the proportion of photons generated with respect to injected electrons. The proposed mechanism giving rise to low differential quantum efficiency such as heating and leakage currents are not sufficient to explain the observed behaviour. The linear dependency between  $\eta$  and injected current has been discovered in GTE Laboratories [32].

From Figure 2.13, we can see that the power output is linearly related to the increment of  $\eta$  (2.7). However, there are difficulties in designing a laser source with a high differential quantum efficiency. The average  $\eta$  for existing laser source ranges from 0.03 to 0.20 ( or 3% to 20% ) only.

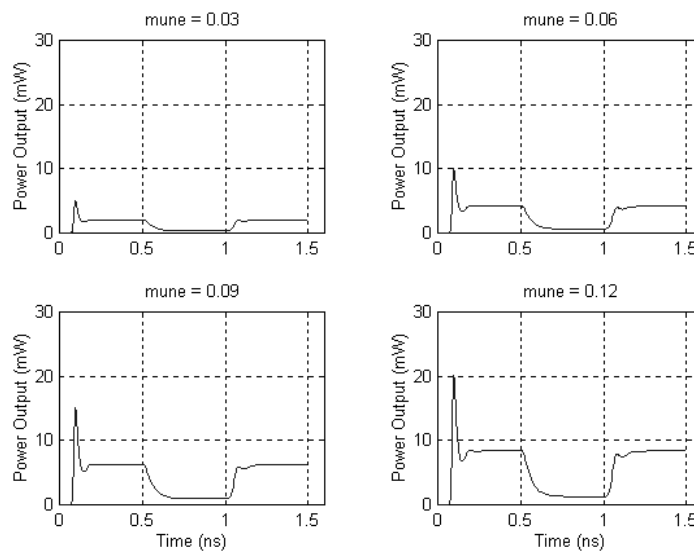


**Figure 2.13** : Power output of various differential quantum efficiency at 2 Gbit/s

### 3.2.2.5 Effects of the photon life-time - $\tau_p$

Photon life-time,  $\tau_p$  is related to the cavity structure of the semiconductor laser. Small value of  $\tau_p$  corresponds to short cavity structure of the laser source. From (2.16), we see that  $\tau_p$  is inversely proportional to the power output,  $m(t)$ . In (2.17), we notice that we could reduce frequency chirp by

reducing  $\tau_p$ . And Figure 2.13 shows that the turn-on delay can be improved by reducing  $\tau_p$ . Thus, it is essential to reduce  $\tau_p$  by observing the importance of these three considerations.

However, referring Figure 2.14, we notice that small value of  $\tau_p$  gives rise to large overshoot in the output response. For instance where  $\tau_p = 3ps$ , the overshoot is about 120%, which is undesirable. There is no overshoot been observed for  $\tau_p$  greater than 30ps but again large value of  $\tau_p$  would cause severe frequency chirp, turn-on delay and as well as low power output.

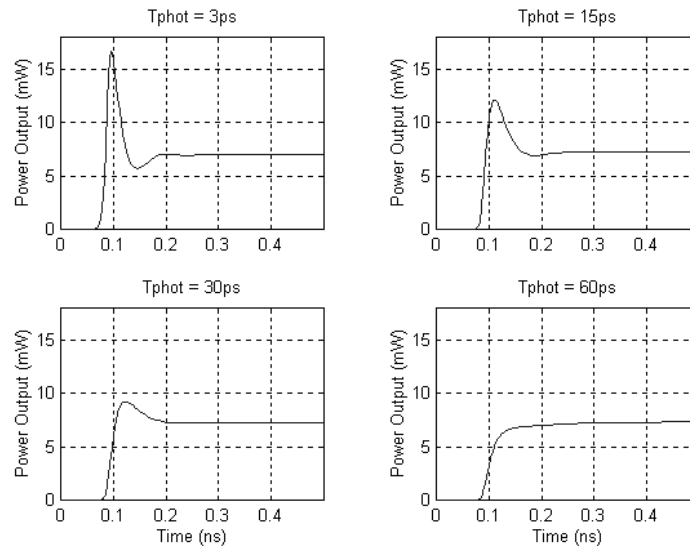


**Figure 2.14** : Power output of various photon life-time at 2 Gbit/s

In conclusion, there is no better solution apart from compromising all the factors discussed above. Therefore, one optimum solution need to be obtained for design implementation.

### 3.2.2.6 Effects due to the carrier life-time - $\tau_n$

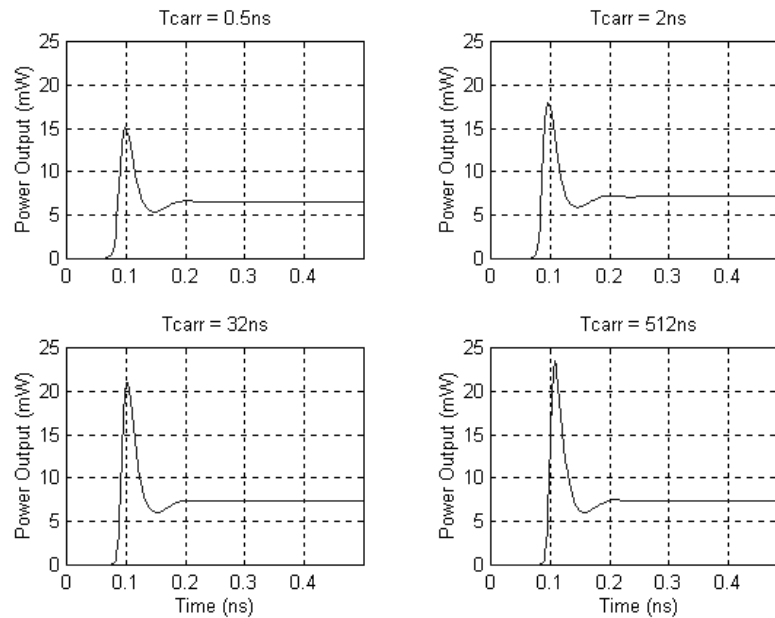


**Figure 2.15** : Power output of various carrier life-time at 2 Gbit/s

The carrier lifetime,  $\tau_n$  is related to the loss of electrons due to both spontaneous emission and non-radiative recombination [3]. From Figure 2.15, we notice that the overshoot of the output response is proportional to the carrier lifetime,  $\tau_n$ . For example where  $\tau_n = 512\text{ns}$  the overshoot is 230%, compares with  $\tau_n = 0.5\text{ns}$  which is only 100%. It is found that the turn-on delay has no direct relationship with  $\tau_n$ . However, there seems to be a minimum turn-on delay between  $\tau_n = 0.5\text{ns}$  and  $\tau_n = 2\text{ns}$ .

In conclusion, we should reduce  $\tau_n$  for the sake of not having the overshoot effect in our design implementation.

### 3.2.2.7 Effects due to the gain compression factor - $\varepsilon$

The inclusion of gain compression factor,  $\varepsilon$  in the laser rate equations (2.1)-(2.3) is a phenomenological approach which can represent a number of mechanisms, including spatial hole burning and lateral carrier diffusion [33][34], spectral hole burning, and other nonlinearities [35].

Deducing from results of Figure 2.16 good damping effect ( less relaxation oscillations ) and small overshoot can be achieved by having a larger value of  $\varepsilon$ . For instance, oscillations of four cycles with overshoot of 330% (  $\varepsilon = 0.5 \times 10^{-23}$  ) can be reduced to one oscillation cycle with 130% overshoot for the case where  $\varepsilon = 2.5 \times 10^{-23}$ . Thus, one can foresee that the output response will be fully oscillating for  $\varepsilon = 0$ .

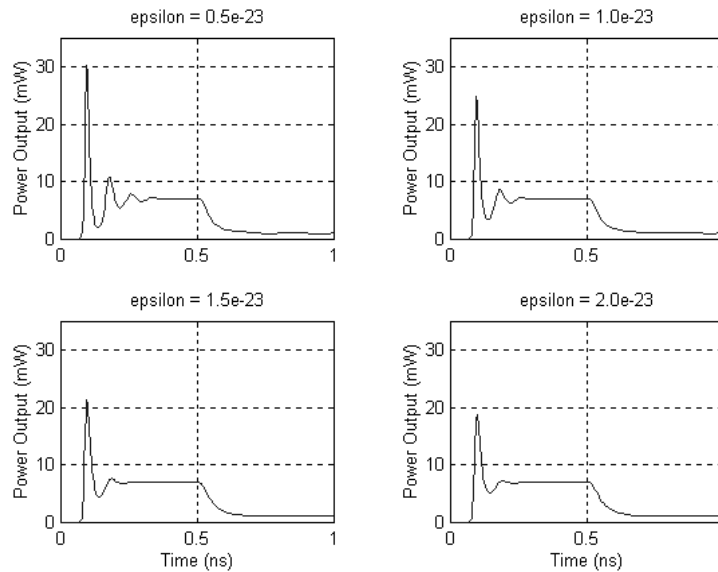


**Figure 2.16** Power output of various gain compression factor at 2 Gbit/s

In conclusion, reasonable large value of  $\epsilon$  is desirable to overcome the relaxation oscillation which would cause some additional unnecessary bandwidth for optical communication systems.

### 3.2.2.8 Power Output and Eye Diagrams Analysis

Binary input stream pulses are encoded with either using *RZ*, *NRZ* or Manchester line coding in the code generator. The encoded input signal current is used to drive the semiconductor laser source by using a biasing circuit. This optical power output,  $m(t)$  will be transmitted into the optical fibre in the next module.

Shown in Figure 2.17 is the typical optical power output waveforms. It is encoded with binary bit sequence of 1011 0111 using *NRZ* format at 2.5 Gbit/s transmission. In Figure 2.26 we notice that the whole output pulse has been shifted by 0.1ns, i.e. 25% of the bit period ( 0.4 ns ). This delay is due to the turn-on delay time.

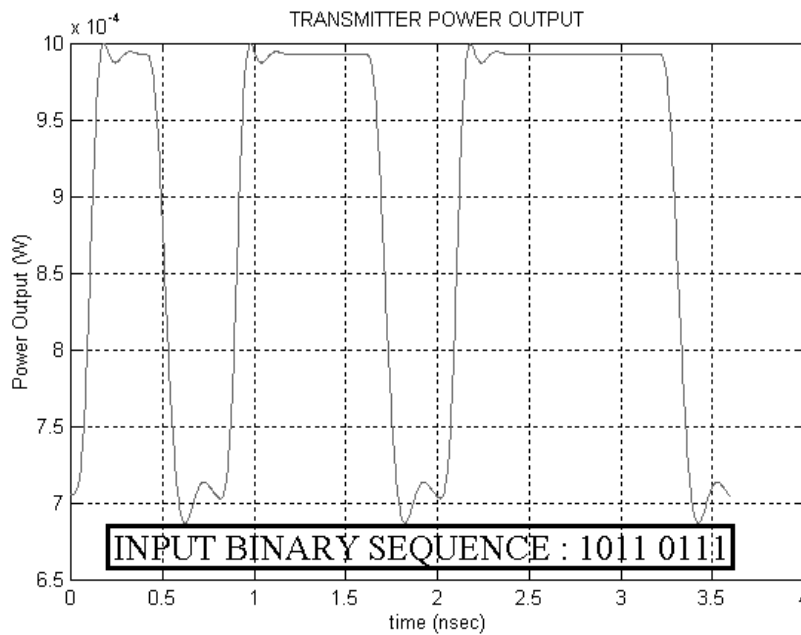


**Figure 2.17** : Power output of the optical transmitter with input bits 1011 0111 for NRZ format.

### 3.2.2.9 Eye Diagrams Analysis

The eye diagram technique is a simple but powerful measurement method for assessing the data-handling ability of a digital transmission system. This method has been used extensively for evaluating the performance of wire systems and can also be applied to optical fibre data links. To measure system performance with the eye diagram method, a variety of word patterns should be provided. A convenient approach is to generate a random data signal. **MOCSS**<sup>©</sup> uses eight different 3-bit long combinations to simulate the eye diagrams. The output of each is overlapped and hence the eye diagram.

Shown in Figure 2.18 is the simulated eye diagrams of various bit rates for a particular laser source with rise time 130ps. As the transmission bit rate increases, the eye opening reduces to a limit where the eye does not exist any more. Due to the indecisive decision level, it is impossible for the receiver to correctly decode the optical signal. Thus, the performance of a laser source is limited by the transmission rate. In Figure 2.18, the performance of the 5 Gbit/s transmission is undesirable. Hence, this particular laser source could only afford to transmit at 3.3 Gbit/s or below. However, it is more recommended to place the limit to 1 Gbit/s as the signal will be further distorted by the dispersion of optical fibre which in turn would produce a bad undesirable eye diagram at the receiving end.

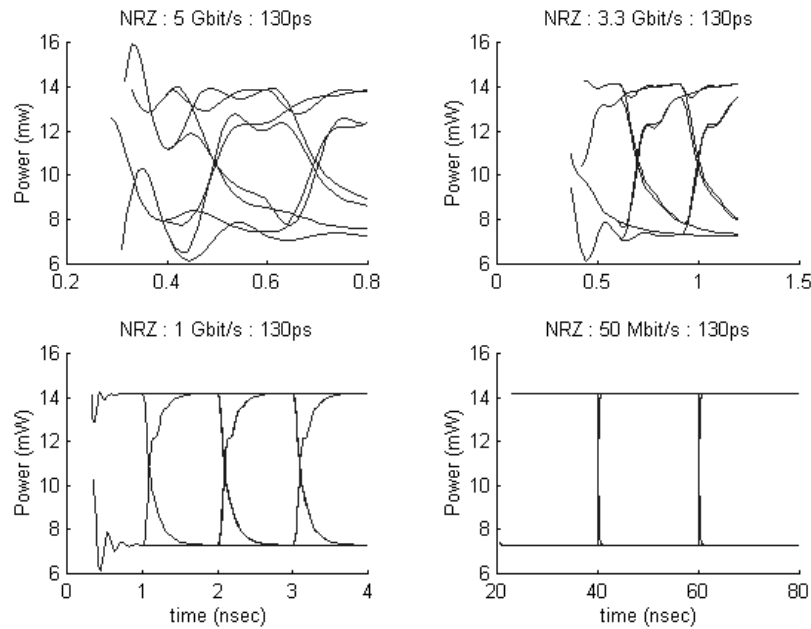


**Figure 2.18** Eye diagrams of the optical transmitter at various bit-rates

The same laser source is used for this analysis. Notice that the maximum achievable transmission bit rate for Manchester line coding is half of NRZ. Basically, it is because only a minimum half of bit period is used to encode a pulse. Thus, we conclude that system performance of an optical transmitter measured by eye diagrams technique is limited by the laser rise time constant and as well as the choice of line coding.

### 3.2.3 Software

A new noise equivalent circuit model for laser diode is presented. It enables the noise analysis of laser diode and its relevant circuit to be complemented in a unified manner using circuit analytical software SPICE and allows the straightforward calculation of the intrinsic shot noise together with modulation response, terminal impedance, transient response and non-linear distortion. A concept of equivalent input intrinsic shot noise of laser diode is proposed to establish this model [12].

### 3.2.4 Laser models

There has been a growing interest in employing directly modulated semiconductor lasers, capable of being modulated at microwave frequencies ( in GHz range ) for transmission over fibre optic links. A 20 GHz bandwidth 1.3  $\mu\text{m}$  InGaAsP/InP Straight-Wall Mass-Transport Buried Heterostructure ( SW-MTBH ) laser diode was developed to operate in a microwave fibre optic link [6]. This laser diode has wide bandwidth, high dynamic range, low-noise and good modulation properties which making it attractive to be an optical source for microwave fibre optic applications. Even though there are many lasers which are capable to transmit at higher bit-rate ( Table 2.1 ), SW-MTBH laser

is claimed to be the best due to its overall performance which includes reliability in wide-range of operating temperature and low cost of production.

Our model includes all these advanced laser sources for completeness and allows users to specify their own laser sources if necessary. Although these newest developed optical sources can operate in the ultra-high speed regime, their field performance has not proven and normally these lasers would be operating in the moderate high speed region around the 2.48 Gits/sec of the STM-16 level. For higher bit rate operation one should employ external modulation techniques with the laser diode operating in the CW mode. This is described in the next section of this article.

Laser Type for Direct Modulation	Abb.	Bandwidth	Year	Refs
Buried Heterostructure	BH	4 GHz	1982	[19]
Ridge Waveguide	RW	4.5 GHz	1984	[20]
Etched Mesa Buried Heterostructure	EMBH	7 GHz	1984	[20]
Constricted mesa ( V-groove Mass Transport Buried Heterostructure )	V-MTBH	15 GHz	1987	[16]
Vapour-Phase-Regrown Buried Heterostructure	VPR-BH	24 GHz	1990	[13]
Multi-Quantum Well Active Region	MQW	20 GHz	1992	[14]
P-doped Strained Multi-Quantum Well Active Region	pS-MQW	25 GHz	1992	[15]
Semi-Insulating Buried Crescent	SIBC	22 GHz	1992	[17]
Straight-Wall Mass Transport Buried Heterostructure	SW-MTBH	20 GHz	1994	[6]

**Table 2.1** Advanced optical laser sources operating in the ultra-high speed regime.

Laser sources has been successfully modelled by using laser rate equations ( solved by Runge-Kutta algorithm ). In order to simulate the real system, laser noise ( *Langevin force* ) is incorporated into the rate equations. A special laser source has also been included for ultra high speed system simulation analysis. The dynamic responses of the lasers, for example relaxation oscillations, frequency chirp and turn-on delay are simulated and confirmed with the experimental results[51].

The effect of each parameter of the laser rate equations to the response of the laser source has been analysed and discussed in details. All these results can be used as a guideline to design a laser source. A design menu has been developed and is available in **MOCSS**® for design purposes. The generation of the eye diagrams has been developed and it can be used to measure the performance of a particular optical transmitter system.

### 3.2.5 Tunable Transmitters

In WDM signal transmission, it is desirable that the transmitter emits very narrow spectral width and the optical carriers exhibit their distinctive optical spectrum. The distributed feedback lasers are normally chosen together with an external modulator such the travelling wave LiNbO<sub>3</sub> Mach-Zhender interferometric type or the electro-optic absorption III-V modulators. The DFB lasers has a Bragg diffraction grating fabricated into the active region at the p-n junction, and only the mode near the Bragg wavelength of the periodic grating index variation is generated. As a result it can be made tunable by changing the Bragg wavelength or the period of variation of the grating index. This can be implemented by temperature tuning the laser or using external fibre grating as an external distributed feedback cavity. A number of mechanisms for tuning other laser types have also been modelled.

Wavelength variable sources can be designed accordingly with the spectral characteristics of the semiconductor gain medium and tunable grating of the DBR. The spectra of the multiplexed optical sources can be obtained at any position during the propagation of the lightwaves along the optical fibres or optical amplifiers. Such multiplexed optical spectra can be observed in Section 5 where case studies of optical WDM communications are described.

### 3.3 External Modulator

Semiconductor lasers generally exhibit a limited modulation bandwidth that allows bit rate of up to 10 Gb/s. Higher data rate transmission may be possible by continuously CW driving the laser at a specific current just to produce a continuous wave carrier. The lasing CW lightwaves are then modulated by an external optical modulator, an electro-optic or electro-absorption type. A popular modulator type is the titanium diffused LiNbO<sub>3</sub> Mach-Zehnder modulator, which was modelled with bandwidth up to 75 Ghz. is realised by a fabrication structure [54]. With this modulation bandwidth, bit rates up to 60 Gb/s can be transmitted.

The external modulator is driven by a frequency referenced generator which sets the frequency of the electrical pulses generated by a bit pattern generator. This voltage pulses are then electrically

amplified with sufficient current to drive the travelling wave electrode. These pulses represent a digital bit stream applied to the electrodes of the modulator to change through the electrooptic effects the refractive index of the LiNbO<sub>3</sub> waveguides in one of the arm of the interferometric modulator.

For extremely high speed modulation the electrode is a travelling wave type of coplanar structure or asymmetric coplanar structure. The optical signal waves is split into two arms of the waveguide, where one lightwave path is induced by an electro-optic phase change due to the applied voltage. Lightwaves in the two arms of the Mach-Zhender merge at the modulator output they add constructively or destructively depending on their phase difference to produce an optical replica of the applied voltage signal pulses. The cross section of such an optical interferometric modulator is shown in Figure 2.19 and its operating characteristics in Figure 2.20. An experimental set up for modulation of the external modulator is given in Figure 2.21.

Some important parameters specified for the modulator included the modulation bandwidth, the insertion losses, the bias electrical voltage, the phase shift voltage, the on/off or extinction ratio, and the interferometric interaction length. The power transfer characteristic for the modulated optical continuous wave has the following nonlinear form

$$P_{out} = P_0 \exp \left[ - \left( \frac{V}{V_0} \right)^a \right] \tag{2.47}$$

where  $P_0$  is the effective intensity of the input light which included insertion losses,  $V_0$  the FWHM voltage and  $a = 4$  for the modulator. The bias voltage was chosen at the middle of the exponential decay for the best linear operation.

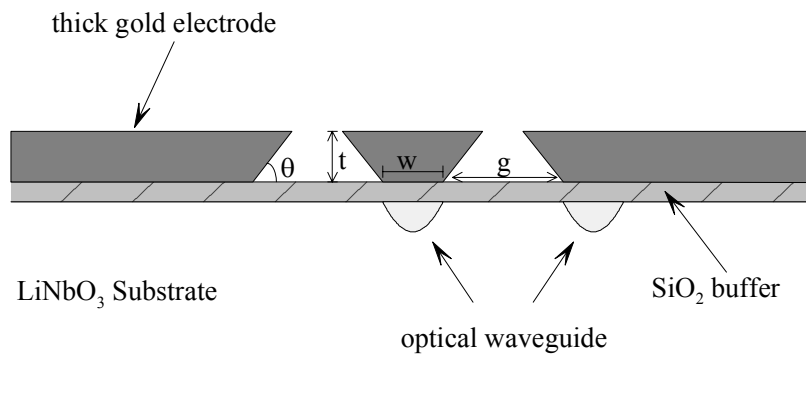


**Figure 2.19** Practical thick electrodes of the travelling-wave interferometric modulator.

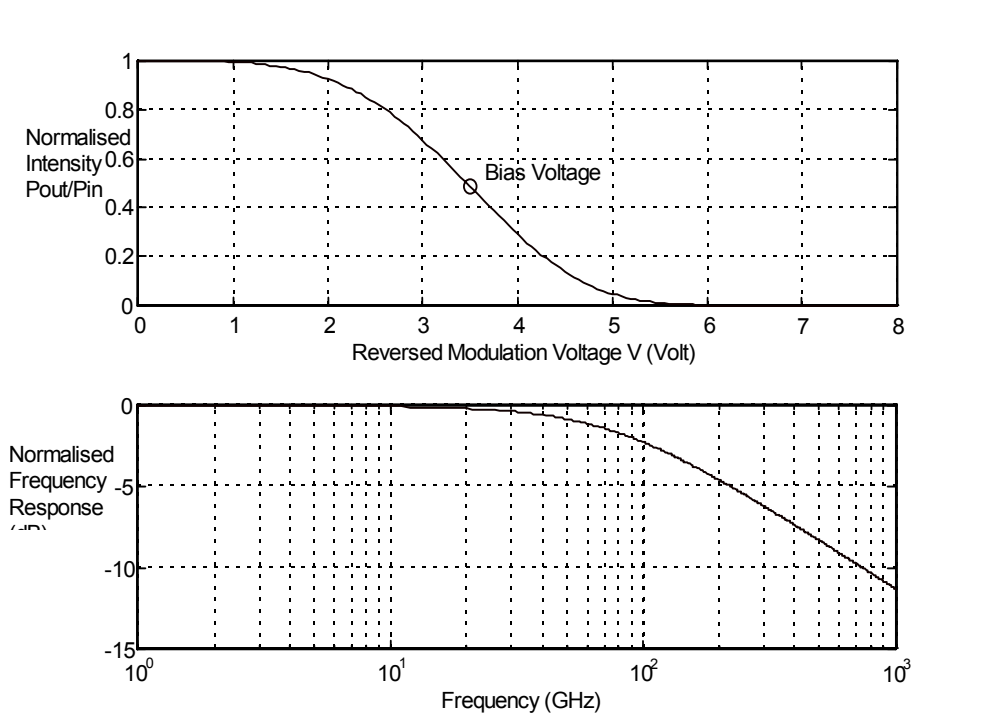


**Figure 2.20** Operational characteristics of the interferometric modulator

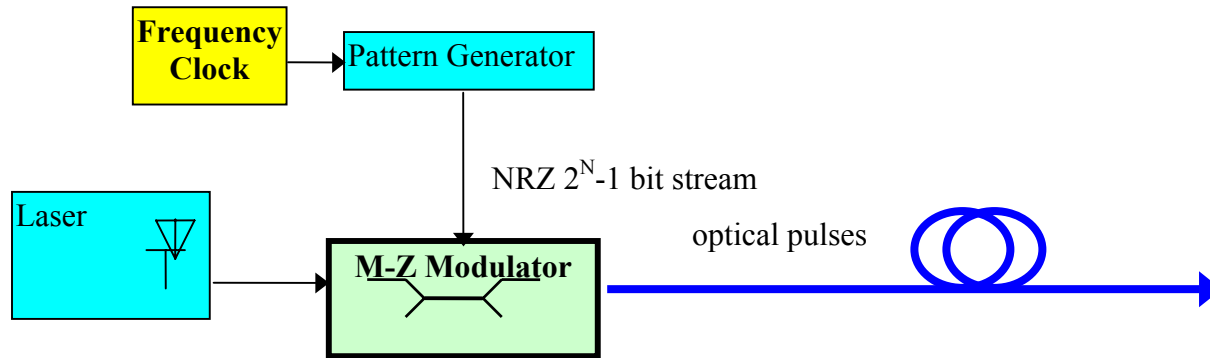


**Figure 2.21** Schematic diagram of an optical transmitter incorporating an external interferometric modulator.

#### 4 In-Line Optical Amplifiers

Modern optical fibre communications are operating with photonic amplification rather than OE and EO conversion, electronic amplification and regeneration. In-line optical amplifiers have now become standard optical components for ultra-long and ultra-high speed as well as for WDM optical communications systems. The optical amplifiers can be periodically inserted or cascaded *in line* in long-haul optical transmission systems to compensate for the optical transmission loss. Similarly they can be employed for boosting optical signal power wherever necessary, such as immediately after the external transmitter before transmitting through the optical fibre propagation medium or immediately after a long length of an optical fibre transmission system. Optical amplifiers are well known in three types: semiconductor-type laser optical amplifiers, fibre distributed type Raman amplifiers and erbium doped fibre amplifiers (EDFA). However the EDFAs are the most preferred optical amplification medium in practical systems and networks[53, 54].

The core diameter of the EDFAs is normally smaller than that the transmission fibre channel. Thus connection loss between the amplifiers and the transmission fibres occurs. EDFAs have now been chosen for optical transmission systems because they operate within the minimum fibre loss wavelength window of  $1.55\mu\text{m}$ . Further they provide high gain, low noise, wide bandwidth and are polarisation independent. Therefore, the characteristics of this type of fibre amplifiers are modelled in our simulation system.

##### 4.1 Operation Characteristics of EDFAs

Erbium ions in silica fibres occupy discrete energy levels are well known and not given here. The energy levels are formed by Stark-splitting caused by local electric fields, which are known as

thermal or homogeneous broadening. It is assumed that the inhomogeneous broadening is due to the randomness of glass structure much less significant. This is in fact true for most rare-earth ions in glass at room temperature [53].

An erbium doped fibre is pumped with a high power laser diode, using a wavelength selective coupler which combines pump and signal powers so that they co-propagate in the amplifying fibre. Associated optical components such as optical isolators are also used to optimised the stability of the amplification process in the EDFA. The pump light excites erbium ions into their higher energy level. An optical isolator may be included to prevent amplifier oscillation due to spurious reflections, and an optical bandpass filter is used to extract the signal beam at the amplifier output [54]. In practice, a highly efficient doped fibre is needed to minimise the level of pump power.

The state transitions  $4I_{15/2}-4I_{11/2}$  or  $4I_{15/2}-4I_{13/2}$  correspond to signal amplification in the 1550 nm band require pump wavelengths of 980 nm or 1480 nm in the erbium absorption bands respectively. Semiconductor lasers operating near these wavelengths are specifically developed to pump power in EDFAs in these regions. To achieve high gain, large pump power is required to totally invert the erbium ions population from the ground level  $4I_{15/2}$  to the excited energy level  $4I_{13/2}$ . The 980nm pump level  $4I_{11/2}$  is relatively unstable and erbium ions quickly decay to the long lived metastable state  $4I_{13/2}$  in a non-radiative manner. Signal power is amplified by stimulated emission of photons dropping from the excited state back to the ground state, when light is emitted in phase with the signal frequency. In addition, the metastable state ions also randomly emit photons, which get amplified over the whole amplifier spectrum and interfere with the amplified signal. This is the dominant amplified spontaneous emission (ASE) noise in EDFAs. In our model we choose to pump the EDFAs at 1480 nm and the operating channel wavelengths can be located across the full gain spectrum of the EDFAs [54].

## 4.2 Gain Characteristics of EDFAs

Erbium doped silica fibres basically consist of three atomic energy levels as discussed above. Erbium ions can be in the ground state, pumped to the metastable state, or in the pump level during pumping. They may also have a fourth level at the pump photon energy  $hf$ , which can cause excited state absorption. In modelling the amplifier, a *two level* system for the Er ions is assumed for the reason that the population in the third level (pump band) and other levels is negligible. This is valid provided the pump rate is relatively slower than the fast non-radiative decay of ions in other levels to the  $I_{13/2}$  metastable level [54].

A two-level rate equation for generation in a semiconductor laser can be used to model optical pumping and amplification in the EDFAs [3], thus the two energy levels under consideration are the ground state and the excited metastable state. The rate of change of the inversion population in the excited state due to spontaneous and stimulated emission is given by [3]

$$\frac{\partial N_2(z,t)}{\partial t} = \frac{\sigma_{ak} \Gamma_k P_k(z)}{a_{eff} h\nu_k} N_1(z) - \frac{\sigma_{ek} \Gamma_k P_k(z)}{a_{eff} h\nu_k} N_2(z) - \frac{N_2(z)}{\tau_{SP}} \quad (3.1)$$

where for the conservation of particle the total erbium ions density is

$$N_t(z) = N_1(z) + N_2(z) \quad (3.2)$$

and  $N_1$  is the ground state population. The parameters in (3.1) for the EDFAs are  $\sigma_{ak}$  - *absorption cross section at frequency  $\nu_k$  ( $m^2$ )*,  $\sigma_{ek}$  - *emission cross section at frequency  $\nu_k$  ( $m^2$ )*,  $P_k$  - *power at frequency  $\nu_k$* ,  $a_{eff}$  - *effective erbium doped core radius*,  $h\nu_k$  - *photon energy*,  $\tau_{SP}$  - *spontaneous lifetime of the metastable state*,  $\Gamma_k$  - *overlap integral between the signal and the dopant mode*.

The first term in (3.1) describes change in the metastable population through absorption of signal or pump energy of frequency  $\nu_s$  by ground state ions having absorption cross section  $\sigma_{ak}$ . The second term describes depletion of the metastable level through stimulated emission of cross section  $\sigma_{ek}$ . The third term describes spontaneous emission of photons from excited ions having a metastable lifetime  $\tau_{SP}$ . Steady-state modelling of the EDFA operation can be applied when it has a long metastable lifetime and the gain medium can efficiently store signal energy to smooth out amplifier fluctuations. By neglecting the temporal characteristics of the EDFA when the modulation frequency of the amplified signal is high relative to the pumping rate or the spontaneous and stimulated emission rates, the steady state solution for a metastable population condition in (3.1) is

$$N_2(z) = \frac{\sum_k P'_k(z)}{1 + \sum_k P''_k(z)} N_t(z) \quad (3.3)$$

where the powers are normalised to their threshold and saturation values [6] such that

$$P'_k(z) = \frac{P_k(z)}{P_{th}} \quad (3.4)$$

$$P''_k(z) = \frac{P_k(z)}{P_{sat}}$$

$$P_{th} = \frac{\pi a_{eff}^2 h \nu_k}{\Gamma_k \sigma_{ak} \tau_{SP}} \tag{3.5}$$

where

$$P_{sat} = \frac{\pi a_{eff}^2 h \nu_k}{(\sigma_{ak} + \sigma_{ek}) \Gamma_k \tau_{SP}}$$

Note that pump and signal powers are not constant but change along the amplifier length due to absorption, stimulated and spontaneous emission. Considering firstly a noise free amplification by neglecting spontaneous emission, which can later be included for the amplified power, distributed power along the amplifying medium is described by [55].

$$\frac{dP_k(z)}{dz} = [\sigma_{ek} N_2(z) - \sigma_{ak} N_1(z)] \Gamma_k P_k(z) \tag{3.6}$$

that indicates that the signal power is amplified by stimulated emission of metastable ions and partly absorbed by ground state ions. Similarly the pump power can be amplified by stimulated emission while partly absorbed by ground state ions along the amplifier length. With pump bands below 1520nm, the absorption profile is much higher than the gain profile, as showed in Figure 3.1 below for a EDFA with germanium doped core, the pump power gain will therefore be relatively small.

### 4.3 Absorption and Emission Spectra

The absorption and stimulated emission spectra in Figure 3.1 are measured experimentally [6] [10] in dB/m units of gain or loss. Germanium doping in silicate glass has the effect of raising the fibre refractive index and hence broadening the gain spectrum. The gain and absorption cross sections of the fibre can be directly determined from the measured spectra as

$$\begin{aligned} \alpha_a(\lambda) &= \sigma_a(\lambda) \Gamma(\lambda) N_t \\ \alpha_e(\lambda) &= \sigma_e(\lambda) \Gamma(\lambda) N_t \end{aligned} \tag{3.7}$$

where  $\alpha_a$  and  $\alpha_e$  are the measured absorption and gain coefficients in dB/m,  $\sigma_a$  and  $\sigma_e$  are the absorption and gain cross sections,  $N_t$  is the total erbium ions density, and  $\Gamma$  is the overlap integral between the optical mode and the erbium ions. When erbium ions are uniformly distributed in the core,  $\Gamma$  is usually known and the cross sections can be directly obtained from (3.7). Otherwise if  $N_t$  varies across the core radius, the cross sections may have to be calculated using the Ladenburg-Fuchbauer equation

$$\sigma_{a,e}(\lambda) = \frac{\lambda^4 I_{a,e,peak}(\lambda)}{8\pi c n^2 \tau \int I_{a,e}(\lambda) d\lambda} \tag{3.8}$$

where  $\lambda_{a,e,peak}$  is the wavelength at the absorption or gain peak,  $\tau$  is the metastable lifetime,  $n$  is the refractive index of the glass,  $c$  is the velocity of light, and  $I_{a,e}(\lambda)$  is the measured spectral shape of the absorption and emission coefficients. Indeed, the cross section spectra in Figure 2.1 was calculated using (3.8) assuming  $\Gamma$  was not well known [6].

The absorption cross section at pump band below 1520nm turned out to be relatively large compared to the gain cross section, which implies efficient pumping of erbium ions with small pump power. The two cross-section profiles almost coincide within the signal band of 1530-1545 nm, as valid for the usual assumption. The large absorption at short wavelengths is due to large thermal population in the lower states of the ground level photons, and large fluorescence at long wavelengths due similarly to large thermal population in the excited states.

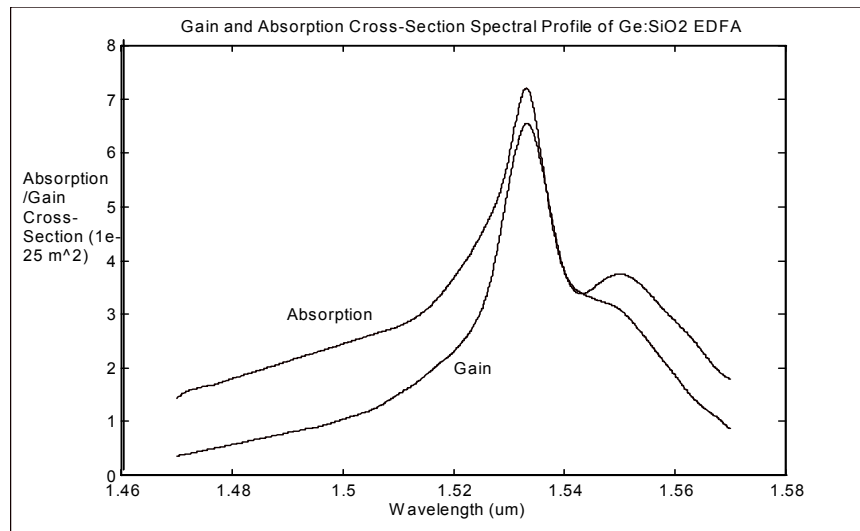


**Figure 2.1** Cross section absorption and emission spectra of Ge:SiO<sub>2</sub> EDFA

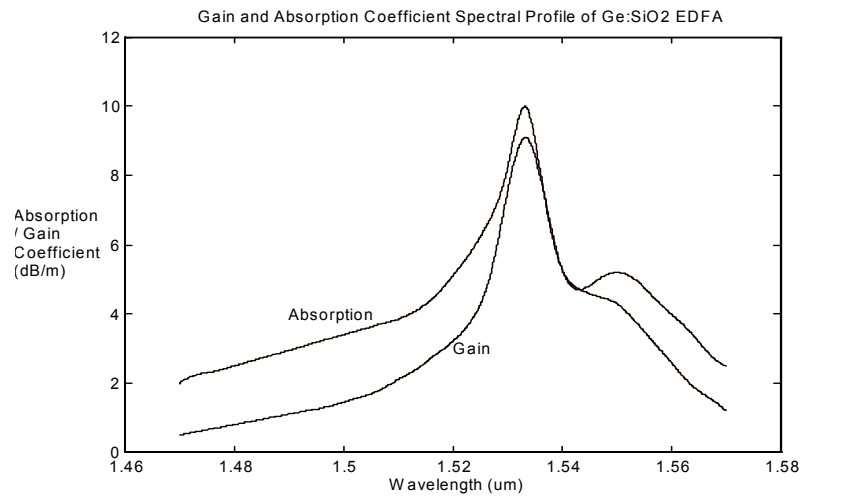


**Figure 2.2** Absorption and emission coefficient spectra of Ge:SiO<sub>2</sub> EDFA

Using (3.2) and substituting for N<sub>2</sub> from (3.3),

$$\begin{aligned} \frac{dP_k(z)}{dz} &= [\sigma_{ek} N_2(z) - \sigma_{ak} (N_t(z) - N_2(z))] \Gamma_k P_k(z) \\ &= \left( (\sigma_{ek} + \sigma_{ak}) \frac{N_2(z)}{N_t(z)} - \sigma_{ak} \right) \Gamma_k P_k(z) N_t(z) \\ &= \left( (\sigma_{ek} + \sigma_{ak}) \frac{\sum_k P_k'(z)}{1 + \sum_k P_k''(z)} - \sigma_{ak} \right) \Gamma_k P_k(z) N_t(z) \end{aligned} \quad (3.9)$$

To eliminate the overlap integral and the cumbersome calculation of the cross sections, the propagation equation can be written just in terms of the absorption and gain coefficients using (3.7)

$$\frac{dP_k(z)}{dz} = \left( (\alpha_{ek} + \alpha_{ak}) \frac{\sum_k P_k'(z)}{1 + \sum_k P_k''(z)} - \alpha_{ak} \right) P_k(z) \quad (3.10)$$

This spatial rate equation is solved numerically using the 4<sup>th</sup>-5<sup>th</sup> order Runge-Kutta function in MATLAB<sup>®</sup>. Typical parameter values at 1.55 μm for the EDFA are as shown.

<b>EDFA parameters used in spatial modelling of gain characteristics</b>
<i>Signal Wavelength</i> λ <sub>S</sub> = 1.55 μm
<i>Pump Wavelength</i> λ <sub>P</sub> = 1.48 μm
<i>Pump Threshold</i> P <sub>Psat</sub> = 1.5 mW
<i>Noise Bandwidth</i> Δν <sub>ASE</sub> = 4460 GHz
<i>Er<sup>3+</sup>-doped Core Radius</i> = 2.2 μm
<i>Pump Absorption Coefficient</i> α <sub>Pa</sub> = 2.5 dB/m
<i>Signal Absorption Coefficient</i> α <sub>Sa</sub> = 4.3 dB/m
<i>Pump Gain Cross-section</i> σ <sub>Pe</sub> (λ <sub>P</sub> ) = 5 × 10 <sup>-26</sup> m <sup>2</sup>
<i>Signal Gain Cross-section</i> σ <sub>Se</sub> (λ <sub>S</sub> ) = 3.9 × 10 <sup>-25</sup> m <sup>2</sup>
<i>Pump Absorption Cross-section</i> σ <sub>Pa</sub> (λ <sub>P</sub> ) = 1.8 × 10 <sup>-25</sup> m <sup>2</sup>
<i>Signal Absorption Cross-section</i> σ <sub>Sa</sub> (λ <sub>S</sub> ) = 3.1 × 10 <sup>-25</sup> m <sup>2</sup>
<i>Excited State Spontaneous Lifetime</i> τ <sub>SP</sub> = 10 ms
<i>Overlap integral between signal mode and erbium ion</i> Γ <sub>S</sub> = 0.58

$$\text{Overlap integral between pump mode and erbium ion } \Gamma_P = 0.62$$

#### 4.4 Amplification Characteristics

##### 4.4.1 Signal Amplification along the Fibre Length

The results are as shown in Figure 3.2. For signal amplification, the launched pump power must be above a threshold value  $P_{Pth}$  at the EDFA input to achieve minimum population inversion of erbium ions. The signal gain increases along the amplifier length as stimulated emission of erbium ions continues with sustaining pump power. The pump power also attains a small gain due to small gain coefficient at the pump frequency. Eventually at a particular point in the amplifier fibre the pump intensity decays below its inversion threshold  $P_{Pth}$ , and the signal is reabsorbed by the ground state ions and the gain starts to drop. The amplified signal at this point is termed as  $P_{Sth}$  corresponding to  $P_{Pth}$ . A signal gain is considered reaching a saturation level  $P_{Ssat}$  shortly after this value.

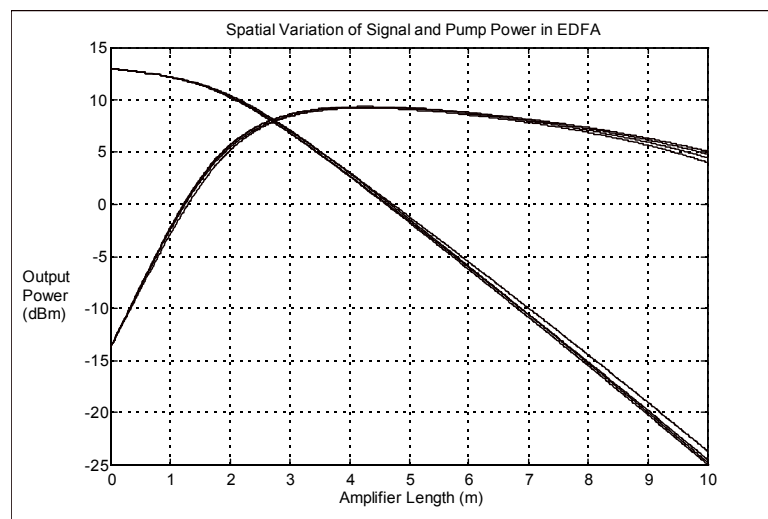


Figure 3.3(a) Pump and signal powers variation along amplifier length

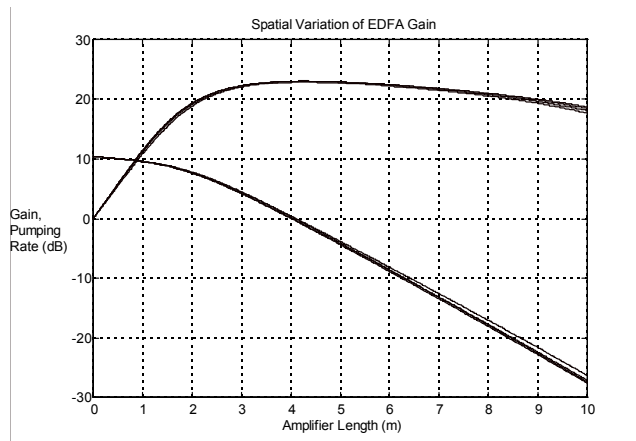


Figure 3.3(b) Pumping rate and signal gain variation along amplifier length

Therefore for a given input pump power, there exists an optimal fibre length within which signal gain up to a maximum value can be achieved. Figure 3.3 shows that this optimal length increases with the optical pump power. In practice, the length of the Er doped section of the amplifier should be designed so that an exact to minimise the ASE noise or and reaches an optical length to absorb sufficient pump power for amplification gain.

These characteristic curves allow the choice of an amplifier length by adjusting the input pump power to obtain the required loss compensation, or to obtain the highest gain with minimum pump power if the amplifier length is justifiable.

#### 4.4.2 Signal Gain As A Function of Pump Power

The gain characteristics of the EDFA as a function of input pump power and amplifier length are described in this sub-section. Different gain and absorption characteristics of other doped fibre materials can easily be inserted in our modelling. Analytical solutions of the rate equations given in (3.10) can be obtained as a transcendental equation which relates *the signal gain G, the amplifier length L and the launched pump power  $P_{Pin}$*  as followed [2] :

$$\ln\left(\frac{P_{Pin}}{P_{Pth}} - \frac{1}{2}\alpha_p L - \frac{1}{2}\frac{\alpha_p}{\alpha_s}\frac{\ln 10}{10}G\right) + \frac{1}{2}\alpha_p L - \frac{1}{2}\frac{\alpha_p}{\alpha_s}\frac{\ln 10}{10}G = \ln\left(\frac{P_{Pin}}{P_{Pth}}\right) \quad (3.11)$$

where  $G=10\log(P_S(L)/P_S(0))$  dB. This is a very useful equation for an experimental design of EDFA as it allows the evaluation of the gain characteristics by measurement of only three parameters,  $\alpha_s$ ,  $\alpha_p$  and  $P_{Pth}$ . The equation was solved numerically to give a set of characteristic curves for different launched pump powers or amplifier lengths.

In order to obtain the *gain characteristics as a function of pump power*, (3.11) can then be rewritten as

$$kG = \frac{P_{Pin}}{P_{Pth}} \left( 1 - e^{\left( kG - \frac{1}{2} \alpha_p L \right)} \right) - \frac{1}{2} \alpha_p L \tag{3.12}$$

where  $k = \frac{1}{2} \frac{\ln 10}{10} \frac{\alpha_p}{\alpha_s}$  and is solved numerically for different amplifier lengths. The resulting characteristic curves are as shown in Figure 3.4.

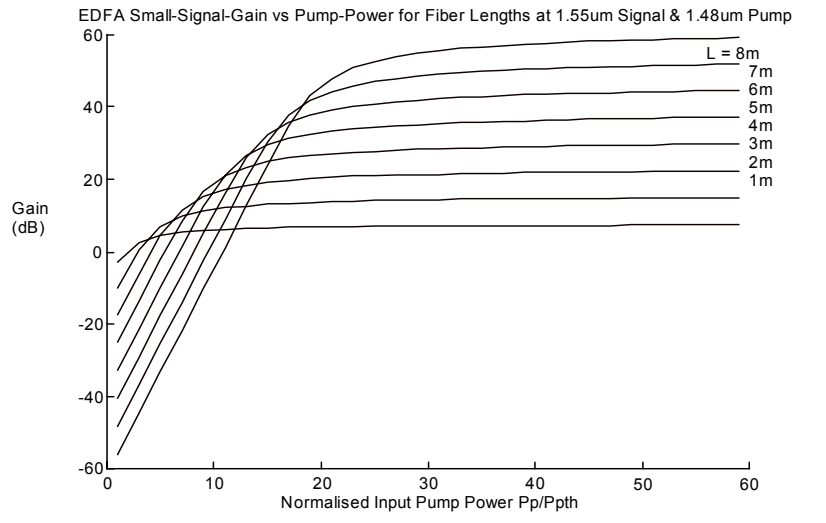


Figure 3.4 Signal gain variation with pump power for different EDFA lengths.

The curves show that the gain saturates when more pump power than sufficient for population inversion is launched into an amplifier fibre of a given length. Note that with a long fibre, a pump power slightly greater than the inversion threshold  $P_{Pth}$  may not be sufficient for signal amplification over the entire fibre length, and the gain is negative at the output due to absorption of signal by the fibre. Thus a long fibre requires larger pump power. The parameters used in the calculation were experimental values as measured in [2]:

<b>Parameters For Gain Characteristics Calculation</b>
Pump Wavelength $\lambda_p = 1.48 \mu\text{m}$
Signal Absorption Coefficient $\alpha_s = 0.175 \text{ m}^{-1}$
Pump Absorption Coefficient $\alpha_p = 0.076 \text{ m}^{-1}$
Signal mode cross section area $a_s = \text{pi} * (\text{core\_radius})^2$
Pump mode cross section area $a_p = \text{pi} * (\text{core\_radius})^2$ , assuming core uniformly doped
Excited state spontaneous lifetime $\tau_{SP} = 10 \text{ ms}$
Planck's constant $h = 6.626 \times 10^{-34} \text{ Js}$

#### 4.4.3 Signal Gain As A Function of Amplifier Length

To obtain the gain characteristics as a function of amplifier length, equation (3.12) is solved with the normalised pump power  $P_p/P_{Pth}$  constant. A set of gain curves is obtained for different pump powers in Figure 3.5. The maximum gain attainable was found to be increasing with pump power, so was the amplifier length for maximum gain.

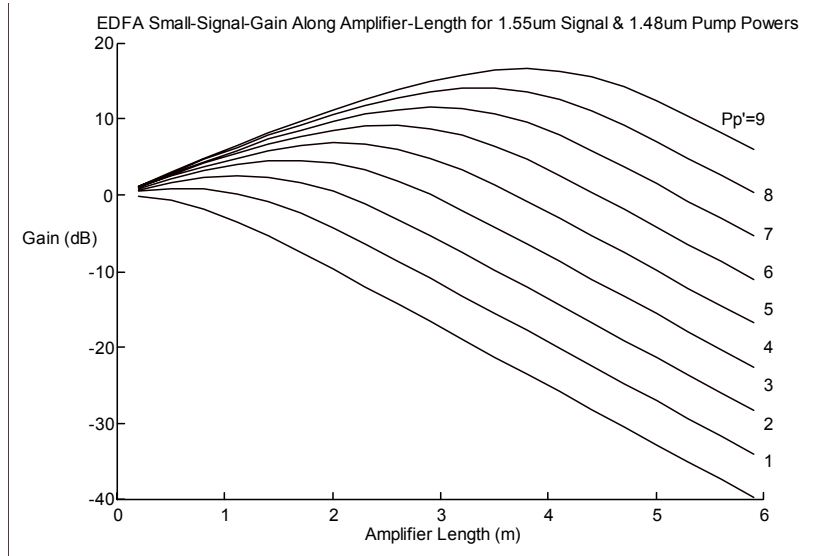


Figure 3.5 Signal gain variation with amplifier length for different pump powers.

The curves show that the gain started to drop after reaching a maximum as the amplifier length increases because a pump power is not sufficiently strong to cause adequate population inversion beyond a point in a long fibre, and the fibre will just reabsorb the signal. This implies that the length of the amplifier has to be optimised to achieve maximum gain for a certain pump power.

These gain characteristics calculated by the transcendental equation in (3.11) are in good agreement with experimental curves as confirmed by [2]. They are referred to as small signal gains in the sense of linear amplification, as prior to falling into saturation due to amplifier noise as described below.

#### 4.4.4 The Bisection Method For Solving A Nonlinear Equation

Equation (3.12) is a nonlinear equation and it certainly is difficult to solve for an exact solution. If it can be rewritten in a general explicit form of  $f(x) = 0$  then any value of  $x$  satisfying this equation is a root of  $f$  [5]. Hence by denoting  $x=G$  and all other terms appear as constants, an approximate value for  $G$  can be obtained for a given pump power input  $P_{Pin}$  at a specific amplifier length  $L$  :

$$kG + \frac{1}{2} \alpha_p L - \frac{P_{Pin}}{P_{Pth}} \left( 1 - e^{\left( kG - \frac{1}{2} \alpha_p L \right)} \right) = 0 \tag{3.13}$$

The simplest method to approximate the root of  $f(G)=0$  is the bisection method, which just requires  $f$  to change sign over some continuous interval  $[a, b]$ , so that  $f(a)f(b)<0$ . From the intermediate value theorem, this implies that there must be at least one root  $x$  of  $f$  within the interval.

The basic procedure is to bisect the function  $f$  at the midpoint of the interval  $c=(a+b)/2$ , then if  $f(a)f(c)<0$  the interval is halved to  $[a, c]$ , or else the interval is halved to  $[c, b]$ . The procedure repeat until the value  $x=c$  is within some small tolerance value, then we satisfy with the value  $c$  as a root of  $f$ . The algorithm for the bisection method is then

*Given a function  $f(x)$ , an interval  $[a, b]$  over which  $f$  is continuous and  $f(a)f(b)<0$ , and a tolerance  $e$*

*Set  $c$  to  $(a+b)/2$*

*Repeat*

*if  $f(a)f(c)<0$  then*

*set  $b$  to  $c$*

*else if  $f(a)f(c)>0$  then*

*set  $a$  to  $c$*

*set  $c_L$  to  $c$*

*set  $c$  to  $(a+b)/2$*

*until  $|c-c_L| < e$*

Then  $c$  is an approximate root of  $f(x)=0$ . Although the procedure is simple, this method is superior because it always converges. The value of  $e$  was taken as 0.005. Using this method, a gain curve is obtained by solving (3.13) for a set of roots  $G$  over a range of pump power  $P_p$  with the amplifier length constant, or over a range of amplifier lengths with the pump power constant.

#### 4.5 Modelling of Optical Amplifier Noises

The dominant noise in EDFA is due to spontaneous emission. While the signal power get amplified in the gain medium, lightwaves generated due to spontaneous emission of photons in random directions also get amplified. This amplified spontaneous emission (ASE) power  $P_{ASE}$  contributes to the amplified signal power  $P_k$  as noise sources, thus it can be written:

$$P_k(L) = G_k P_k(0) + P_{ASE}(L) \tag{3.14}$$

where  $L$  is the length of the doped optical amplifier,  $G_k$  is the signal gain at frequency  $\nu_k$ , and the ASE contribution when included in the spatial rate equation in (3.9) is obtained as [6]

$$P_{ASE}(v_k) = 2 \left( \frac{N_2}{N_2 - \frac{\alpha_{ak}}{\alpha_{ek}} N_1} \right) h v_k \Delta v_k (G_k - 1) \quad (3.15)$$

where  $\Delta v_k$  is the bandwidth of a single Fourier component and is related to the window  $T$  of the time based signal as  $1/T$ . The frequency dependence of the ASE power was stated to indicate photons emitted in spontaneous manner have random phase and could take on frequency over the entire amplifier bandwidth. The overall noise bandwidth  $\Delta v_{ASE}$  is therefore effectively almost the whole spectrum of the amplifier, and power amplification over the band contributes to the amplified signal in the form of white noise.  $\Delta v_{ASE}$  was estimated from the gain cross-section profile  $\sigma_e(v)$  in Figure 3.2 as [6]

$$\Delta v_{ASE} = \int_0^{\infty} \frac{\sigma_e(v)}{\sigma_{e,peak}} dv \quad (3.16)$$

and is found to be 4460 GHz for the Ge:SiO<sub>2</sub> gain spectrum considered.

#### 4.5.1 Modelling ASE Power As a Random Noise Source

In practice it is usually observed that noise statistics of the amplified light follows a Gaussian distribution. By considering noises as random variables generated by many independent sources, it can be reasonably assumed that the probability density function of their sum approaches Gaussian under fairly general conditions. The effect of amplifier noises can therefore be modelled as a Gaussian random process with a noise variance  $P_{ASE}$  [11].

The approach to signal amplification was to multiply the electrical field of the input signal  $E_K(t, 0)$  by the total field gain  $\sqrt{G_T}$  in the time domain.  $G_T$  is obtained at the output of the amplifier through interaction of the power of each time sample of the input signal with the pump power in the amplifier fibre.

$$E_K(t, L) = \sqrt{G_T} E_K(t, 0) \quad (3.17)$$

Random ASE noise was then included by generating complex spectral components whose real and imaginative parts are Gaussian random variables with variance  $P_{ASE}$  corresponding to the average noise power. These components are superimposed over the Fourier spectrum of the signal to produce fluctuations in the time-based signal.

In MATLAB<sup>®</sup> programming environment the spectrum was obtained by applying the discrete Fourier transform function  $FFT(x)$  which uses a radix-2 fast-Fourier-transform algorithm when  $x$  is a vector with length of a power of 2. For this reason, the temporal signal was intentionally sampled

to obtain  $2^N$  points. We also made use of a standardised Gaussian random number generator  $Z = N(0, 1)$  which has zero mean and unit variance and transformed it to a complex random variable with variance  $P_{ASE}$  by

$$E_k(Z_1, Z_2) = (Z_1 + jZ_2)\sqrt{P_{ASE}} \quad (3.18 a)$$

and each of these variables then generated added to a spectral component  $E_k(f_j)$  of the signal

$$E_k(f_j) = FFT(E_k(t))_j + E_k(Z_{1j}, Z_{2j}) \quad (3.18 b)$$

The amplified time signal plus noise was then obtained by applying the inverse discrete Fourier transform function  $IFFT(x)$  to the modified spectrum

$$E_k(t) = IFFT(E_k(f)) \quad (3.19)$$

#### 4.5.2 Signal Degradation In Direct Detection

To determine how severe the extent of noise could impair the amplified signal, it would be necessary to consider detection of the signal. Consider a photodetector which generates a photocurrent  $I$  upon detection of a light signal, the photocurrent  $I_{Samp}$  corresponds to the amplified signal power is

$$I_{Samp} = RGP_S(0) + \sqrt{P_{ASE}} + i_N \quad (3.20)$$

where  $R = \eta q/h\nu$  is the responsivity,  $\eta = 1$  is assumed for unit quantum efficiency, and  $i_N$  represents the current fluctuations which can be expressed as a noise variance  $\langle i_N^2 \rangle$  combining a bunch of noises with single-sided spectral density [8]

$$\langle i_N^2 \rangle = 2qRGP_S + 4qRn_{SP}h\nu(G-1)\Delta\nu_{ASE} + 4R^2n_{SP}GP_Sh\nu(G-1) + 4R^2(n_{SP}(G-1)h\nu)^2\Delta\nu_{SP-SP} \quad (3.21)$$

where the spontaneous emission noise factor  $n_{SP}$  is introduced as

$$n_{SP} = \frac{N_2}{N_2 - \frac{\alpha_{as}}{\alpha_{es}} N_1} \quad (3.22)$$

From left to right, (3.18) consists of the signal shot noise, the ASE shot noise, the ASE-signal beat noise, and the ASE-ASE beat noise.  $\Delta\nu_{ASE}$  and  $\Delta\nu_{SP-SP}$  are the effective bandwidth of the ASE and ASE-ASE beat noises respectively. The dominant terms are immediately obvious as those possessing  $G^2$ . However it is known in practice that most of the ASE-ASE beating can be effectively removed by an optical bandpass filter [2]. Therefore we are left with one term as the dominant noise to model with, namely the ASE-signal beat noise.

Since in practical transmission high and low pulses are generated by non zero modulation intensity, the ASE-signal will contribute equally to both a bit '1' and bit '0' pulse. The noise current therefore adds in the same manner to the amplified signal in (3.20) regardless of its information:

$$I_{Samp} = RGP_s(0) + \sqrt{P_{ASE}} + 2RG\sqrt{n_{sp}hvP_s} \quad (3.23)$$

To assess the extent of noise added to the amplified signal by the EDFA, it is convenient to introduce a parameter called the **amplifier noise figure**  $F_N$  which measures the signal-to-noise ratio (SNR) degradation of the amplified signal:

$$F_N = \frac{SNR_{IN}}{SNR_{OUT}} \quad (3.24)$$

By considering the amplifier as a photodetector limited mostly by shot noise, the SNR of its input signal is

$$(SNR)_{in} = \frac{\langle I \rangle^2}{\sigma_s^2} = \frac{I_s^2}{2qI_s\Delta f} = \frac{(RP_s)^2}{2qRP_s\Delta f} = \frac{P_s}{2hv\Delta f} \quad (3.25)$$

where  $\Delta f$  is the detector bandwidth. The SNR of the amplified signal would be

$$(SNR)_{out} = \frac{\langle I \rangle^2}{\sigma_s^2 + \sigma_{ASE}^2} = \frac{I_s^2}{(2qI_s + 4RI_s(G-1)n_{sp}hv)\Delta f} = \frac{RGP_s}{(2q + 4R(G-1)n_{sp}hv)\Delta f} \approx \frac{P_s}{4n_{sp}hv\Delta f} \quad (3.26)$$

Therefore

$$F_n = \frac{SNR_{in}}{SNR_{out}} = 2n_{sp} \quad (3.27)$$

which indicates that for the usual case of  $G \gg 1$ , even with an ideal amplifier, when there is complete population inversion of erbium ions and  $n_{sp} = 1$ , the SNR of the amplified signal is degraded by 3dB at minimum.

Figure 3.7 showed the noise figure variation along the amplifier length, corresponding to ions populations variation due to simultaneous and spontaneous emission and ground state absorption.

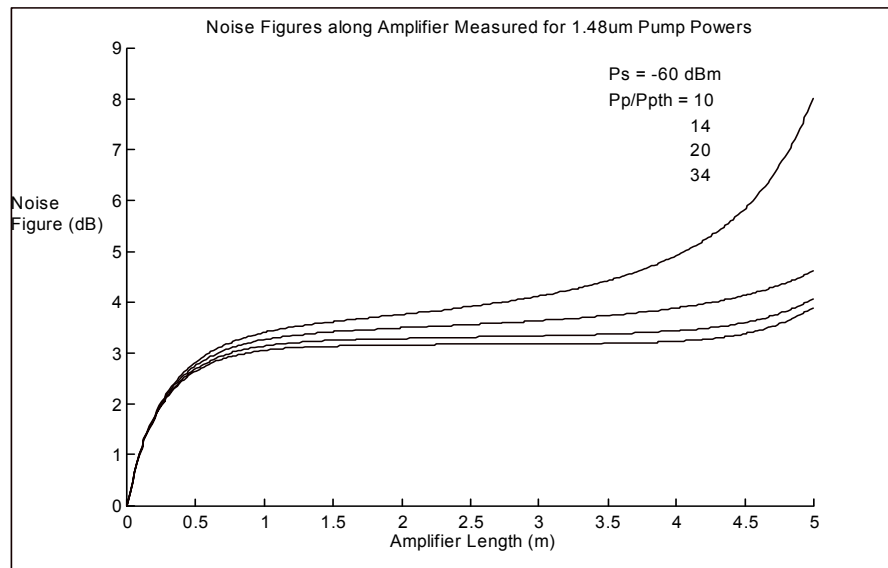


**Figure 3.7** Noise figure variation along amplifier length.

When the amplified signal is detected at the receiver with a photodiode, the incoming power will have to include the interaction of signal and ASE beating noise in the photodetection process, as mentioned above :

$$P_S(L) = GP_S(0) + \sqrt{F_N hv \Delta v_{ASE} G} + 2q^2 G^2 F_N P_S / hv \tag{3.28}$$

This will in turn require an excess power to be added to the detected signal for correct detection of the degraded or penalised signal, the so called power penalty, at the receiver for a given sensitivity.

#### 4.6 Multiplexer / Demultiplexer

Multiplexers for WDM systems have been primarily of two main types: wavelength dependent directional couplers and Mach-Zehnder interferometers. They can be easily fabricated with current silica technology and have high peak transmission. But their sinusoidal spectral response makes them to have low crosstalk suppression over a narrow wavelength region.

Waveguide array multiplexer has been the recently developed type and favoured due to its merits of low insertion loss, high crosstalk suppression, and polarisation independent response. The modelled device has a periodic spectral response with repeating transmission peaks, the spacing between which known as the free spectral range was 1600 GHz or 13 nm, within which the WDM channels could be accommodated. The spectral response about a pass wavelength has a Gaussian form, which is centred about a specific wavelength to filter out one single channel :

$$H_{Mux}(\delta f) = \exp \left\{ - \left( \frac{\Delta x \delta f}{\Delta f \omega_0} \right)^2 \right\} \tag{3.29}$$

where  $\delta f$  is the frequency shift from the centre frequency,  $\Delta x$  is spacing of the input/output waveguides,  $\Delta f$  the frequency channel spacing and  $\omega_0$  the spot size of the multiplexer.

The full-width-half-maximum of this Gaussian passband was calculated as about 30 GHz by

$$FWHM = \frac{2\sqrt{\ln 2}\omega_0\Delta f}{\Delta x} \quad (3.30)$$

which could filter channels as narrow as 1 nm and suppress adjacent channels by more than 30 dBm.

## 5 Signal Guided Propagation in Optical Fibre

Pulse propagation in optical fibre is simulated by applying the *split-step Fourier method* to numerically solve the nonlinear Schrodinger equation (NSE), which includes the effect of first order and second order GVD, self phase modulation (SPM) and cross phase modulation (XPM) due to fibre nonlinearity, and fibre attenuation,. This is a well established mathematical model and is extensively modelled fro all fibres in the transmission system, ie. for DSF and DCF.

A slow varying pulse envelope  $A(z,t)$  which can be the envelop of a summation of a number of optical channels of the WDM system, is found to propagate inside a nonlinear dispersive optical fibre in the following manner :

$$\frac{\partial A}{\partial z} + \frac{\alpha}{2} A + \frac{i}{2} \beta_2 \frac{\partial^2 A}{\partial T^2} - \frac{1}{6} \beta_3 \frac{\partial^3 A}{\partial T^3} = i\gamma_k \left( |A_k|^2 + \sum_{j=1, j \neq k}^N 2|A_j|^2 \right) A_k \quad (4.1)$$

where  $\alpha$  is the fibre loss,  $\beta_2$  and  $\beta_3$  are the second and third order GVD factors,  $\gamma$  is the nonlinearity parameter, and  $T = t - z/v_g$  is a frame of reference moving with the pulse at group velocity  $v_g$ . The first and second terms on the right hand side account for self phase modulation and cross phase modulation of the optical field with the  $N-1$  adjacent channels respectively.

### 5.1 Lightwaves Beam Propagation Method using Split Step Model

The instantaneous pulse envelope  $A(z, t)$  propagating inside the fibre is calculated by solving equation (4.1) numerically using the *split-step Fourier method*. Expressing equation (4.1) as

$$\frac{\partial A}{\partial z} = (\hat{D} + \hat{N})A \quad (4.2)$$

where  $\hat{D}$  is the dispersion differential operator and  $\hat{N}$  is the nonlinearity operator :

$$\hat{D} = -\frac{\alpha}{2} - \frac{i}{2} \beta_2 \frac{\partial^2}{\partial T^2} + \frac{1}{6} \beta_3 \frac{\partial^3}{\partial T^3} \quad (4.3)$$

$$\hat{N} = i\gamma_k \left( |A_k|^2 + \sum_{j=1, j \neq k}^N 2|A_j|^2 \right) \quad (4.4)$$

As this two operators appear to add by superposition, dispersive and nonlinear effects can be considered to act independently. That is, the two effects *split*. Next consider dividing the fibre length into small *steps* of length  $h$ . The exact solution of (4.1) describes the pulse envelope in segment  $z+h$  relative to its shape in the preceding segment  $z$ :

$$A(z+h, T) = \exp(h\hat{D}) \exp(h\hat{N}) A(z, T) \quad (4.5)$$

where the exponential operator  $\exp(h\hat{D})$  is evaluated in the Fourier domain :

$$\exp(h\hat{D})B(z, T) = \{F^{-1} \exp[h\hat{D}(i\omega)]F\} B(z, T) \quad (4.6)$$

by replacing the differential operator  $\partial/\partial T$  by  $i\omega$ . This equation is numerically solved using the *Finite-Fourier-Transform* (FFT) algorithm. To improve the accuracy of the split-step Fourier method, the pulse is made to propagate in the following manner :

$$A(z+h, T) = \exp\left(\frac{h}{2}\hat{D}\right) \exp\left(\int_z^{z+h} \hat{N}(z') dz'\right) \exp\left(\frac{h}{2}\hat{D}\right) A(z, T) \quad (4.8)$$

Intuitively, this equation says that a pulse emerges out of the preceding fibre segment and enters the current segment would propagate in a *purely dispersive* medium in the first half of the segment, then stops at middle of the segment and picks up *all* nonlinear effects in that segment, then set off to complete the remaining half of the *purely dispersive* segment. The pulse would then enter the subsequent segments and propagate in the same manner until it reaches the fibre end.

The self-phase-modulation SPM refers to the nonlinear phase shift in the optical wave caused by the optical field itself. Such effect is generally negligible at low power levels ( normally below 10 mW) but becomes significant when the peak intensity of the pulse is sufficiently high to cause appreciable change in the refractive index of silica fibre. This intensity induced index variation, referred to as the Kerr nonlinearity, produces a nonlinear phase shift in the carrier wave and leads to spectral broadening of the pulse. For WDM systems, the nonlinear effects are expected to further enhance with the phase shift for a channel depends not only on the power of that channel but also on the power in the adjacent channels, the so called cross phase modulation (XPM).

In general, dispersion and nonlinearity act together along the length of the fibre. The Split Step Method obtains an approximate solution by assuming that in propagating the optical field over a small distance  $h$ , the dispersive and nonlinear effects can be pretended to act independently. More

specifically, propagation from  $z$  to  $z+h$  is carried out in two steps as shown in Figure 4.1. The algorithm for this model is implemented in MATLAB.

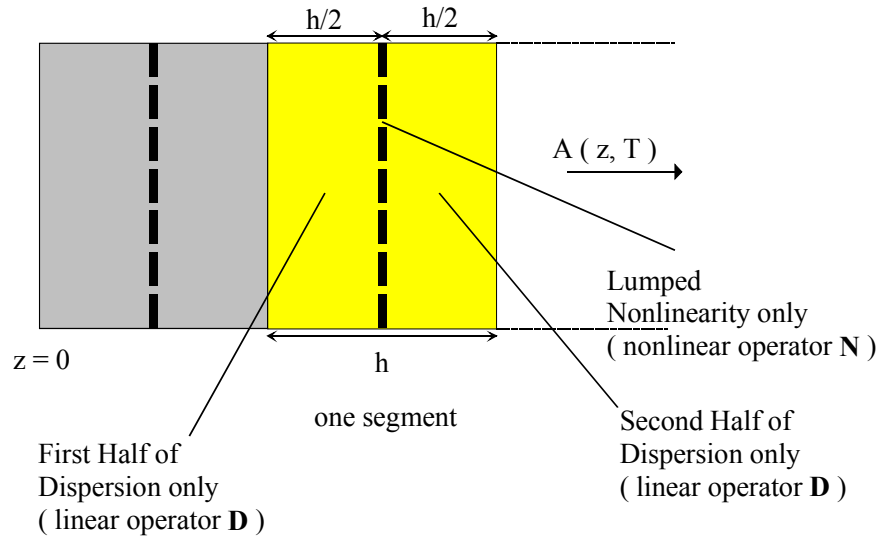


**Figure 4.1** Schematic illustration of symmetrised split step model used for numerical simulations.

## 5.2 Algorithm for the Split Step Model

This algorithm is developed to synthesise the Split Step Model using the numerical methods. Various aspects of accuracy of the simulation of solitons evolution have been closely examined and considered. The algorithm is developed in the MATLAB platform.

**Step 1** : This step corresponds to the first half dispersion only region shown in Figure 4.1. In this process, only the dispersion ( the linear operator part ) acts alone and  $N = 0$ . Thus, we have

$$A_{D1}\left(z + \frac{h}{2}, T\right) = F^{-1} \left\{ \exp\left(\frac{h}{2} \tilde{D}(j\omega)\right) \cdot F\{A_o(0, T)\} \right\} \quad (4.9)$$

where  $F$  is the Fast Fourier Transform and  $A_o(0, T)$  is the optical multiplexed signals of the optical channels of different carriers or that of a siggle channel or it can be that of a fundamental soliton given by

$$A_o(0, T) = \text{sech}(\tau) \exp\left(\frac{j\xi}{2}\right) \quad (4.10)$$

where  $\tau$  and  $\xi$  are the normalised time and distance. The WDM signals is in fact a summation of all the electric fields representing the optical intensity channels propagated along the optical fibre transmission line. The linear operator  $D(j\omega)$  is obtained by replacing

the differential operator by  $j\omega$  where  $\omega$  is the Fourier frequency. Thus, the equation is given by

$$\tilde{D}(j\omega) = \frac{j}{2}\beta_2\omega^2 - \frac{j}{6}\beta_3\omega^3 - \frac{\alpha}{2} \quad (4.11)$$

**Step 2** : The Split Step Model can be expressed in the following expression :

$$A(z+h, T) = \exp\left(\frac{h}{2}\tilde{D}\right) \exp\left(\int_z^{z+h} \tilde{N}(z')dz'\right) \exp\left(\frac{h}{2}\tilde{D}\right) A(z, T) \quad (4.12)$$

where the integral has to be evaluated more accurately by employing the trapezoidal rule and the approximated integral is given by

$$\int_z^{z+h} \tilde{N}(z')dz' \approx \frac{h}{2} \{ \tilde{N}(z) + \tilde{N}(z+h) \} \quad (4.13)$$

However, the implementation of (4.13) is not simple since  $N(z+h)$  is unknown at the mid-segment located at  $z+h/2$  (Figure 4.1 ). It is necessary to follow an iterative procedure that is initiated by replacing  $N(z+h)$  by  $N(z)$ . Equation (4.12) is then used to estimate  $A(z+h, T)$  which in turn to calculate the new value of  $N(z+h)$  from eqn.(4.8). Thus, the overall algorithm of *Step 2* can be expressed in the following steps :

$$A_{D1}\left(z + \frac{h}{2}, T\right) = F^{-1} \left\{ \exp\left(\frac{h}{2}\tilde{D}(j\omega)\right) \cdot F\{A(z, T)\} \right\} \quad (4.14)$$

$$A_{N1}\left(z + \frac{h}{2}, T\right) = \exp\left(\frac{h}{2}\{ \tilde{N}(z) + \tilde{N}(z+h) \}\right) A_{D1}\left(z + \frac{h}{2}, T\right) \quad (4.15)$$

$$A_{D1+N1}\left(z + \frac{h}{2}, T\right) = F^{-1} \left\{ \exp\left(\frac{h}{2}\tilde{D}(j\omega)\right) \cdot F\left\{ A_{N1}\left(z + \frac{h}{2}, T\right) \right\} \right\} \quad (4.16)$$

Hence, the predicted  $N(z+h)$  is found to be :

$$\tilde{N}(z+h) = j\gamma \left\{ \left| A_{D1+N1}\left(z + \frac{h}{2}, T\right) \right|^2 \right\} \quad (4.17)$$

The predicted  $N(z+h)$  will be substituted into (4.15) in order to get a more accurate prediction of (4.17). Thus, this process is done iteratively.

**Step 3** : The predicted  $N(z+h)$  would then be used to calculate the lumped region which is shown in Figure 4.1. In this process, only the nonlinear (nonlinear operator part) acts alone and  $D = 0$ .

$$A_{N2}\left(z + \frac{h}{2}, T\right) = \exp\left(\frac{h}{2}\{\tilde{N}(z) + \tilde{N}(z+h)\}\right)A_{D1}\left(z + \frac{h}{2}, T\right) \quad (4.18)$$

**Step 4** : This step corresponds to the second half dispersion only region shown in Figure 4.1. In this process, only the dispersion ( linear operator part ) acts alone and  $N = 0$ . Thus, we have

$$A(z+h, T) = F^{-1}\left\{\exp\left(\frac{h}{2}\tilde{D}(j\omega)\right) \cdot F\left\{A_{N2}\left(z + \frac{h}{2}, T\right)\right\}\right\} \quad (4.19)$$

**Step 5** : Repeat *Step 1* by substituting  $A(z+h, T)$  from equation (4.19) into  $Ao(0, T)$  of (4.9) for further propagation into the next segment defined in Figure 4.1.

### 5.3 Representation of The Optical Signal

NRZ signal is considered with modulating current pulse shape in the form

$$I_p(t) = \begin{cases} I_{\max}(1 - \exp(-t / t_{rise})^2), bit1 \\ I_{\max} \exp(-t / t_{rise})^2, bit0 \end{cases} \quad (4.20)$$

The modulation current is given by

$$I_m(t) = I_{bias} + I_p(t) \exp(j\omega_m t) \quad (4.21)$$

where  $\omega_m$  is the modulation frequency. The optical field of the modulated signal is computed for transmission in the fibre :

$$E(t) = \sqrt{P_S(t)} \exp(j(\omega_c t + \phi)) \quad (4.22)$$

where  $P_S$  is the optical power for the modulated signal at the laser output,  $\omega_C$  is the carrier frequency and  $\phi$  is the phase produced by the intensity induced index change in the semiconductor laser.

In general, the number of sampling points required to represent a signal increases with low bit rate, that is when the modulation frequency is far away from the optical carrier frequency. The Nyquist sampling rate needed to be higher than or equal to twice the highest frequency in the signal, which is the highest carrier frequency, in order to reproduce a faithful representation of the sequence.

The number of samples is accordingly

$$N = \frac{TotalTime}{SamplingTime} = TotalTime \times SamplingFrequency$$

where N is rounded to the nearest power of 2. The number of sampling points needed was reduced with the carrier frequency shifted by an offset of 192 THz . The total bandwidth required for the 1540-1560 nm region is 8000 GHz . For a 20 Gb/s external modulated WDM signals, the number

of points required within the time window is 4096 to fully resolve the signal in the frequency spectrum.

## 6 Simulation of dispersion compensated WDM optical fibre transmission

These include signal propagation in conventional standard fibre (SMF) of 17 ps/nm-km dispersion at 1550 nm, dispersion-shifted fibre (DSF), and dispersion compensating fibre (DCF). Optimum placement of the DCF along the whole transmission link will be considered, which include pre-compensation, post-compensation, and evenly split pre- and post- compensation. In line amplifiers may be needed after each fibre, especially for DCF with high loss.

Performance is evaluated using eye diagram, calculating signal-to-noise ratio and power penalty at the receiver.

### 6.1 Transmission System configuration

Four optical channels in the 1550 nm region are multiplexed for transmission over a long length of fibre as shown in Figure 5.1. The lightwaves channels are externally modulated at 10 Gbits/sec and multiplexed before propagating through the single mode optical fibres of standard dispersion factor around 17 ps/km.nm. Optical amplifiers are inserted as required when the optical power levels are low with respect to the detection levels of a low noise wideband optical receiver. After transmission through the single mode optical fibres the lightwaves are optically amplified through an optical amplification module where the optical gain is adjusted according to the amplification level required. In this sense the optical amplifier noise can be optimised as the noises can be minimised and the operation level can be adjusted in the linear region.

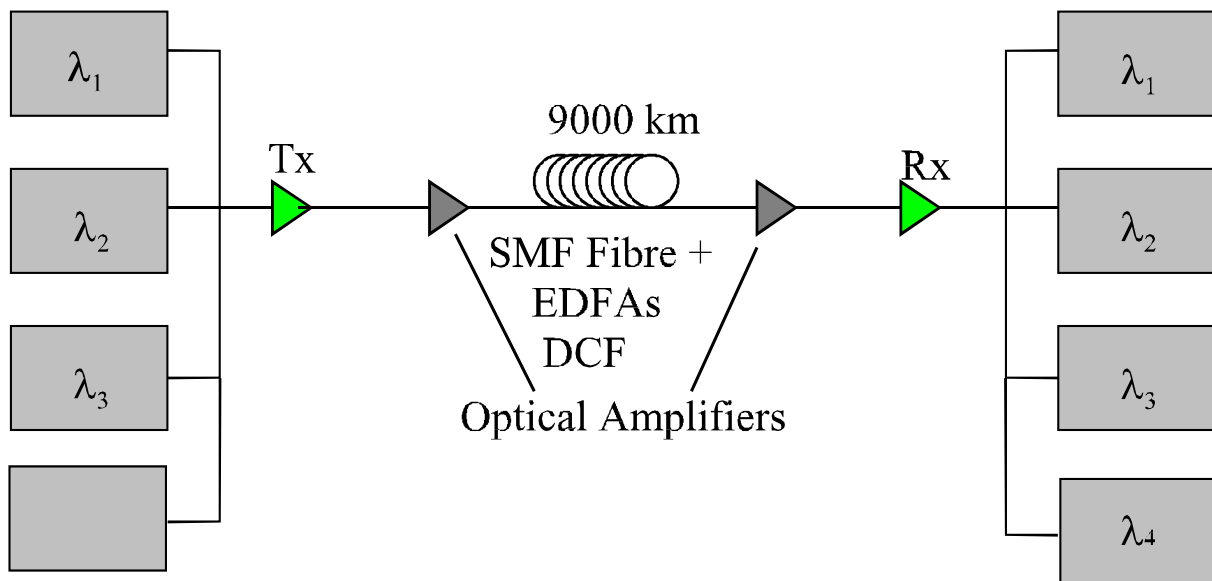
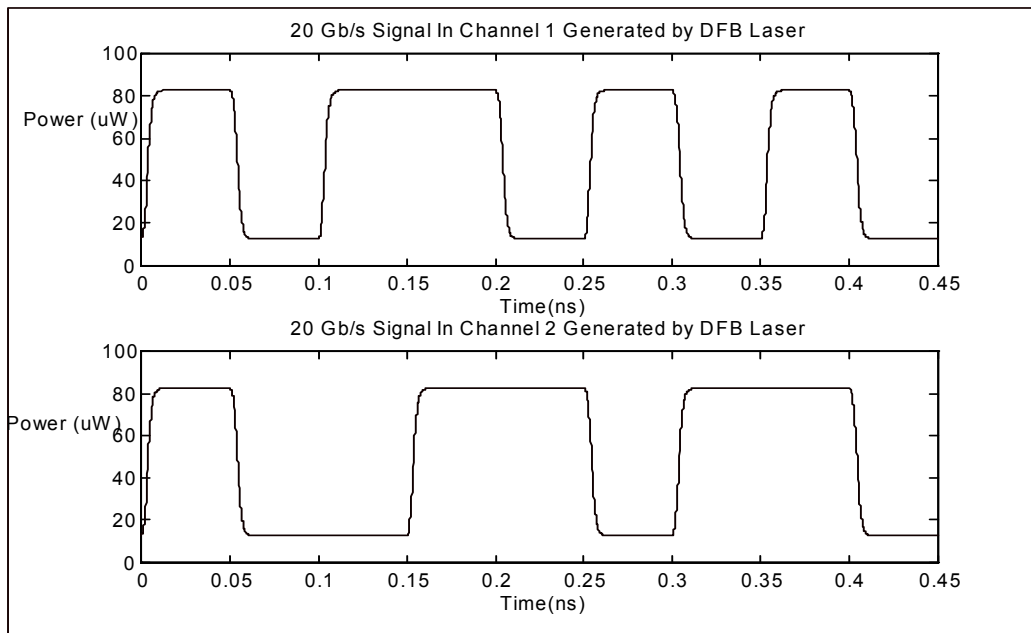


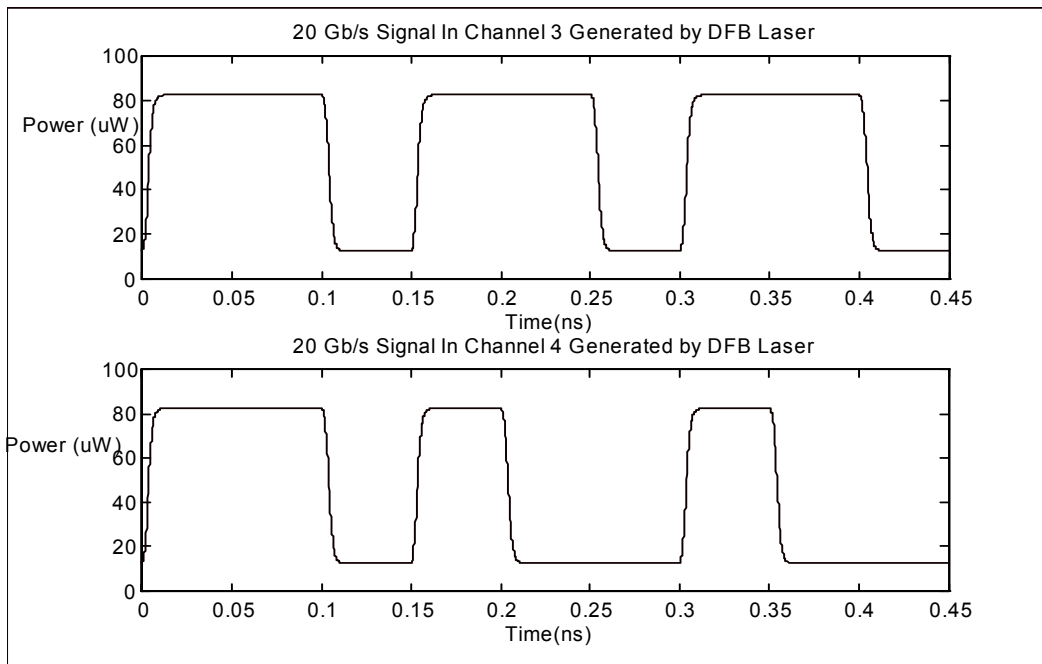
**Figure 5.1** Schematic representation of a long-haul high speed optical communication system with SMF and DCF for compensation

## 6.2 Multiplexed Channel generation

The lasers used in the case studies are DFB lasers which are CW generated and externally modulated using LiNbO<sub>3</sub> optical modulators. The external modulators can operate up to 75 GHz. The multiplexed signals are shown in Figure 5.2 with different digital sequences for channel identification during the modelling. The channels are then optically amplified before transmission through the optical fibres as shown in Figure 5.3. Noises contributed by the optical amplifiers are considered to very small as observed. The multiplexed optical spectrum of the lightwaves propagating in parallel is shown in Figure 5.4. This shows clearly the separation of the optical channels. At this point the lightwaves can be demultiplexed to received the frequency characteristics if required or checking the validity of the optical filtering module. An eye diagram analysis can be conducted by activating the eye diagram propagation, that is to activate all combination of an optical pulse sequence. This would take more computing time as the length of the digital sequence is large. An exemplar of the eye diagram is shown in Figure 5.5 where the eye is completely open at the optical transmitter or a back-to-back detection is achieved in our modelling system. Further the ASE spectrum of the optical amplifier is shown in Figure 5.6 as expected with the spontaneous and amplified stimulated emission characteristics over the gain spectrum of the erbium ion.



(a) and (b)



(c) and (d)

**FIGURE 5.2 (a) -(d):** Four wavelength channels generated at  $\lambda_{1-4}$ : 1550, 1552, 1554, 1548 nm using DFB laser electric fields generated by the rate equations and externally modulated at 20 Gbits/sec.

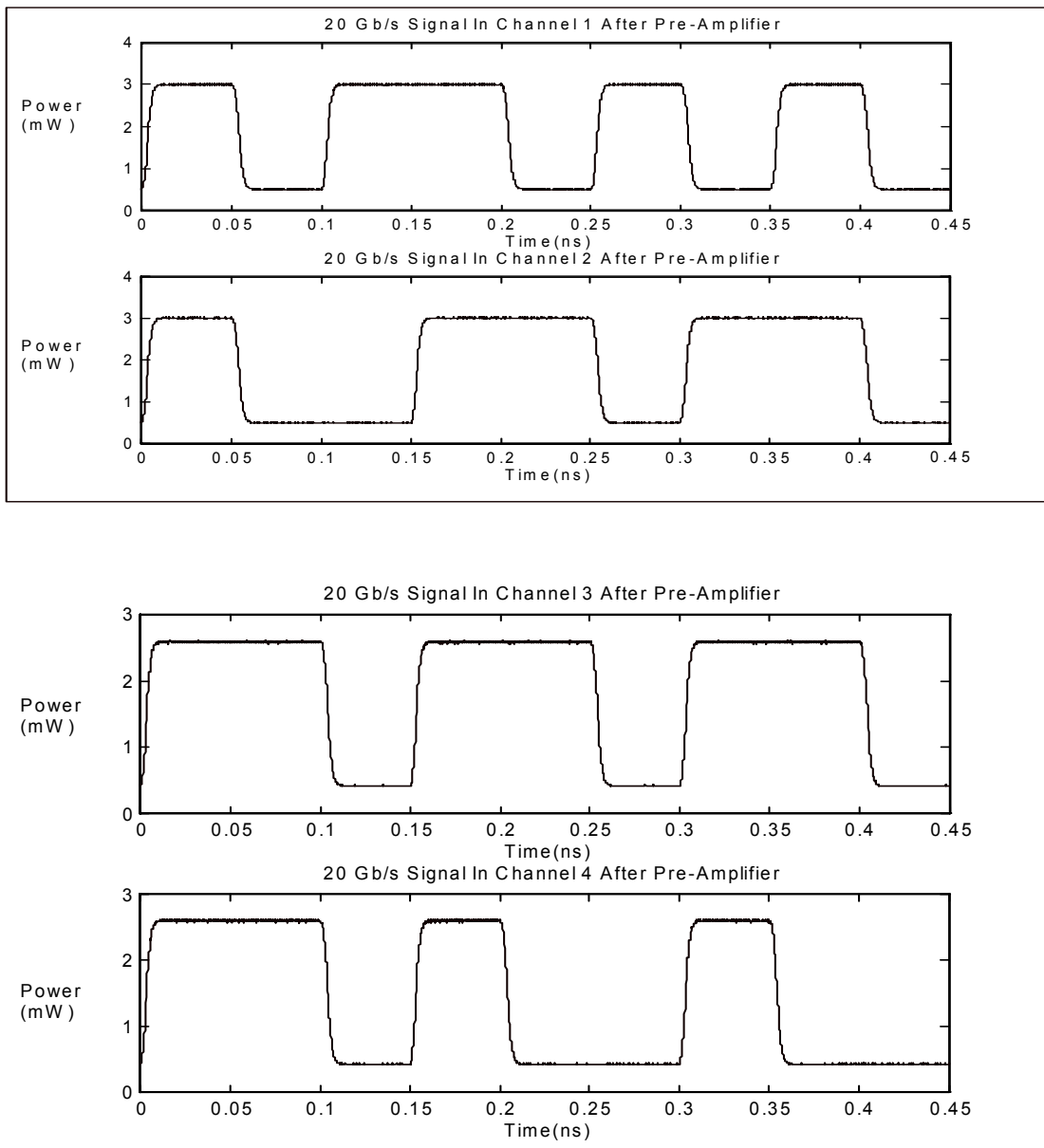


**FIGURE 5.3 (a)-(d):** Optically pre-amplified WDM Channels at transmitters and after the multiplexer. Note unequal amplifier gain : 15.66, 15.68, 15.03, 15.06 dB, with 0.65 dB ripple for WDM channels  $\lambda_{1-4}$  respectively.

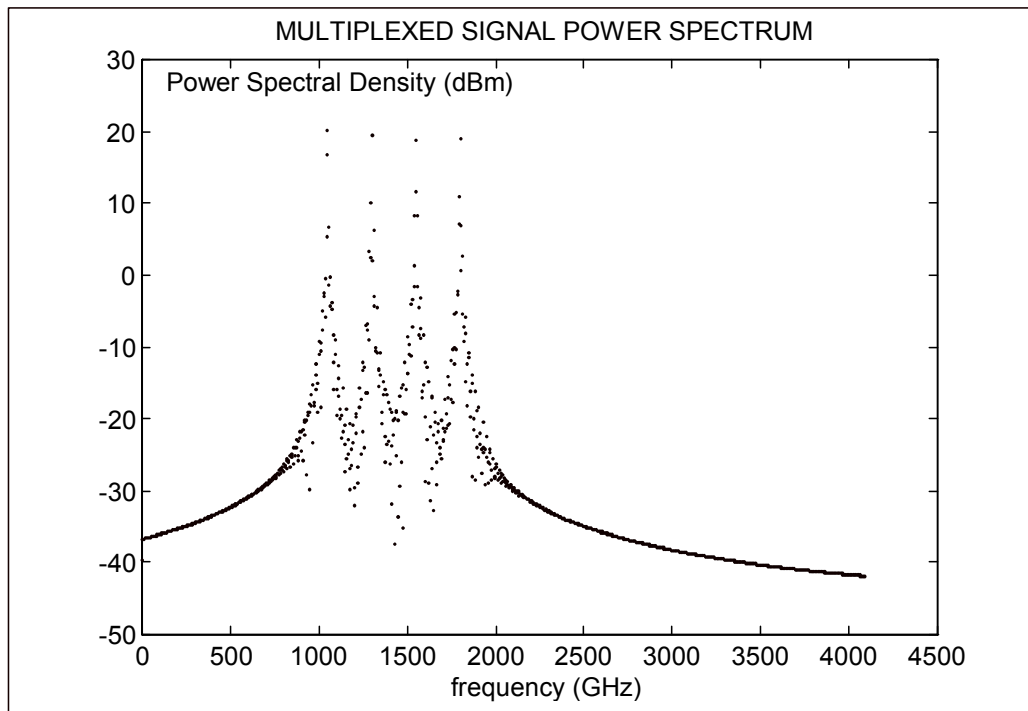


**FIGURE 5.4** Optical spectrum of the multiplexed WDM channels and ASE spectra at the output of the EDFA. The optical frequency is shifted by 192 THz.

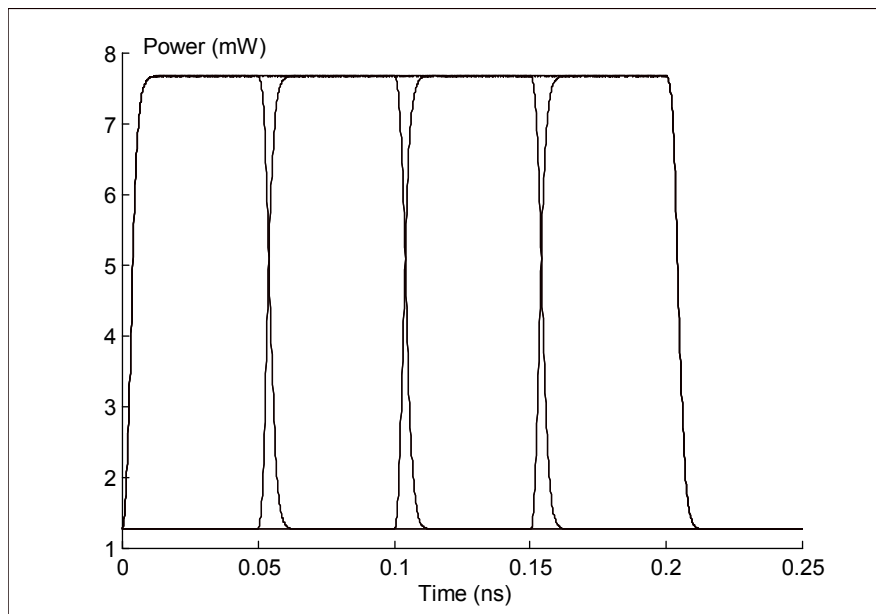


**Figure 5.5 :** Eye diagram at the output of the EDFA cascaded at the output of the external modulator - Channel 1 at  $\lambda_1 = 1550$  nm

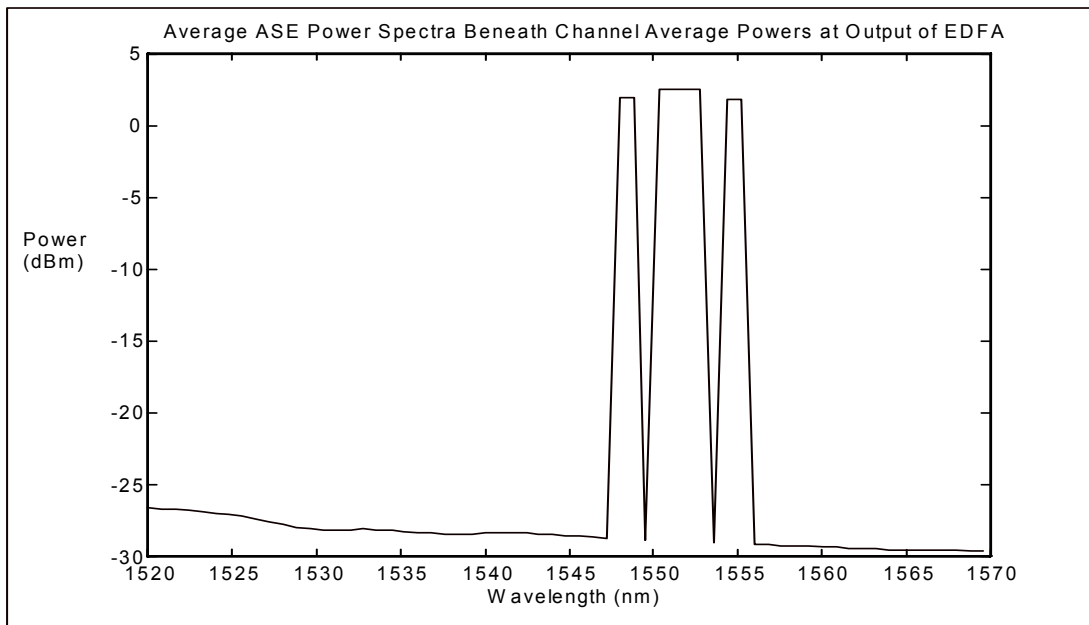


**Figure 5.6** Average ASE power spectra beneath the channel average power at the output of the EDFA.

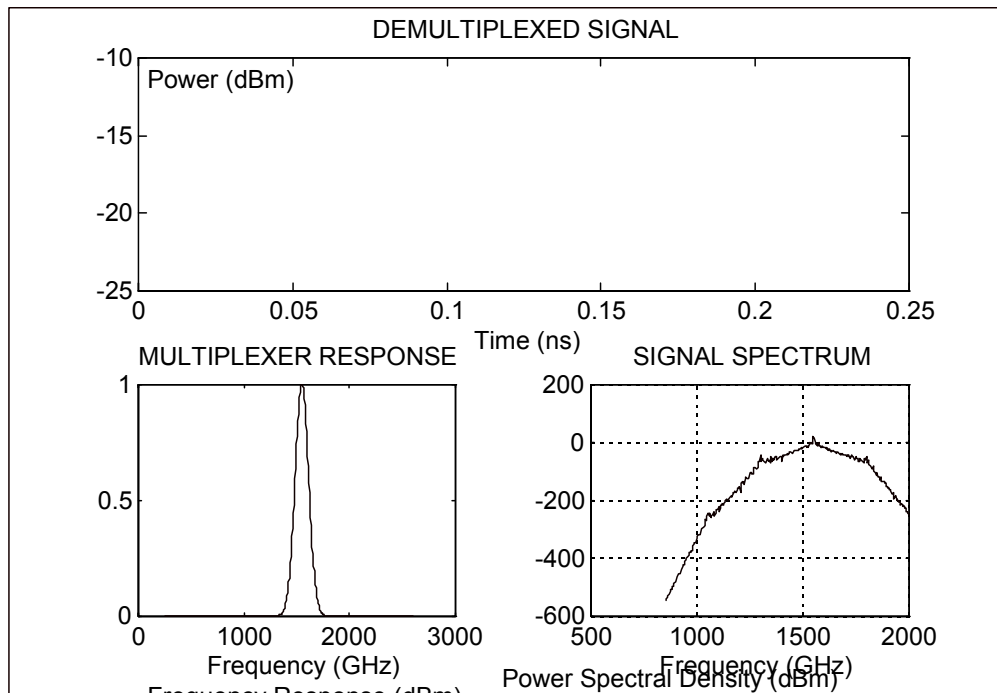


**Figure 5.7** Demultiplexed signals monitored at a section of the transmission channel

### 6.3 WDM transmission through standard optical fibres

The multiplexed signals of the optical channels are then propagated through a standard optical single mode fibre with a total dispersion factor of 17 ps/nm.km in order to shown the broadening effect on the optical pulses as shown in Figure 5.8(a)-(d). Clearly the pulses have been extremely distorted.

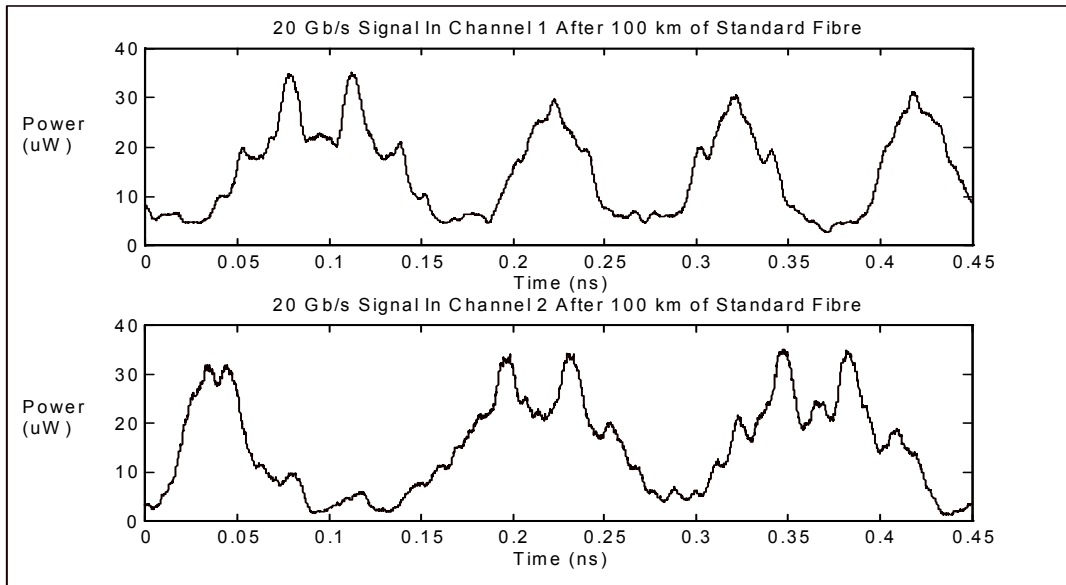


Figure 5.8 (a)-(b)

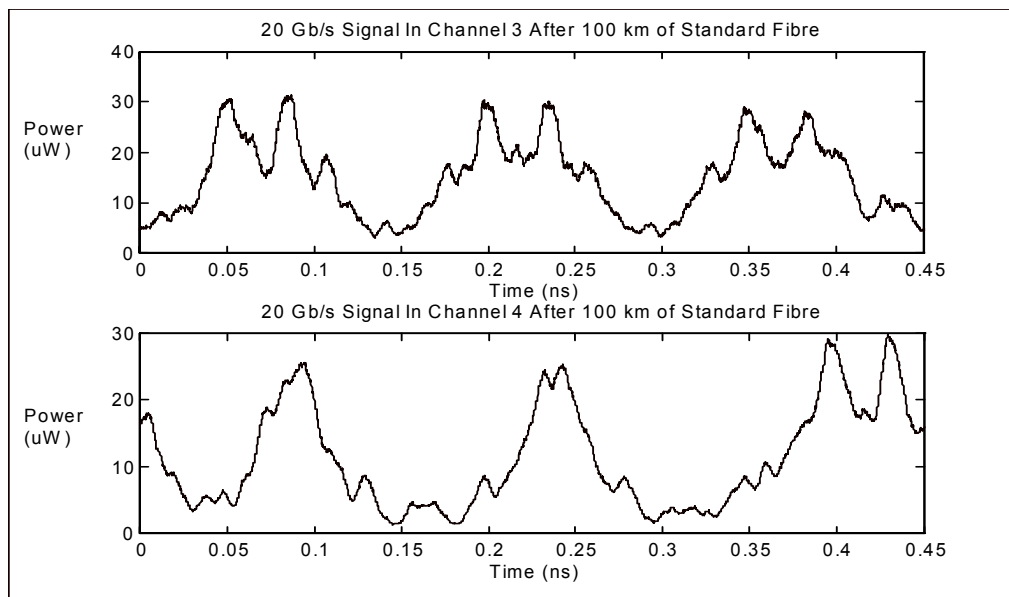


Figure 5.8(c)-(d)

**FIGURE 5.8 (a)-(d)** Dispersed WDM channels after 100 Km transmission through normal standard optical fibre. Total fibre average transmission Loss = 19.46 dB

### 6.4 Compensation of dispersed channels

The distorted optical pulse channels are then passed through a dispersion compensated fibre of a length such that the total dispersion can balance that of the single mode optical fibre. The dispersion characteristics of the DCF is shown in Figure 5.9. A total dispersion factor of about -100 ps/km can be achieved over the wavelength windows of the channels.

After transmission through the DCF the pulse sequences have been recovered as shown in Figure 5.10 (a)-(d). We observed a shift in the pulse positions. This is due to the circulating characteristics of the FFT and IFFT of MATLAB. Some ringing of the pulses can also be observed due to the amplification noises of the amplifiers.

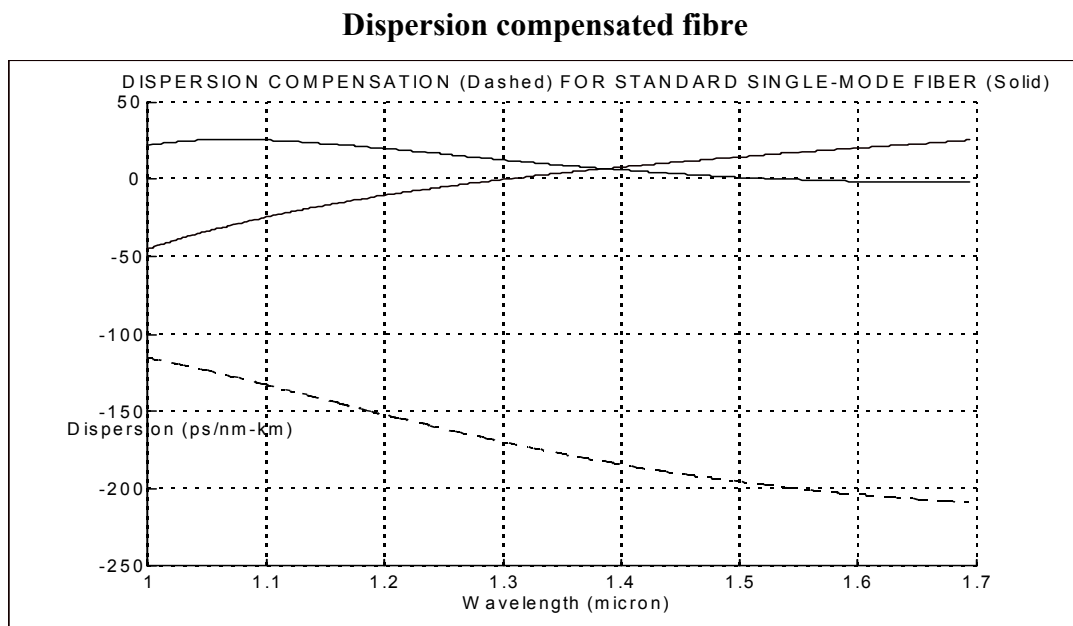


**Figure 5.9** Dispersion characteristics of the DCF - designed and optimised for maximum radius and spotsizes. Material and waveguide (dotted curve) dispersion factor are included.

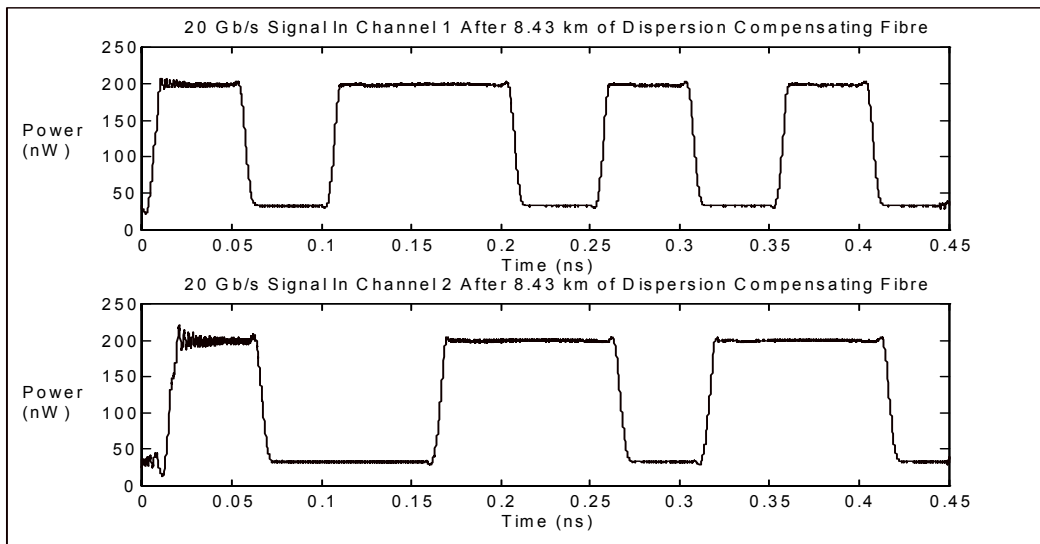


Figure 5.10(a)-(b)

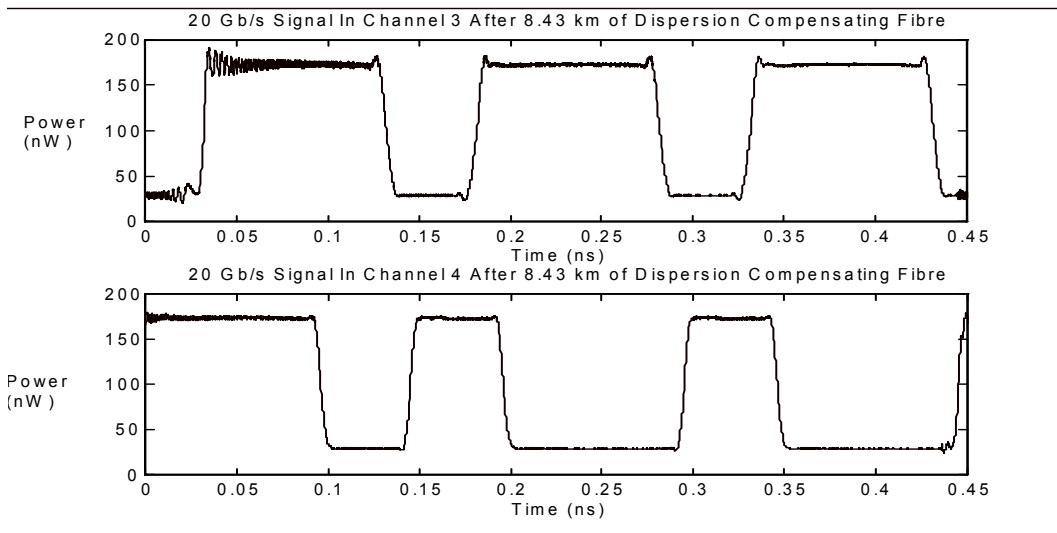


Figure 5.10(c)-(d)

Total fibre loss = 6.63 dB

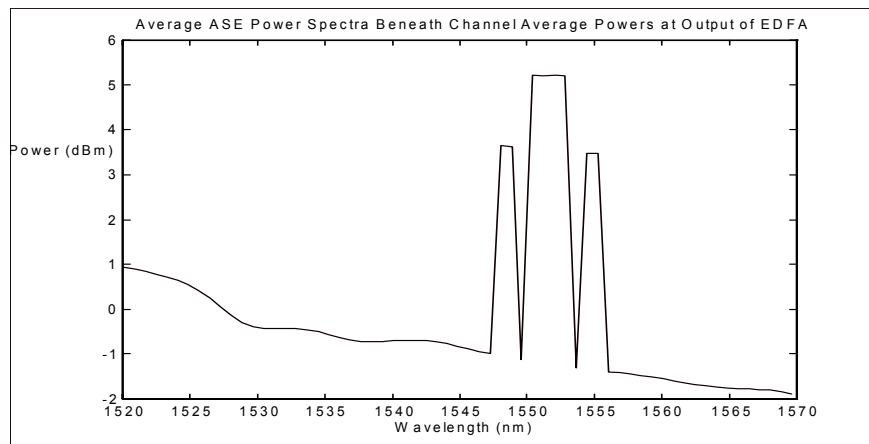
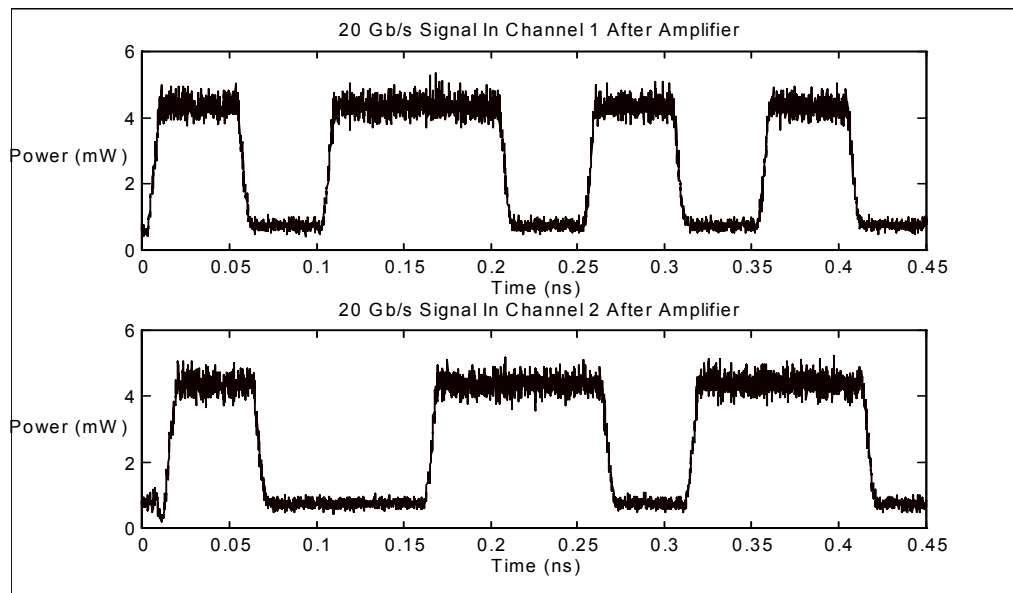


Figure 5.10(e)

**FIGURE 5.10:** WDM channels compensated through CDF fibre.; (a)-(d) Compensated WDM channels after DCF transmission; (e) Optical spectrum of the ASE of the EDFA for WDM channels after transmission through DCF.

### 6.5 Optical amplification of WDM channels

The ASE noise contribution to the optical pulse sequence contribute to the total pulse intensity as shown in Figure 5.11. This noise contribution are considered to be significant when the optical channels propagate progressively through the optical fibre channel. These high frequency noises can also be reduced through a natural filtering effect when the pulses transmitting through the optical fibres. The pulses however are distorted as shown in Figure 5.12 and recovered in near its original form in Figure 5.13. An example of eye diagram analysis can be seen in the next section showing the effectiveness of the modelling platform for WDM optical communications systems.



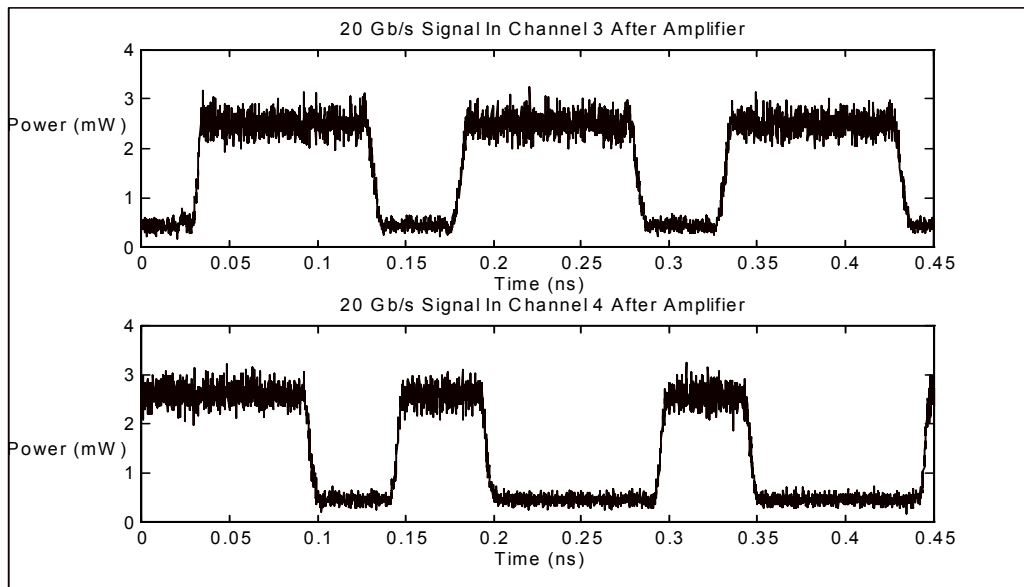
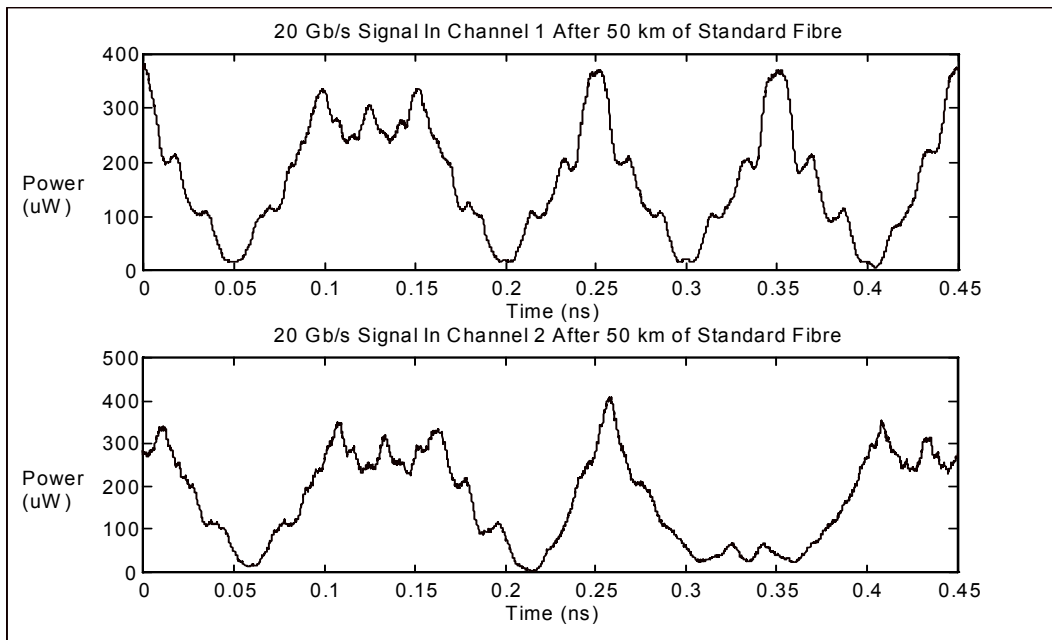
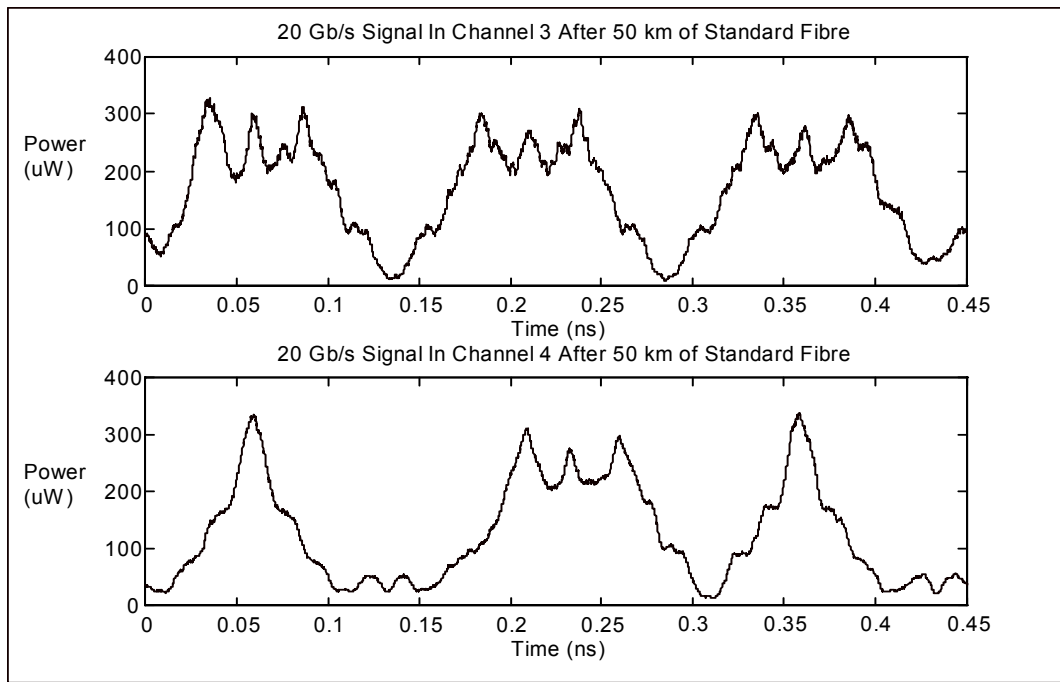


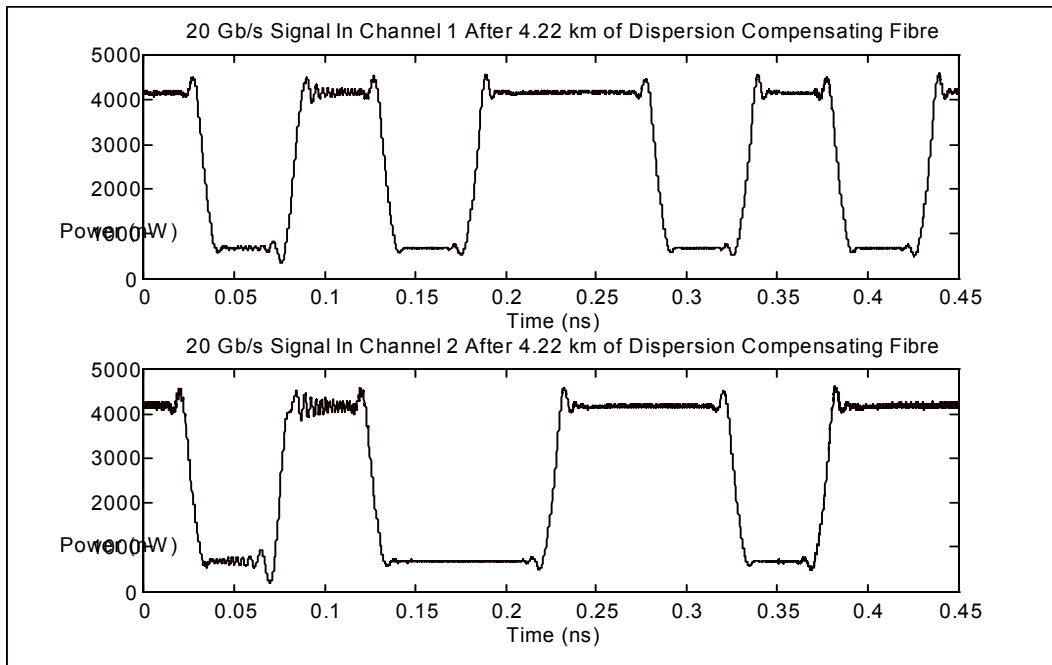
FIGURE 5.11 : WDM channels after the first remote EDFAs for channels 1-4 respectively

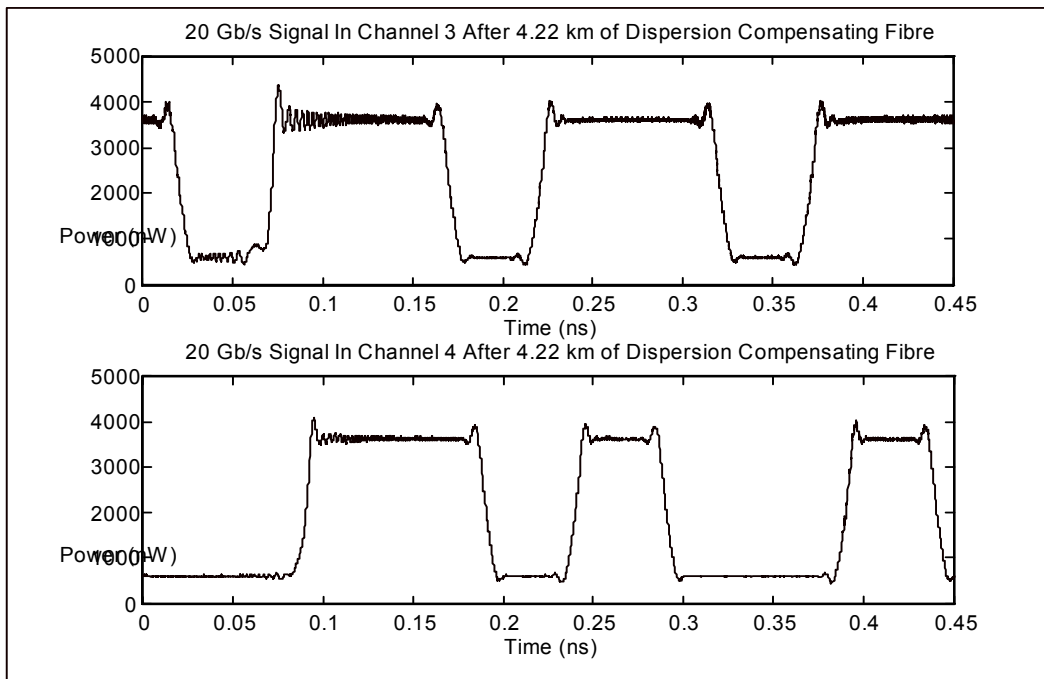
### 6.6 Further transmission and compensation of WDM channels



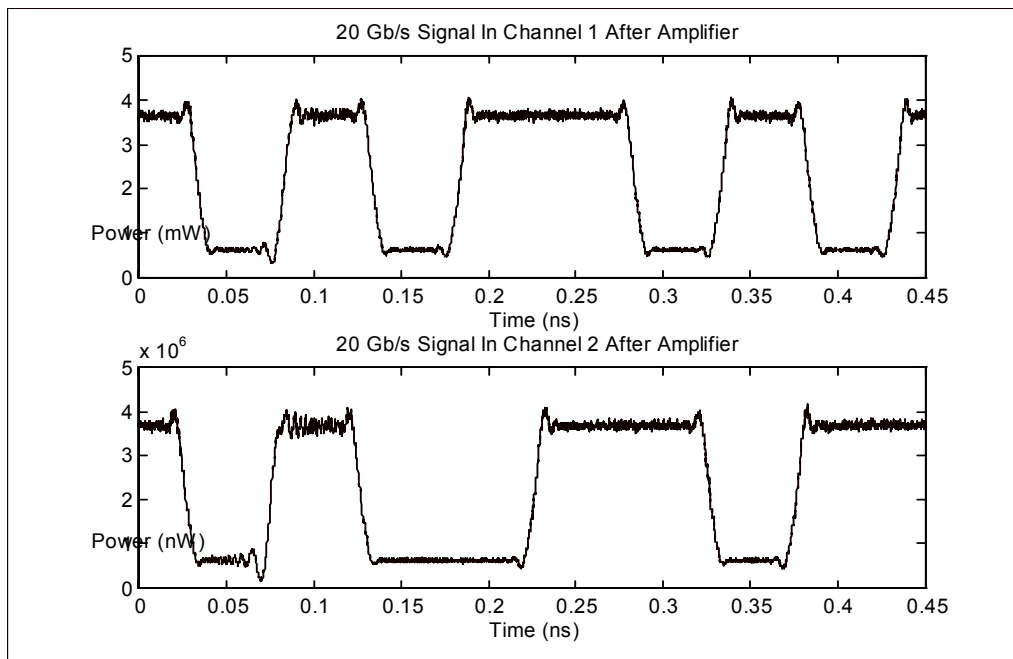


**FIGURE 5.12** : Continuation of optical transmission after the optical amplifiers of four WDM channels. Optical channel average loss = 9.571 dB





**FIGURE 5.13:** WDM channels compensated by DCF . Optical channel loss = 3.14 dB



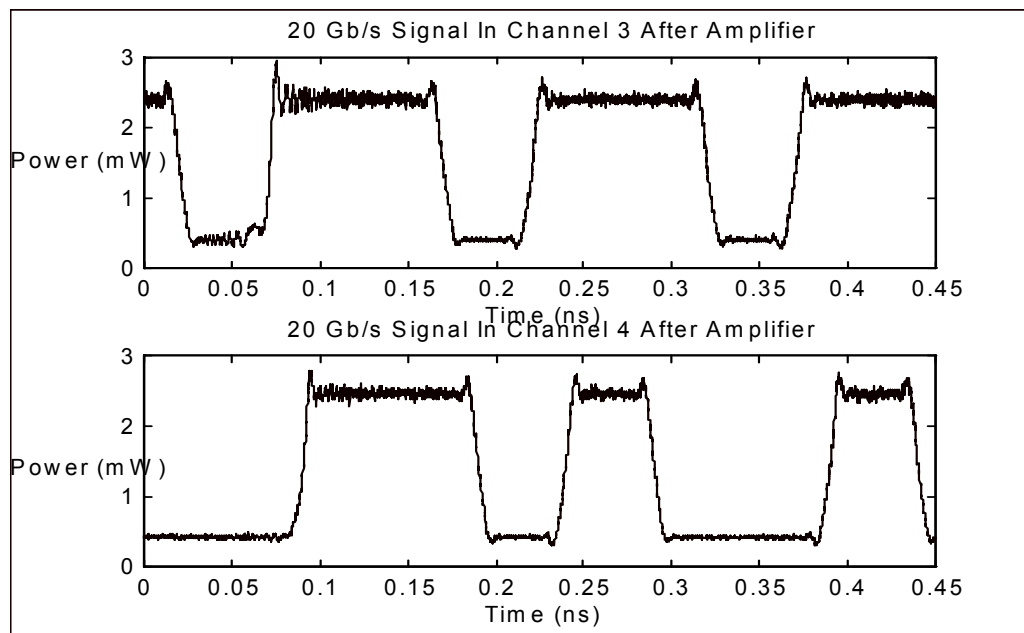


**Figure 5.14** Optically amplified WDM channels after transmitting through DCF.

## 6.7 Multi-channel eye diagram simulation

Four optical channels with the wavelength distributed at 1550 -1553 nm with a 1 nm spacing are multiplexed and transmitted over single mode optical fibres and compensated with dispersion compensated fibre of much shorter length and a dispersion factor of about -100 ps/km.nm. This system configuration is shown in Figure 5.15(a). Figure 5.15 (b) shows the output eye diagram of the transmission length of 50 km before compensated by a dispersion compensated fibre. The optical pulse sequence can be clearly recovered without minimum noise contribution is shown in Figure 5.15(c).

Special Laser Sources + external modulators

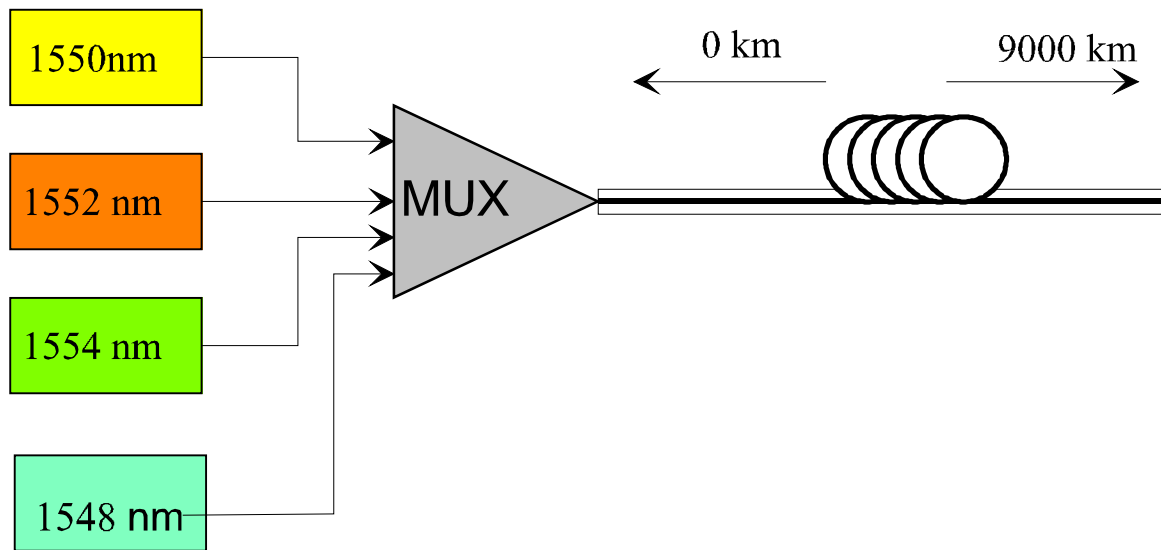


**Figure 5.15(a)** Optical transmitter structures for three wavelength multiplexed optical fibre communications systems.

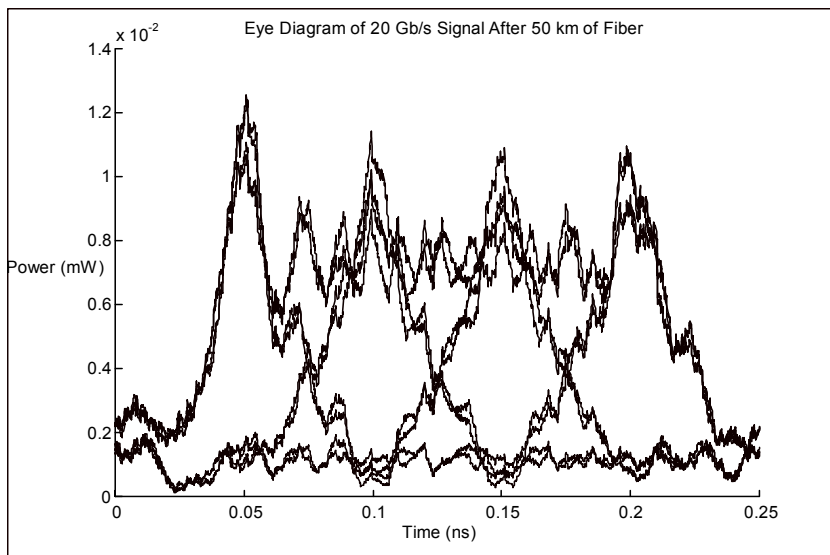


**Figure 5.15(b)** Eye diagram of WDM after transmission through 50 Km of standard optical fibres at +17 ps/(nm.km)

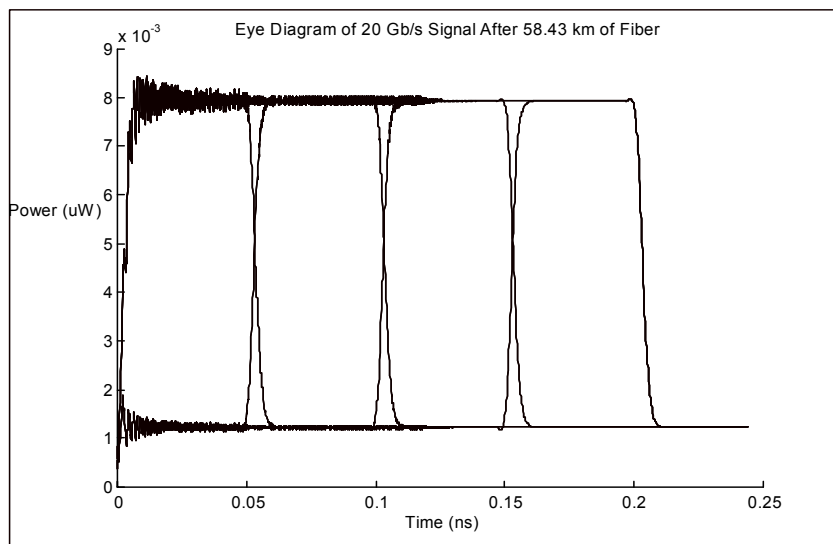


**Figure 5.15(c)** Compensated eye diagram of WDM channels after DCF transmission of 8.43 km at -100 ps/nm/km.

## 7 Conclusion

Fundamental and advanced optical components for WDM dispersion managed optical fibre transmission systems have been comprehensively modelled. Integration of these modular optical sections is demonstrated confirming the validity and accuracy of the modelling utility.

The optical transmitters including laser sources that can be direct or externally modulated. Comprehensive solutions of the rate equations for semiconductor lasers have been solved numerically demonstrating the practicality of the modelling platform. Effects of laser parameters on the output optical pulses are studied and classified for design of laser under pulse operations.

These optically modulated pulse sequences are then propagated through the optical fibres using the nonlinear beam propagation. The cross-phase (XPM) and self-phase (SPM) modulation effects due to several different optical frequency carriers are also included for accurate modelling of the optical transmission systems. Eye diagrams have been used extensively to simulate WDM optical communications systems.

Other enhancing devices such as gain equaliser, in line band-pass filters can be easily added to the package would they become essential. This paper presents a modelling implementation employing simultaneous propagation of several channels in a fibre and monitoring dispersion compensation in each of the channels, multi-channel amplification across the gain spectrum of the EDFA and simulation of a number of different compensation schemes are developed.

The generation of optical carriers under the CW operation of a semiconductor lasers coupled with external modulation technique and /or internal modulation of the injection of current in the laser cavity are described.

Simulation results are given demonstrating the effectiveness of the modelling facility. Further development is needed for the inclusion of the PMD for ultralong and ultra-high speed optical communications is essential.

## 8 REFERENCE

- [1] E. Bowers and M. A. Pollack (1988) 'Semiconductor lasers for telecommunications', in S. E. Miller and I. P. Kaminow (Eds.), *Optical Fiber Telecommunications II*, Academic Press, pp. 509-568.
- [2] M. Senior (1992) *Optical Fiber Communications : principles and practice (2nd edn)*, Prentice Hall.
- [3] G.P. Agrawal, (1992) *Fibre Optic Communication Systems*, Wiley.
- [4] B. Jnr. Jones, (1988) *Introduction to Optical Fibre Communications*, New York : Holt, Rinehart and Winston.
- [5] J. Lowery, (1994) 'Spectral and Dynamic Behaviour of Semiconductor Lasers', in Tut. F , *19th Australian Conference on Optical Fibre Technology ( ACOFT'94 )*.
- [6] A. Atlas, B. de Lary, A. Rosiewicz, R. Panock, (1994) '20 GHz Bandwidth High Dynamic Range 1.3um Buried Heterostructure Laser Modules', *J. Optical Comm.*, pp. 231-237.
- [7] A. Linke, (1985) 'Modulation induced transient chirping in single frequency lasers', *IEEE J. Quant. Elect.*, pp. 593-597.
- [8] Bickers and L.P. Westbrook, (1985) 'Reduction in laser chirp in 1.5um DFB lasers by modulation pulse shaping', *Elect. Lett.*, pp. 103-104.
- [9] Koyama, (1988) 'Frequency chirping in external modulators', *IEEE J. Lightwave Tech.*, pp. 87-93.
- [10] P. Agrawal and N. K. Dutta, (1986) *Long-wavelength semiconductor lasers*, Van Nostrand Reinhold.
- [11] C. Cartledge and A. F. Elrefaie, (1991) 'Effect of chirping-induced waveform distortion on the performance of direct detection receivers using traveling-wave semiconductor optical preamplifiers', *IEEE J. Lightwave Tech.*, pp.209 - 219.
- [12] Rai X. and Xu G., (1994) 'SPICE model for the intrinsic noise of laser diodes', *J. Optical Comm.*, pp. 135-137.

- [13] Meland et al., (1990) 'Extremely high-frequency (24 GHz) InGaAsP diode lasers with excellent modulation efficiency', *Electronics Letters*, pp. 1827 - 1829.
- [14] Lipsanen et al.(1992) 'High-speed InGaAsP/InP multiple quantum well lasers', *Photonics Technology Letters*, pp. 673 - 675.
- [15] Morton et al.,(1992) '25 GHz bandwidth 1.55  $\mu\text{m}$  GaInAsP p-doped strained multi-quantum well lasers', *Electronics Letters*, pp. 2156 - 2157.
- [16] Z. Tsang and Z. L. Liao, (1987) 'Sinusoidal and digital high-speed modulation of p-type substrate mass-transport diode lasers', *IEEE J. Lightwave Tech.*, pp. 300 - 304.
- [17] Huang et al., (1992) 'High-speed, low threshold InGaAsP semi-insulating buried crescent lasers with 22 GHz bandwidth', *IEEE Photonics Technology Letters*, pp. 293 - 295.
- [18] Iga, (1994) *Fundamentals of Laser Optics*, Plenum.
- [19] Hagimoto, N. Ohta and K. Nakagawa, (1982) '4 Gb/s direct modulation of 1.3  $\mu\text{m}$  InGaAsP/InP semiconductor lasers', *Electronics Letters*, pp. 796 - 797.
- [20] R.S. Tucker and I. P. Kaminow, (1984) 'High-frequency characteristics of directly modulated InGaAsP Ridge Waveguide and Buried Heterostructure lasers', *IEEE J. Lightwave Tech.*, pp. 385 - 393.
- [21] Miller et al., (1973) 'Part II : Devices and system consideration', *Proc. IEEE*, pp. 1726 - 1751.
- [22] F. Elrefaie et al., (1988) 'Computer Simulation of Digital Lightwave Links', *IEEE J. Selected Areas Comm.*, pp. 94 - 105.
- [23] S. Kapany, (1967) *Fiber optics: Principle and Applications*, Academic Press.
- [24] C. Kao et al., (1966) *Proceedings of IEE*, p1151.
- [25] P. Kapron, (1970) *Applied Physics Letter*, p423.
- [26] Miya et al., *Electronics Letter*, p106, 1979.
- [27] L. N. Binh, (1990) 'Optical Fibre Communications', *Depat. Elect. Comp. Syst. Eng., Monash University, Clayton Campus, Lecture Notes*.
- [28] H. Malitson, (1965) 'Interspecimen Comparison of the Refractive Index of Fused Silica', *J. Optical Soc. Am.*, pp. 1205-1209.
- [29] J. Adams, (1981) *An Introduction to Optical Waveguides*, Wiley.
- [30] D. Gloge et al., (1980) *Electronics Letter*, p. 366.
- [31] L. Koch et al., (1988) 'High Performance Tunable 1.5  $\mu\text{m}$  InGaAs/InGaAsP Multiple Quantum-well Distributed-Bragg-Reflector Lasers', *1988 IEEE 11th Int. Semiconductor Laser Conf.*, pp. 120-121.

- [32] LaCourse et al., (1988) 'Observation of Strong Carrier Density Increase Above Threshold and Its Effect on P-I and I-V Characteristics of 1.3  $\mu\text{m}$  InGaAsP Lasers', *1988 IEEE 11th Int. Semiconductor Laser Conf.*, pp. 206-207.
- [33] S. Tucker and D. J. Pope, (1983) 'Circuit Modelling of the Effect of Diffusion on Damping in a Narrow-stripe Semiconductor Laser', *IEEE J. Quant. Elect.*, vol. QE-19, pp. 1179-1183.
- [34] J. Channin, (1979) 'Effect of Gain Saturation on Injection Laser Switching', *J. App. Phys.*, vol.50, pp. 3858-3860.
- [35] F. Kazarinov, C. H. Henry, and R. A. Logan, (1982) 'Longitudinal Mode Self-stabilisation in Semiconductor Laser', *J. App. Phys.*, vol.53, pp. 4631-4644.
- [36] Y. Li, C.D. Hussey, (1994) 'Triple-clad single-mode fibers for dispersion flattening', *Opt. Eng.*, pp. 3999-4005, December 1994.
- [37] Monerie, (1982) 'Propagation in Doubly Clad Single-Mode Fibers', *IEEE J. Quant. Elect.*, pp. 535-542.
- [38] L.N. Binh, (1995) *ECS 4344 Optical Fiber Communication Lecture Notes*, Monash University, Vol I.
- [39] S.V. Chung, *PhD Thesis : A Simplified Analysis of Optical Waveguides*, Monash University, 1986.
- [40] L.B. Jeunhomme, (1983) 'Single-Mode Fiber Optics : Principles and Applications', *Optical Engineering/Volume 4.*
- [41] J. Nakagawa et al., (1994) 'Simulation of Dispersion Tolerant Long-Haul Optical Fiber Communication Systems with Distributed In-Line Group-Delay Equalisers', *J.Opt. Comm.*, 15 No. 6, pp. 202-207.
- [42] L. A. Ims et al., (1994) '10 Gbit/s Optical Transmission beyond Dispersion Limit', *J. Optical Comm.*, vol. 15 No. 6, pp. 214-225.
- [43] Y. Li, C.D. Hussey, (1994) 'Triple-clad single-mode fibers for dispersion flattening', *Opt. Eng.*, pp. 3999-4005.
- [44] Monerie, (1982) 'Propagation in Doubly Clad Single-Mode Fibers', *IEEE J. Quant. Elect.*, pp. 535-542.
- [45] S.V. Chung, *PhD Thesis : A Simplified Analysis of Optical Waveguides*, Monash University, 1986.
- [46] S. Park, *PhD Thesis : Low-noise, Broadband Optical Receivers Based on Synthesis and Noise Figure Concepts*, Sydney University, 1993.

- [47] Capasso, (1984) 'Multilayer avalanche photodiodes and solid state photomultipliers', *Laser Focus / Electro-Optics*, Vol. 20, pp.84-101.
- [48] S.R. Forest, (1986) 'Optical detectors : Three contenders', *IEEE Spectrum*, Vol.23, pp.76-84.
- [49] E. Bowers and C. A. Burrus, (1987) 'Ultrawide-band long wavelength PIN photodetectors', *IEEE J. Lightwave Tech.*, Vol. LT-5, pp.1339-1350.
- [50] G. Keiser, (1991) 'Optical Fibre Communications', *McGraw-Hill*, 2nd Edition.
- [51] C. Cartledge, (1989) 'The Effect of Laser Chirping on Lightwave System Performance', *IEEE J. Lightwave Tech.*, Vol. LT-7, pp.568-573.
- [52] K-Y. Chin, (1995) 'Non-linear Fibre Optics : Soliton Communications', *ECS 4324 : Advanced Optical Fibre Communications* , Monash University.
- [53] F. Ruhl, (1994) 'Optical Fibre Amplifiers and Their Applications in Telecommunications', *Aust. Conf. Opt.l Fibre Tech. (ACOFT) 1994 Tutorial*.
- [54] S. Shimada and H. Ishio, "Optical amplifiers and their applications", Chapter 6, J. Wiley, Chichester, 1994.
- [55] S. Shimada and H. Ishio, "Optical amplifiers and their applications", Chapters 5 and 8, J. Wiley, Chichester, 1994.
- [56] T.W. Chua, "Modelling of Travelling Wave Electrode Interferometric optical modulator", M.Eng. Sc. disertaion, Monash University 1996.